JULY 1987 GEOPHYSICAL INVESTIGATION OF NOAH'S ARK (DURUPINAR SITE) MAHŞER VILLAGE, DOĞUBAYAZIT, AĞRI

JOHN R. BAUMGARDNER
UNIVERSITY OF CALIFORNIA
LOS ALAMOS NATIONAL LABORATORY

M. SALİH BAYRAKTUTAN
ATATÜRK UNIVERSITY
FACULTY OF ENGINEERING

NOVEMBER 1987
ERZURUM, TURKEY

ABSTRACT

This report describes the results of the geophysical tests conducted at the Durupınar site (Mahşer Village), 20 km east-southeast of Doğubayazıt, Ağrı, by our research team during the month of July 1987. These tests included a ground-penetrating radar survey, a high precision magnetometer survey, and limited investigations with a one-channel seismograph. In brief, the ground-penetrating radar detected an interface, approximately planar, between four and eight meters below the ground surface, that produces strong reflections of the tranmitted radar pulses. The interface lies beneath at least half the area of the site and represents an abrupt and large change in the dielectric properties of the subsurface medium. Whether this abrupt change in properties is the transition between the overlying clay soil and underlying bedrock or, alternatively, a material other than bedrock such as the petrified remains of a large boat, is impossible to answer with the data presently available. Actual sampling of the underlying material is required for a definitive interpretation. Further, the radar survey shows another moderately reflective interface approximately one meter below the ground surface over most of the site. Again, however, without samples of the subsurface materials, no definitive interpretation of this interface is possible.

The magnetometer survey shows a strong anomaly associated with the rock outcrop near the middle of the boat-shaped site. The localized character of this anomaly and its large amplitude suggest the rock that outcrops at the surface is limited in its lateral extent but probably has many meters of vertical extent.

Finally the very limited amount of seismograph data obtained indicates a layer with moderately high seismic velocity lies at relatively shallow depth (6-8 meters). This material with moderate seismic velocity (2400-3300 m/s) must be something other than the clay soil present at the ground surface.

We recommend core drilling at several locations both inside and outside the site be performed to provide the additional information needed to make proper interpretations of these geophysical tests.

INTRODUCTION

In July 1987 a joint research project between Atatürk University and staff of Los Alamos National Laboratory of the University of California was conducted under the authority of the Turkish Prime Ministry. The purpose of this joint project was to determine, if possible, using geophysical methods whether the boat-shaped formation (Figure 1 and 2) located approximately 20 km east-southeast of Doğubayazıt near Mahşer village--a site first identified in 1959 by Capt. Ilhan Durupınar--contains the remains of Noah's Ark. The geophysical tests included a survey with a ground-penetrating radar, a survey with a proton-precession magnetometer, and limited investigation with a single-channel seismograph.

Leaders of the research team were M. Salih Bayraktutan of Atatürk University and John R. Baumgardner of the University of California. Other members of the team included Thomas T. Anderson; Mahlon T. Wilson of the University of California; Thomas F. Fenner with Geophysical Survey Systems, Inc., manufacturer of the radar; and Şemsi Yazıcı and Necmettin Tamas of Atatürk University. In addition James A. Burroughs, Daniel M. Devaney, and Jeffrey C. Wayman of Seven League Productions provided photographic documentation for the project. Figure 3 is a group photograph of the personnel who participated in this undertaking.

The geophysical instrumentation included a SIR System-8 ground-penetrating radar manufactured by Geophysical Survey Systems of Hudson, New Hampshire. Figure 4 shows the control unit, magnetic tape recorder, graphic recorder, and batteries for the radar. Figure 5 shows the antenna unit used to transmit and receive the radar signals. The antenna was dragged across the site on transects spaced two meters apart. Radar pulses approximately 5 nanoseconds in width were transmitted at a repetition rate of 50 kHz. The return radar signal was recorded on magnetic tape and played back for visual inspection and interpretation on the graphic recorder. The radar survey was performed during the period of 19-23 July 1987.

Other instrumentation included a proton-precession magnetometer Model G-856A and a single-channel signal enhancement seismograph Model ES-125, both manufactured by EGG Geometrics of Sunnyvale, California. The magnetometer survey of the site was conducted 27-28 July by taking readings at two-meter intervals in both coordinate directions. Seismograph investigations of the site was performed 29-30 July. The results of these investigations are discussed in the following sections of the report.

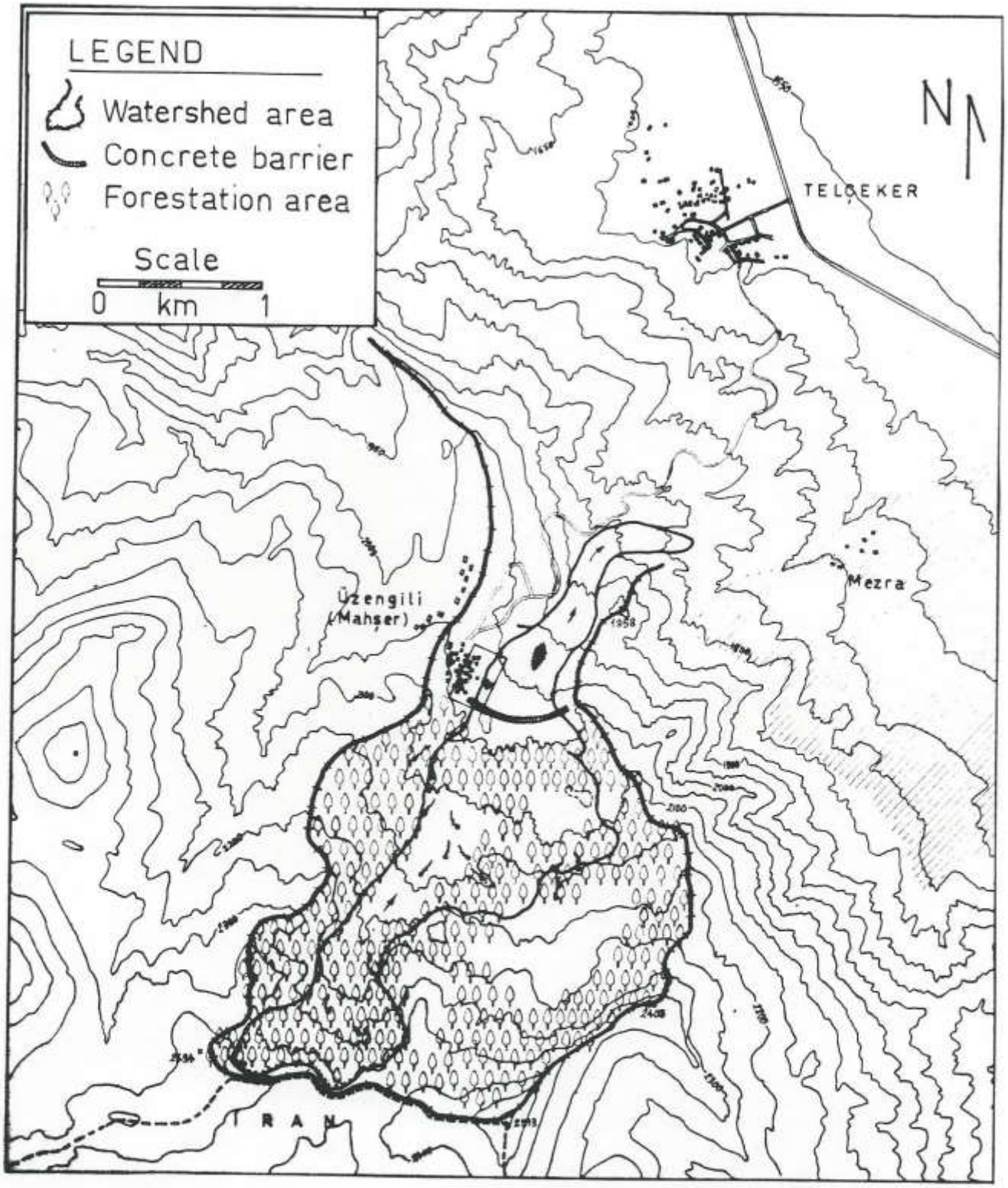

Fig. 1 Topographical map of the area near Mahşer village. The Noah's Ark site is approximately 0.5 km east of the village within an actively moving landslide environment. Features of a plan are shown for stabilizing the terrain including forestation, drainage, and construction of a retaining barrier.

Fig. 2 View of the Noah's Ark site from north toward the south. The significance of the rock outcrop near the middle of the site is an important issue in understanding the site's mode of formation.

Fig. 3 July l987 research team: Thomas Fenner in front; middle row, left to right, James Burroughs, worker from Mahşer village, Jeffrey Wayman, Daniel Devaney, Şemsi Yazıcı, Salih Bayraktutan, John Baumgardner; top row, two bus drivers and Necmettin Tamas. Not shown are Mahlon Wilson and Thomas Anderson.

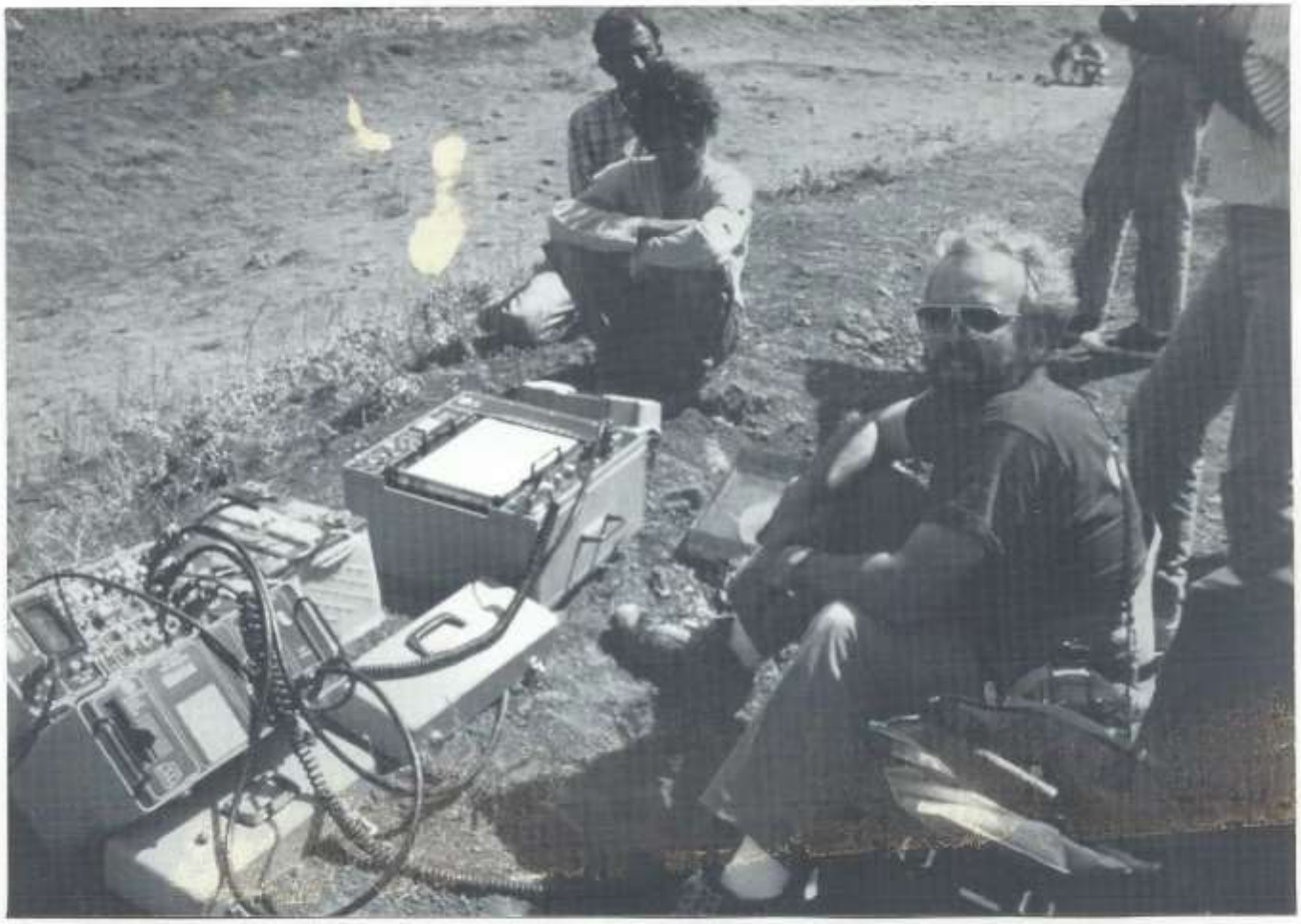

Fig. 4 Ground-penetrating radar including control electronics, magnetic tape recorder, graphic recorder, and batteries. At right is geologist/radar operator Thomas Fenner.

Fig. 5 Radar antenna is moved across the site at as uniform a speed as possible. Radar pulses 5 nanoseconds wide are transmitted 50,000 times per second. Energy reflected by the subsurface structure and received by the antenna is processed to provide a visual representation of the underground structure.

RADAR DATA

Figure 6 shows the x-y coordinate system used for the radar survey. Transects with the radar antenna were made parallel to the x-direction at two-meter intervals. The locations of the transects are denoted by the horizontal lines inside the outline of the site. Figure 7 contains photographically reduced copies of the actual radar data for each of the 71 transects of Figure 6. The left ends of the scans in Figure 7 correspond to the left side of Figure 6. An attempt has been made in Figure 7 to align the x=0 position for each of the transects to the same horizontal position on the page. The widths of the scans vary from transect to transect partly because the speed at which the antenna was dragged across the site was not constant.

All of the scans shown in Figure 7 were obtained with the radar operating at a frequency of 120 MHz in order to achieve the maximum possible penetration. The vertical coordinate in these plots, measured from the topmost horizontal line, represents the roundtrip travel time for the radar signal. The time increment between successive horizontal lines is 20 nanoseconds. For dielectric properties appropriate for clay soil, 20 nanoseconds of roundtrip travel time implies a physical thickness of about one meter. Hence, the interval between horizontal lines in the plots of Figure 7 represents approximately one meter of depth in the ground.

An important consideration in the interpretation of these radar data is the fact that travel time, and therefore depth, is measured with respect to the ground surface. Because there is as much as four meters of topographical variation as one crosses the site, one must be careful to account for this height variation of the ground surface when interpreting the shape of subsurface features.

The most noteworthy feature observable in the data of Figure 7 is the V-shaped reflector that is particularly evident in the transects between y=-6 m and y=-50 m. When the topographical variation of the surface is taken into account, one finds that this feature is almost planar in form. The large amplitude of the back-reflected radar signal suggests a large contrast in the dielectric properties of the two sides of a sharply defined interface. The material above the interfaced presumably is the clay soil observable at the ground surface and exposed to several meters depth in the scarp surrounding the site and in cracks and gullies in the adjacent mudflow environment.

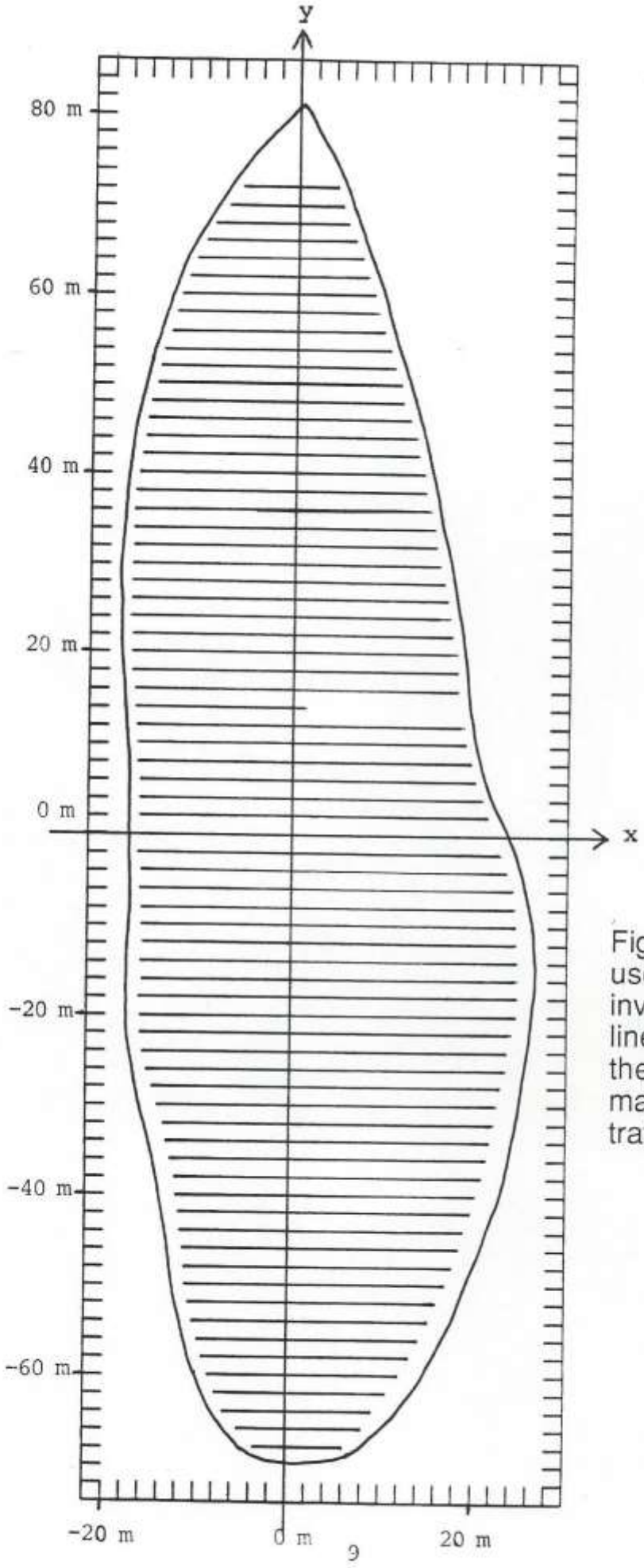

Fig. 6 Coordinate system used for the geophysical investigations. Horizontal lines inside the outline of the site denote transects made in the ground penetrating radar survey.

The crucial issue is the type of material which lies below the interface. Is it bedrock that rises up through the mudflow to form something like a small island around which the flow moves? Or is the material something other than bedrock? At least two considerations suggest that it is not bedrock. The first is that in the transects between y=2 m and y=20 m and x>0 in the vicinity of the rock that outcrops at the surface, one does not observe consistently strong reflections of a similar character. The most likely candidate for the bedrock material is the calc-schist rock that forms the hills on either side of the mudflow channel and that comprises the outcrop near the middle of the site. Since the low amplitude radar returns near the outcrop imply a small dielectric contrast between the clay soil and calc-schist rock, the strong reflections of the prominent V-shaped feature are probably not caused by a transition from clay soil to a calc-schist bedrock.

A second consideration which argues that the material below the relfecting interface may not be bedrock is that in several scans, especially between y=-18 m and y=-38 m, there is a double reflection, suggestive of a layer, rather than a simple transition into a material many meters thick. To find such an extensive, almost planar, layer buried within a channel through which a huge volume of mudflow material has moved in a chaotic fashion is highly anomalous from the standpoint of known landslide and debris flow mechanics. If the layer pertains to a buoyant man-made structure, the layer's present setting suggests that the structure has been transported to the present location by a landslide event where it was stranded upon the rock which now outcrops near the middle of the site.

The next step in resolving these questions is to obtain samples of the subsurface materials by core drilling. Continuous core sampling to a depth of 20 meters should readily indicate the presence or absence of an island of bedrock within the site. It should provide unequivocable evidence as to the nature of the interface producing the strong radar reflections. It could reveal additional structure below the depth the radar could penetrate. The combination of the radar data and ground truth that core drilling can provide would yield a valuable three-dimentional picture of the subsurface structure within this unusual boat-shaped formation. We strongly urge that drilling be performed as soon as weather conditions permit in the spring of 1988.

An additional feature observable in the radar data is a consistent pattern of reflection at a uniform depth of approximately one meter over almost the entire site. It is interesting that in August 1985 we drilled six auger holes at various locations in the site and encountered rock at one meter depth in all holes except one. Core drilling which can penetrate and sample such a layer should clarify its nature and relationship to the rest of the formation.

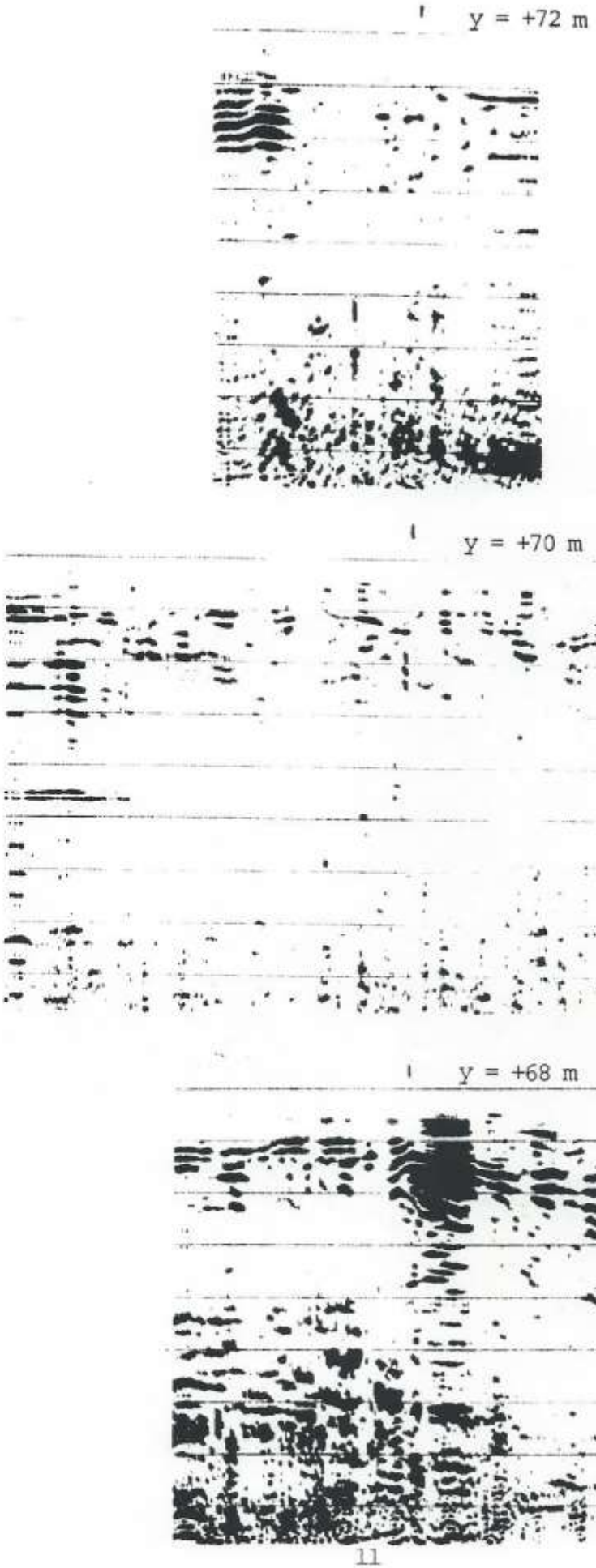

Fig. 7 Actual graphical output for the 71 transects in ground-penetrating radar survey. The small vertical mark above each plot denotes the x=0 point in the scan.

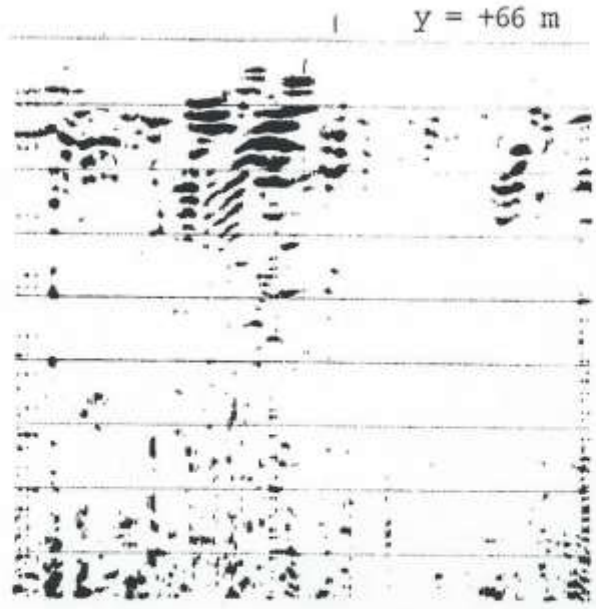
y = +66 m

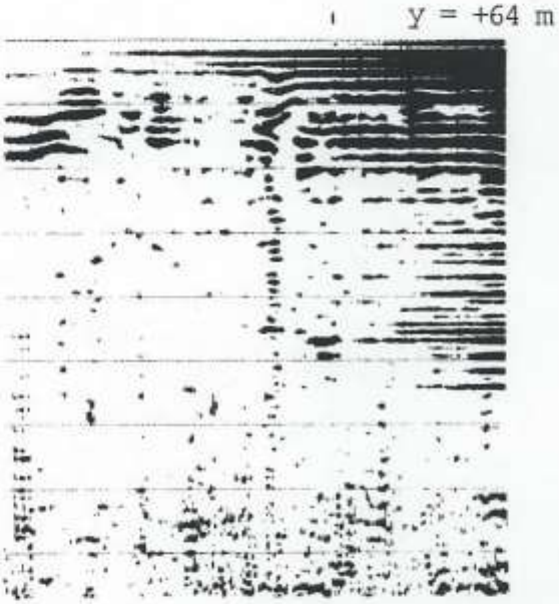
y = +64 m

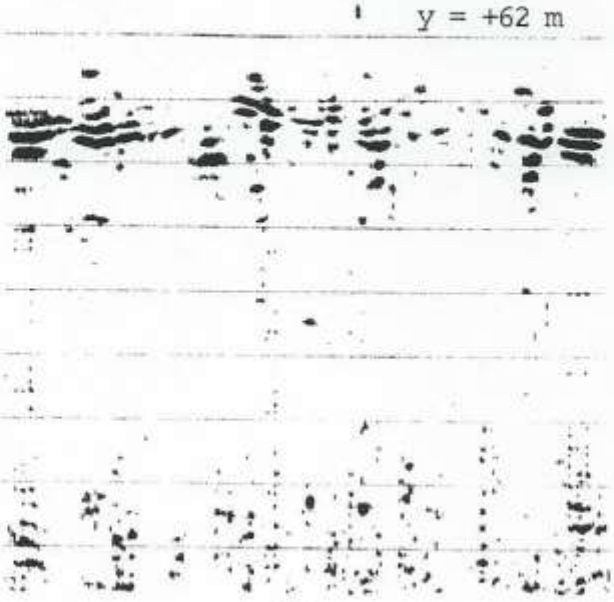
y = +62 m

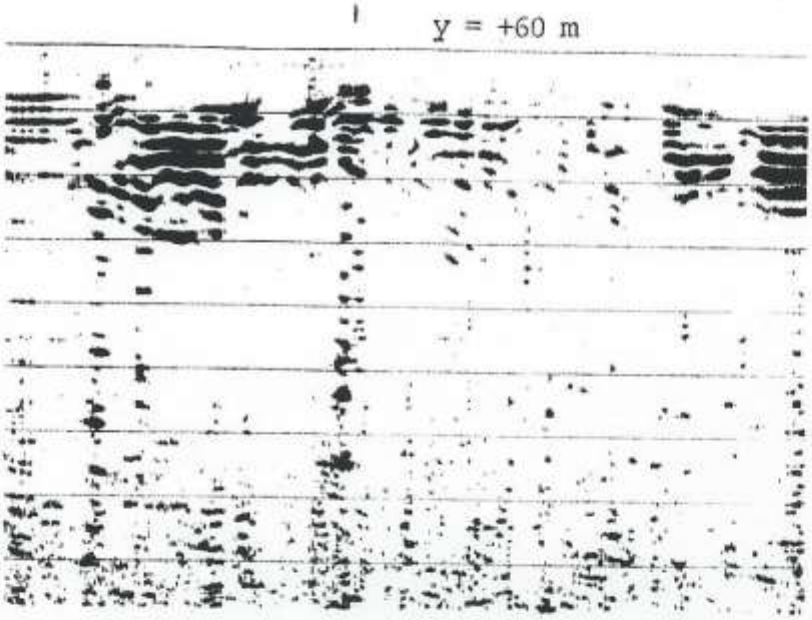
y = +60 m

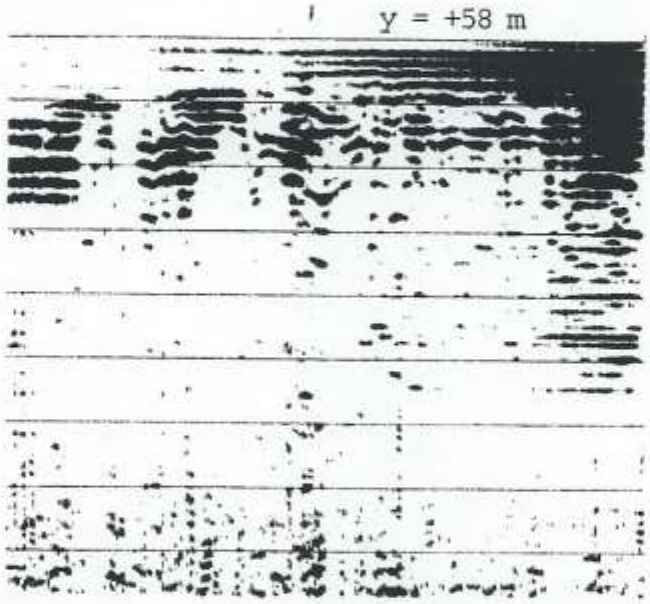
y = +58 m

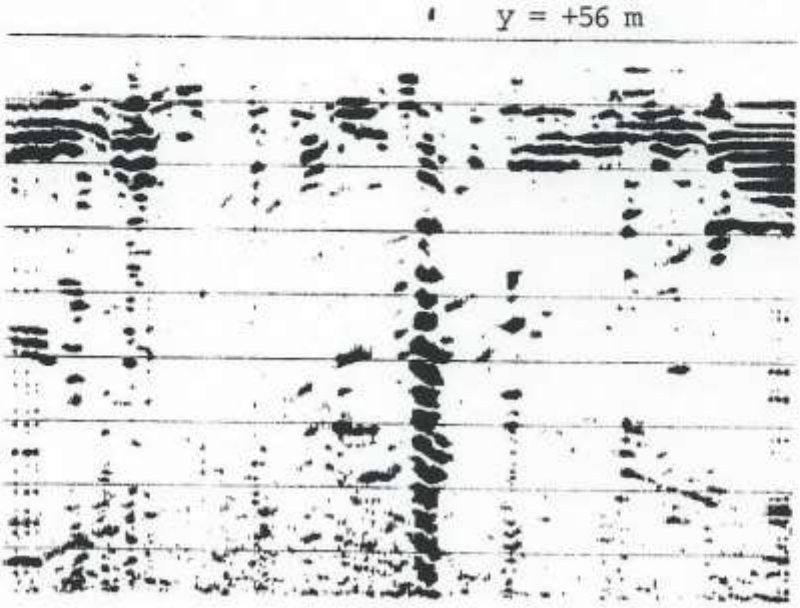
y = +56 m

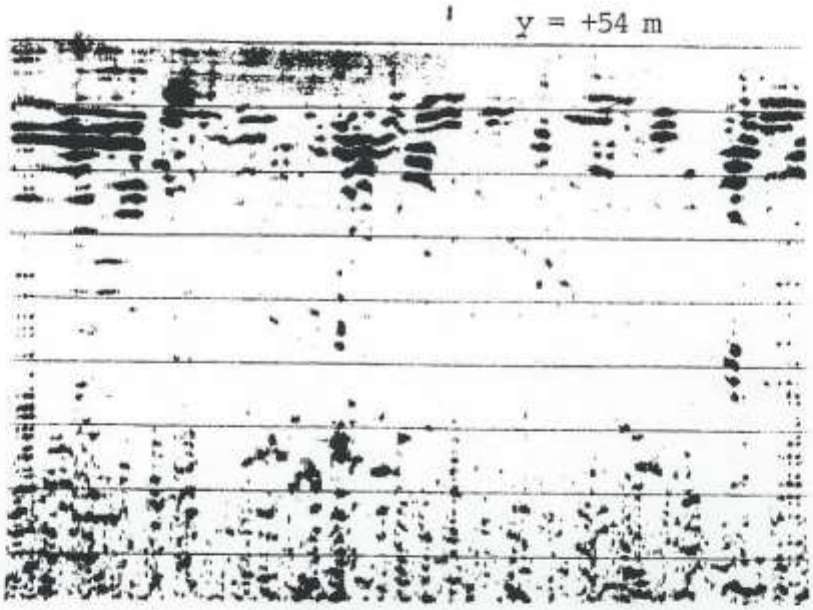
y = +54 m

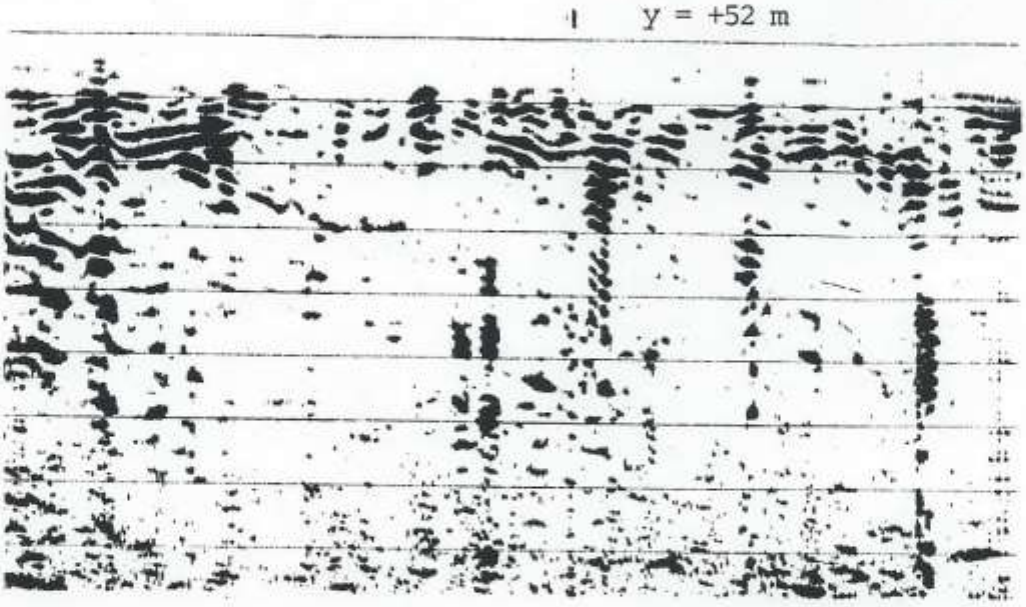
y = +52 m

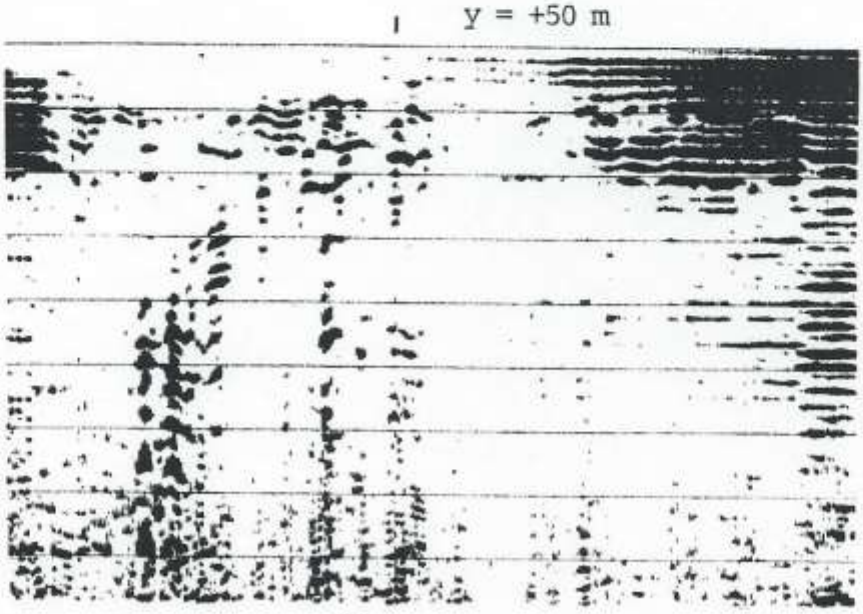
y = +50 m

y = +48 m

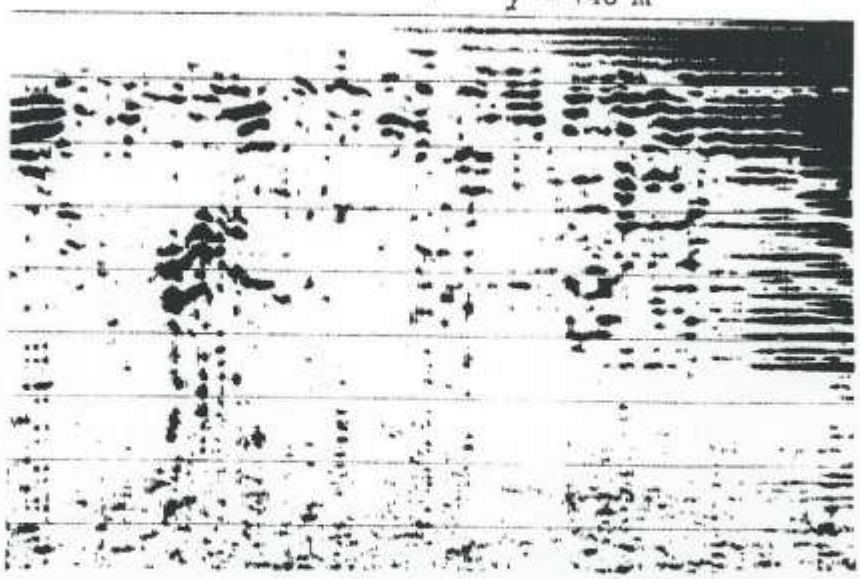

y = +46 m

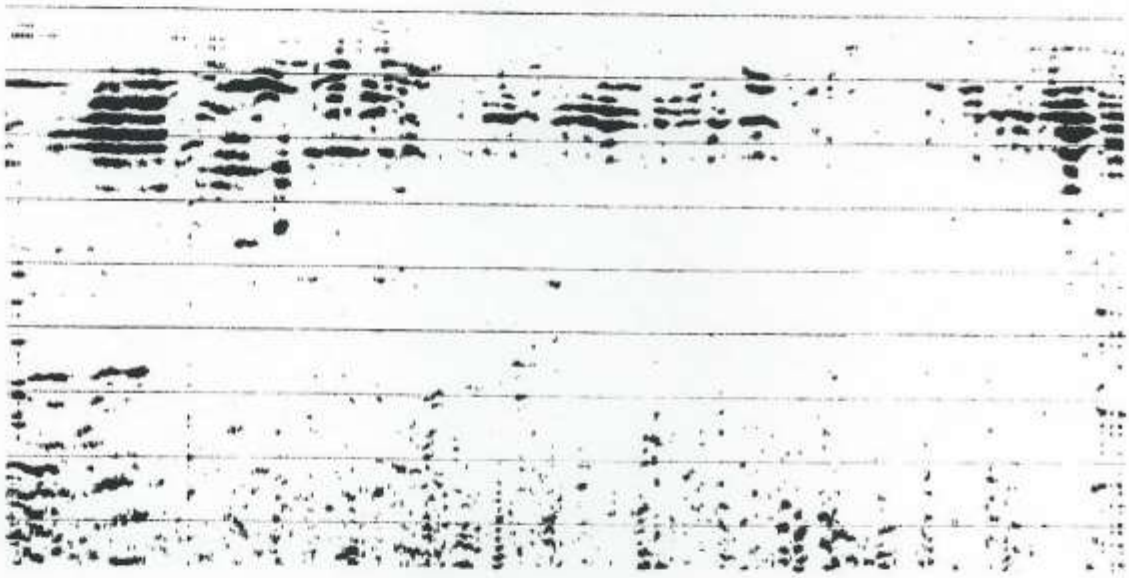

y = +44 m

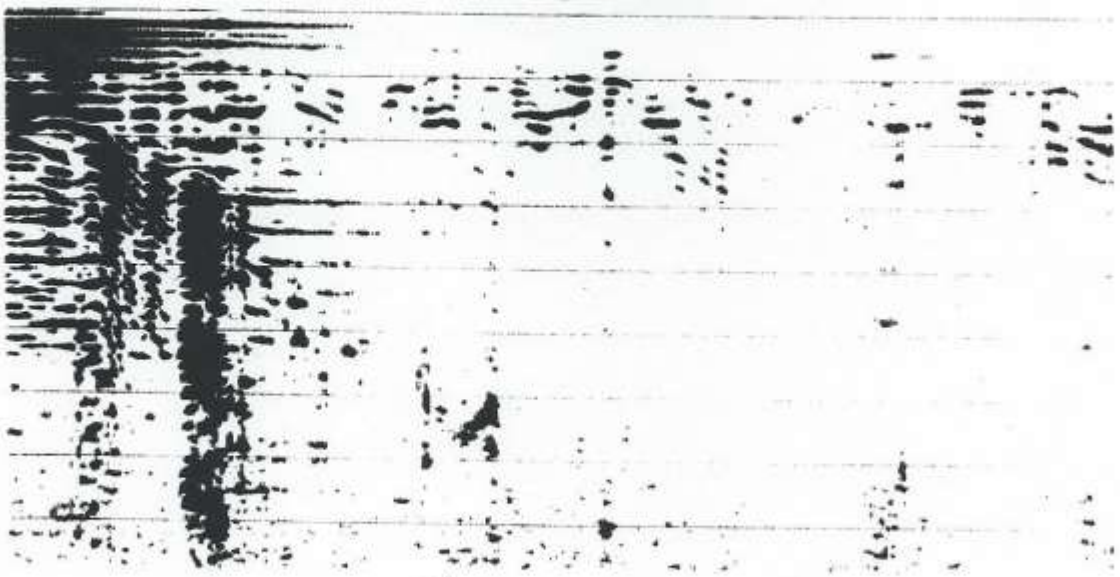

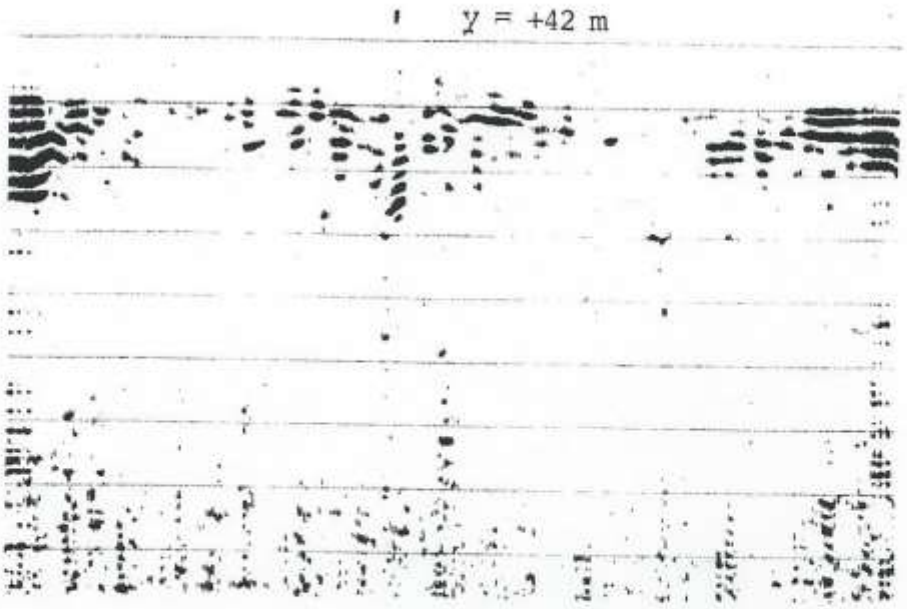
y = +42 m

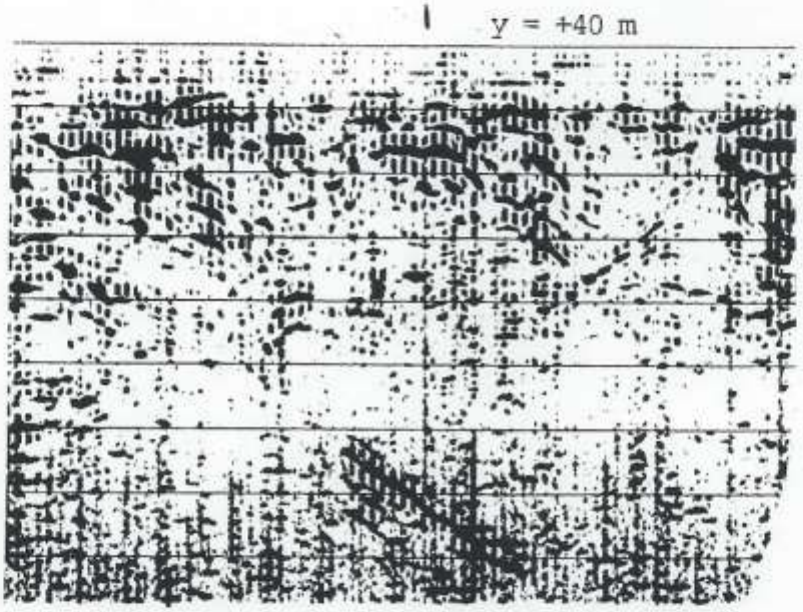
y = +40 m

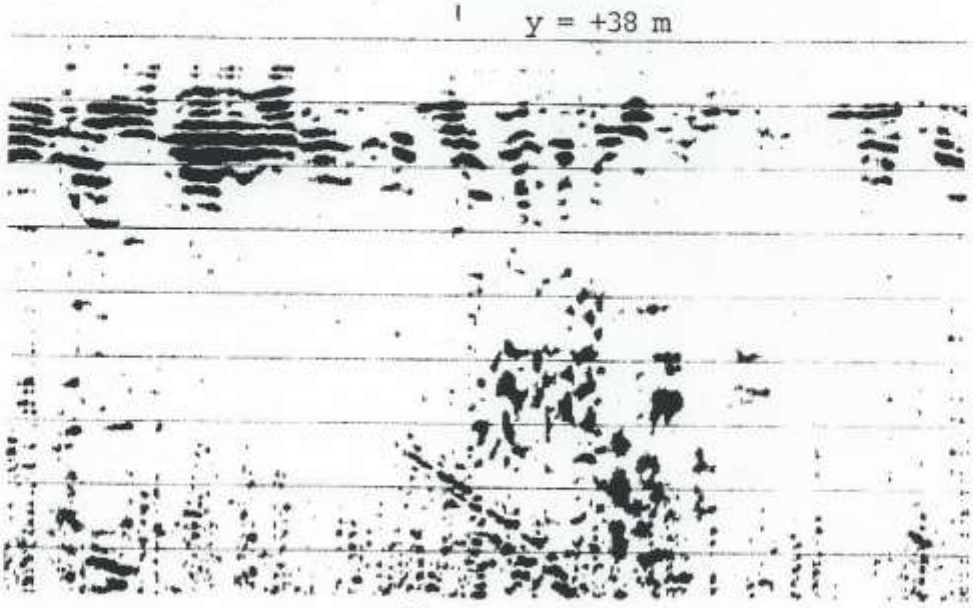
y = +38 m

y = +36 m

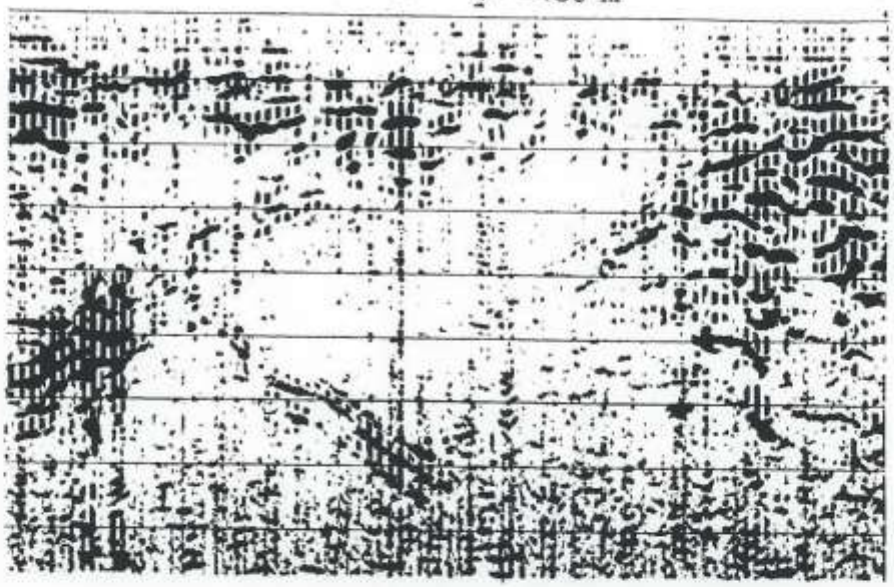

y = +34 m

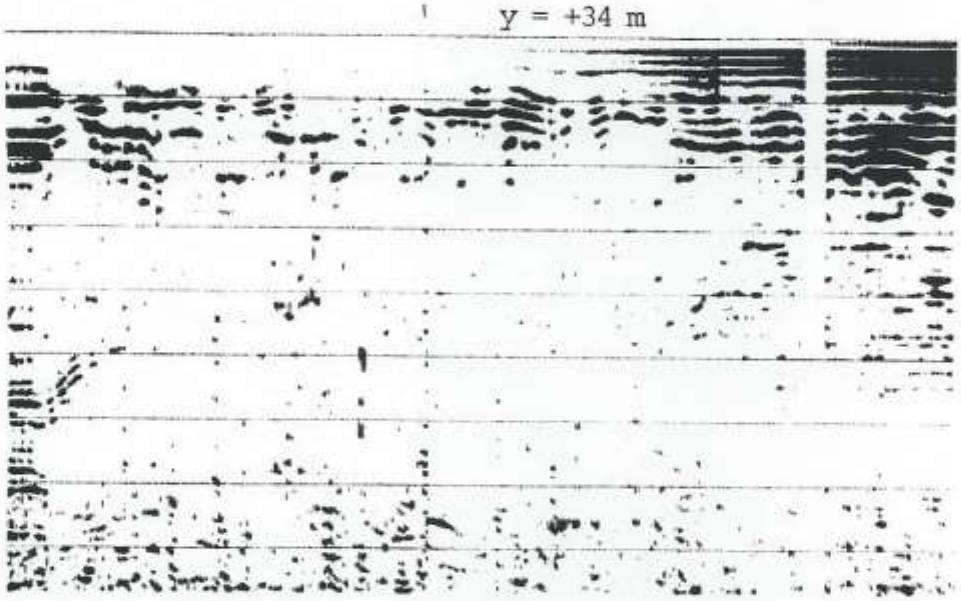

y = +32 m

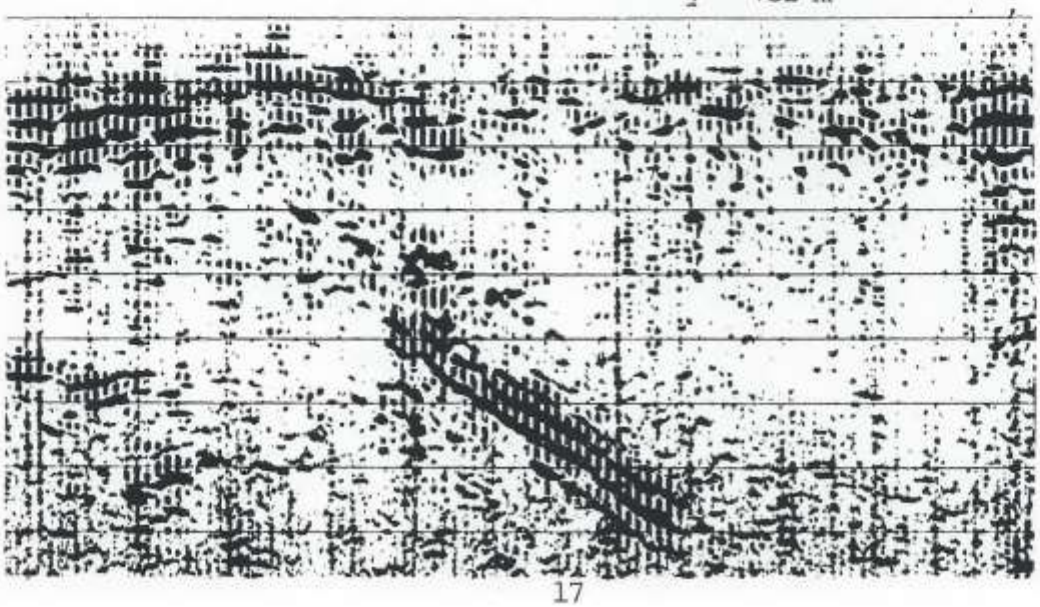

y = +30 m

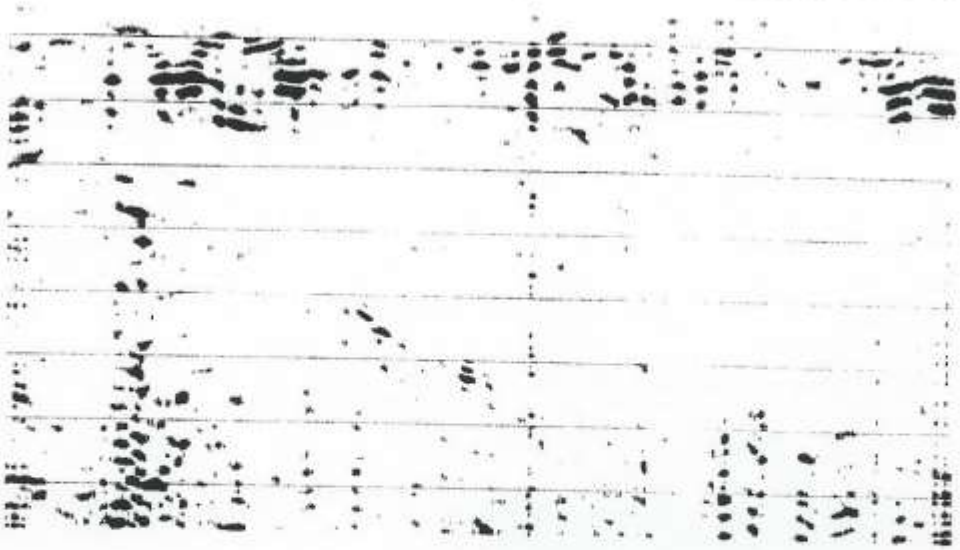

y = +28 m

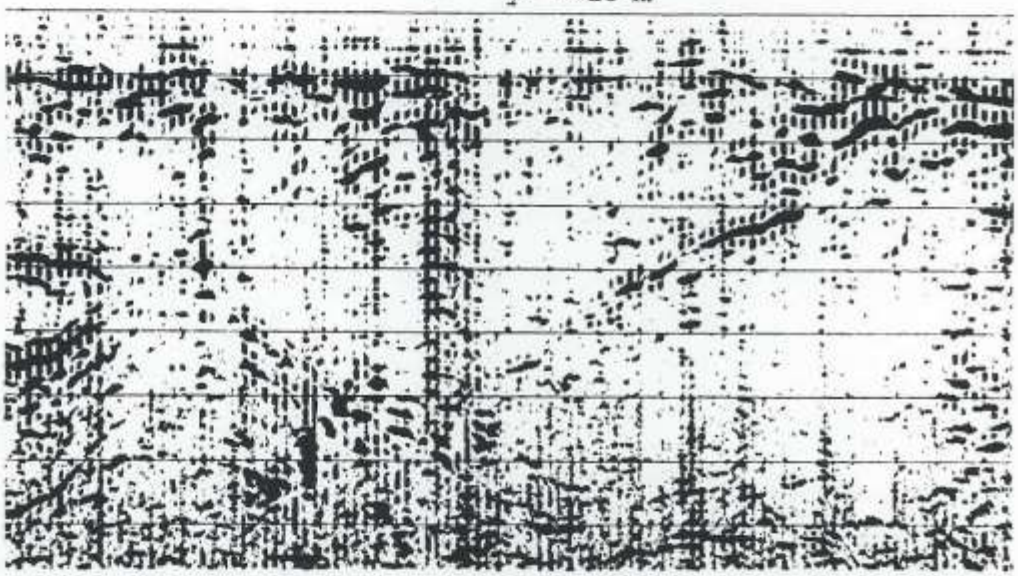

y = +26 m

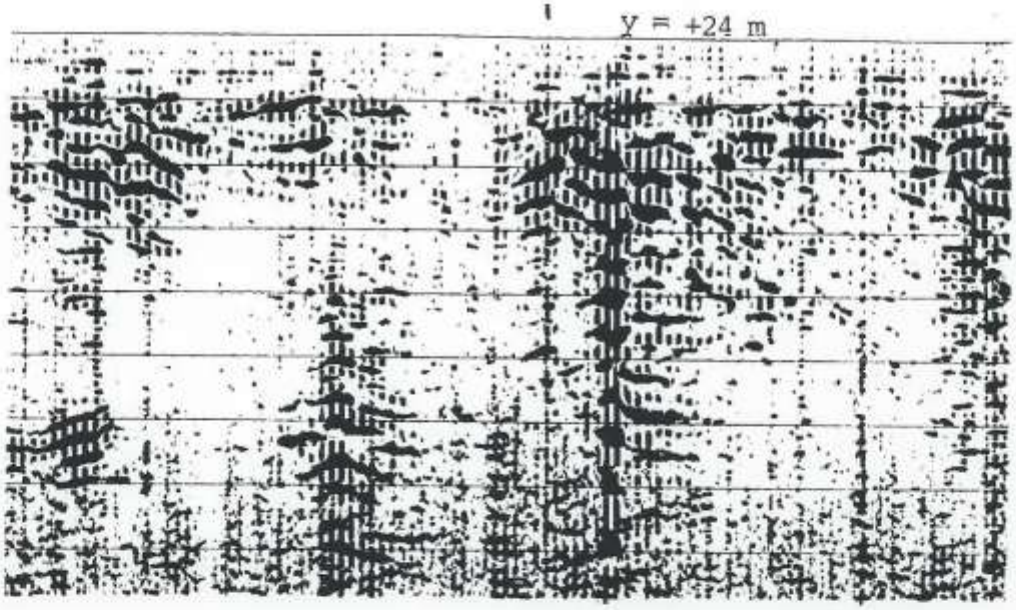
y = +24 m

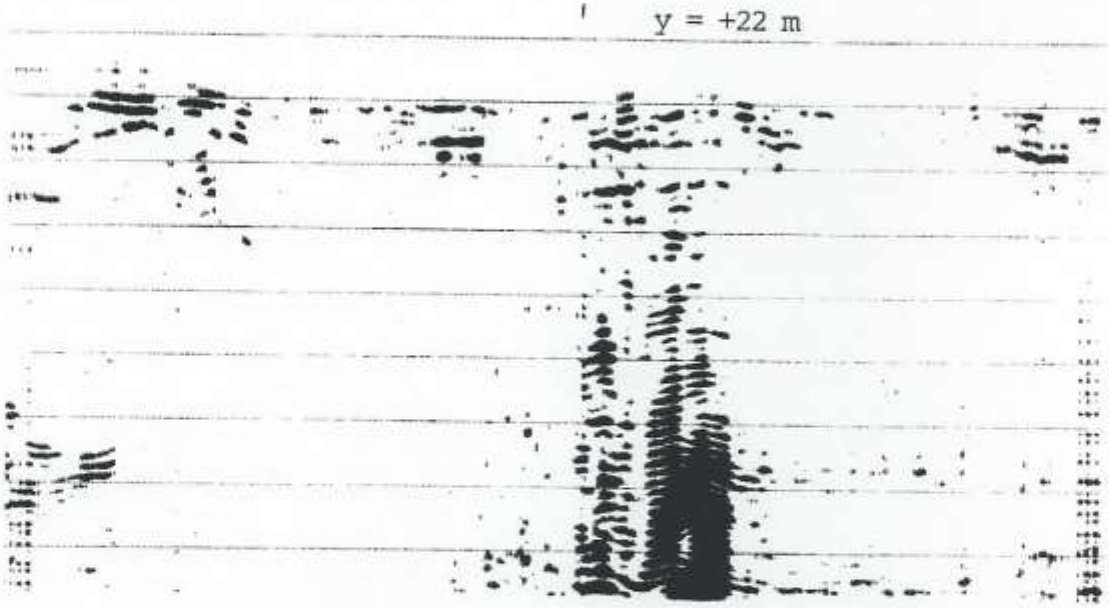
y = +22 m

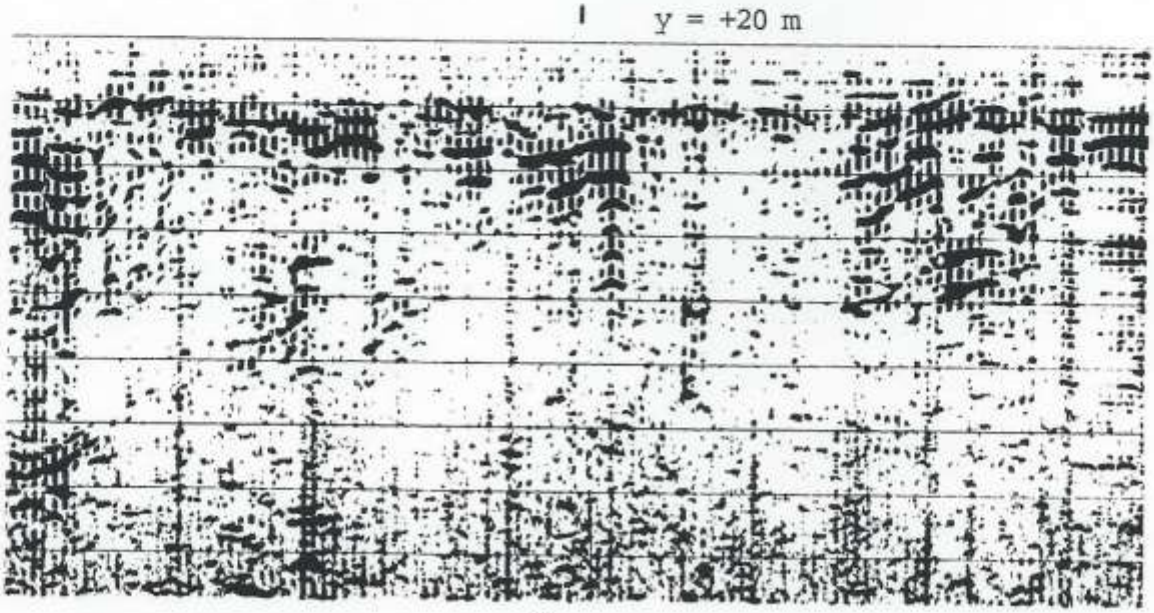
y = +20 m

y = +18 m

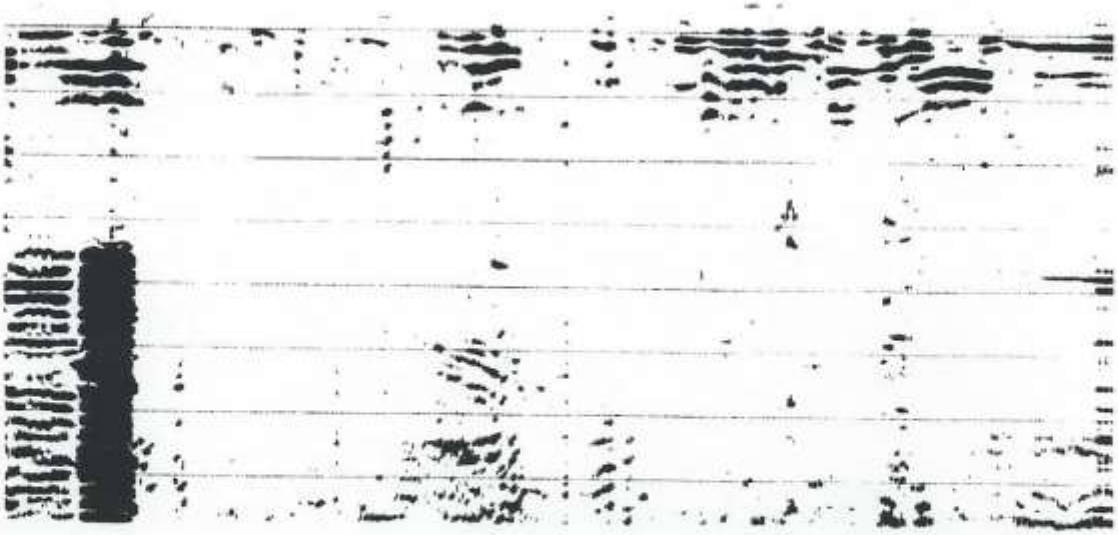

y = +16 m

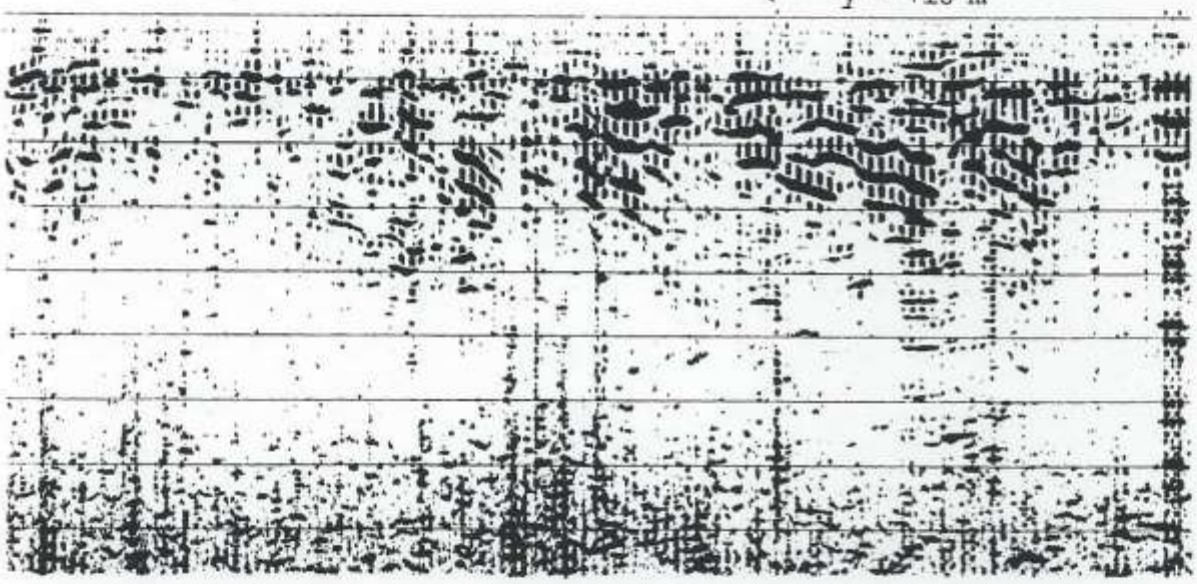

y = +14 m

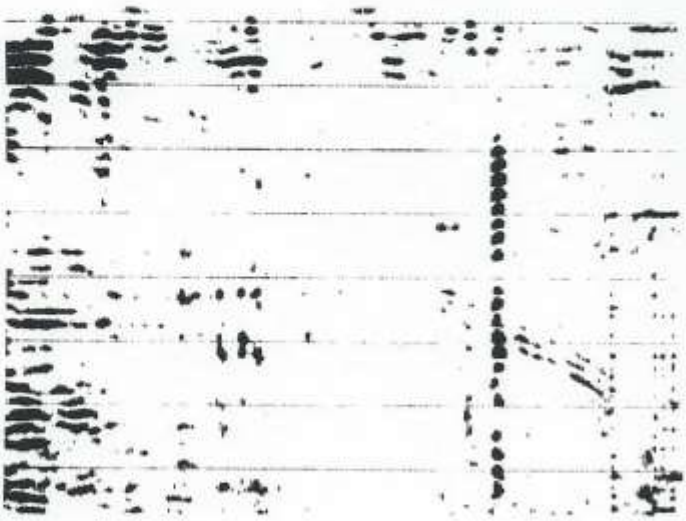

Location of
rock outcrop

y = +12 m

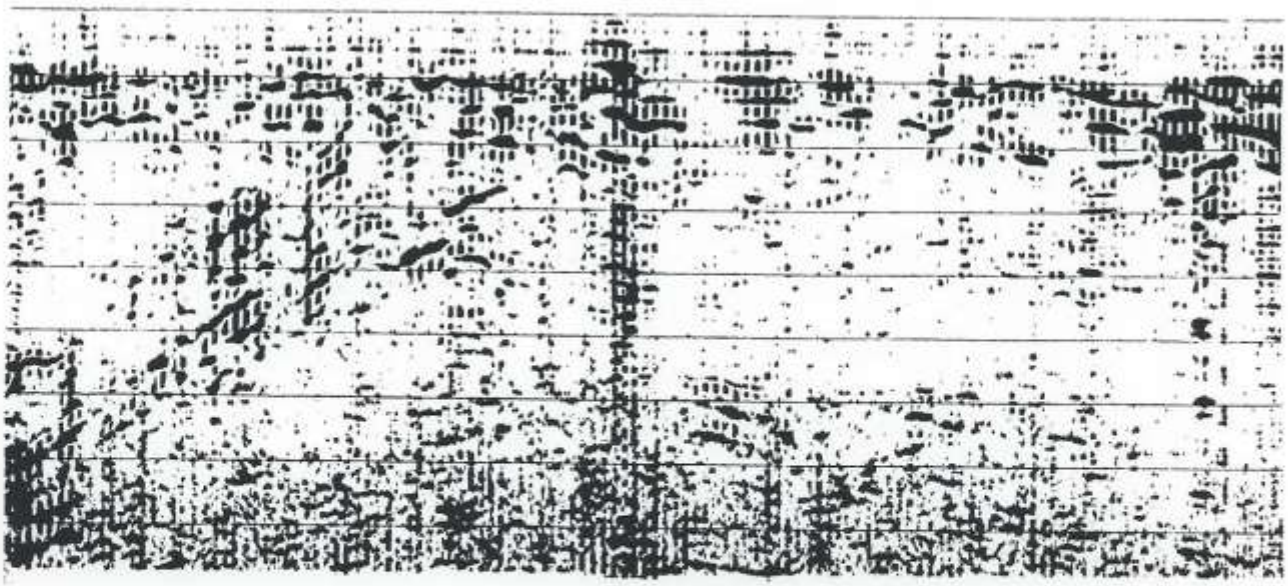

y = +10 m

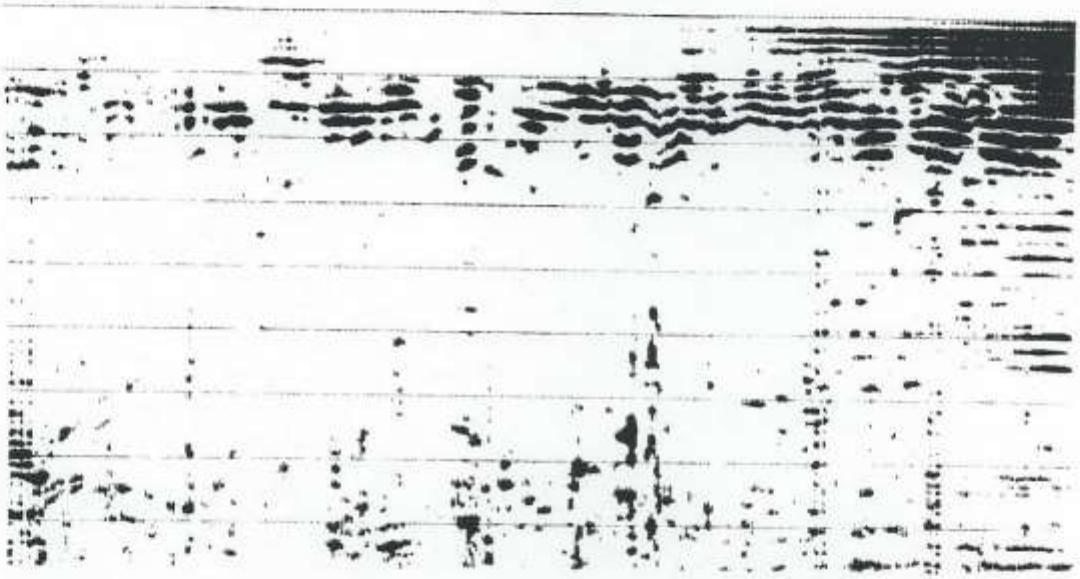

y = +8 m

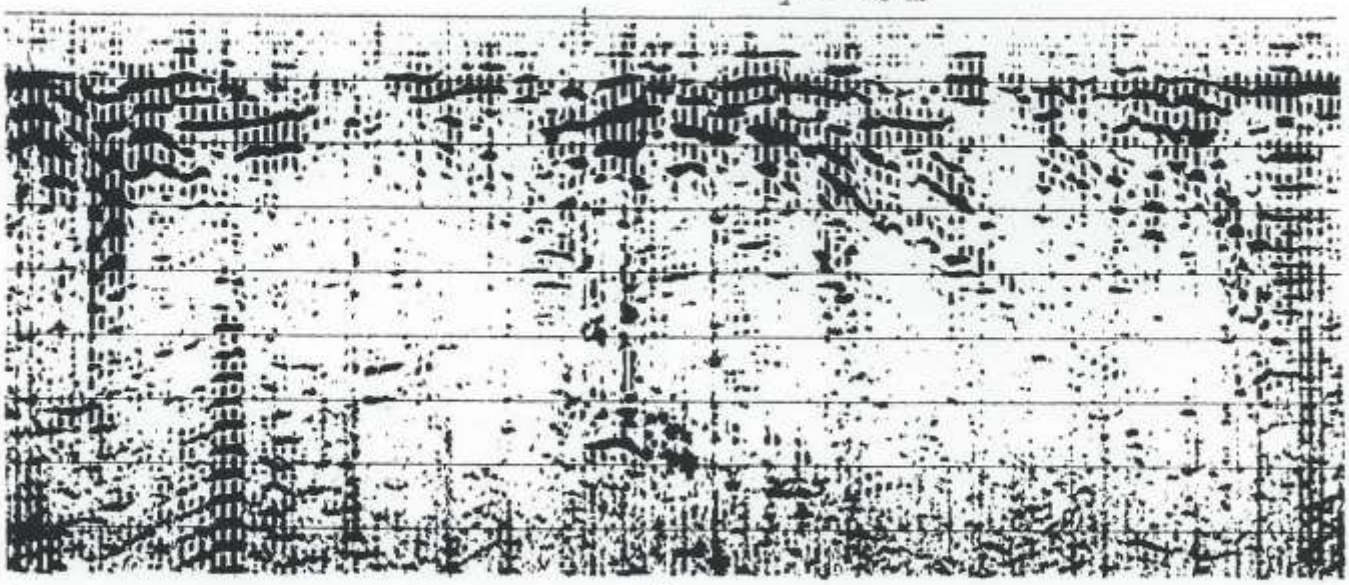

y = +6 m

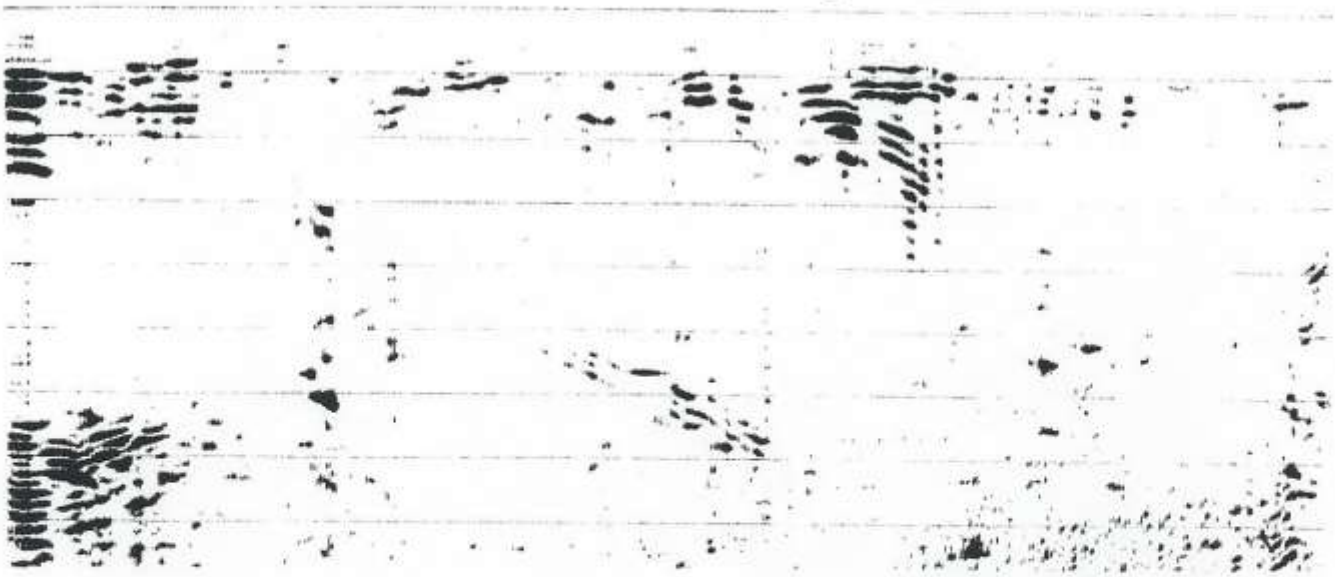

y = +4 m

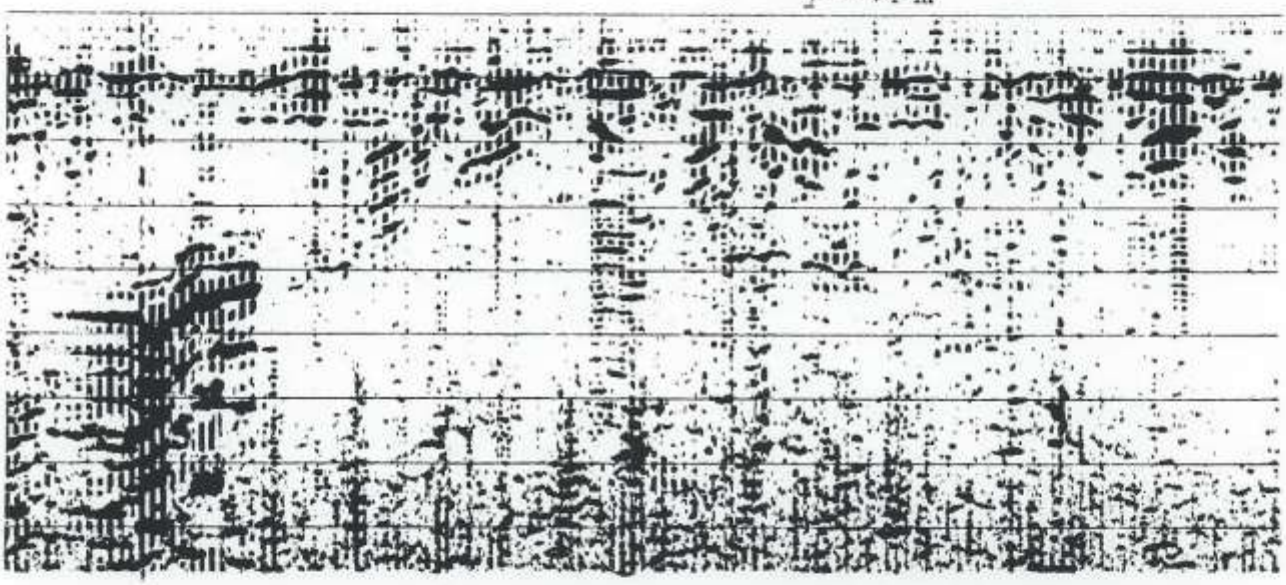

y = +2 m

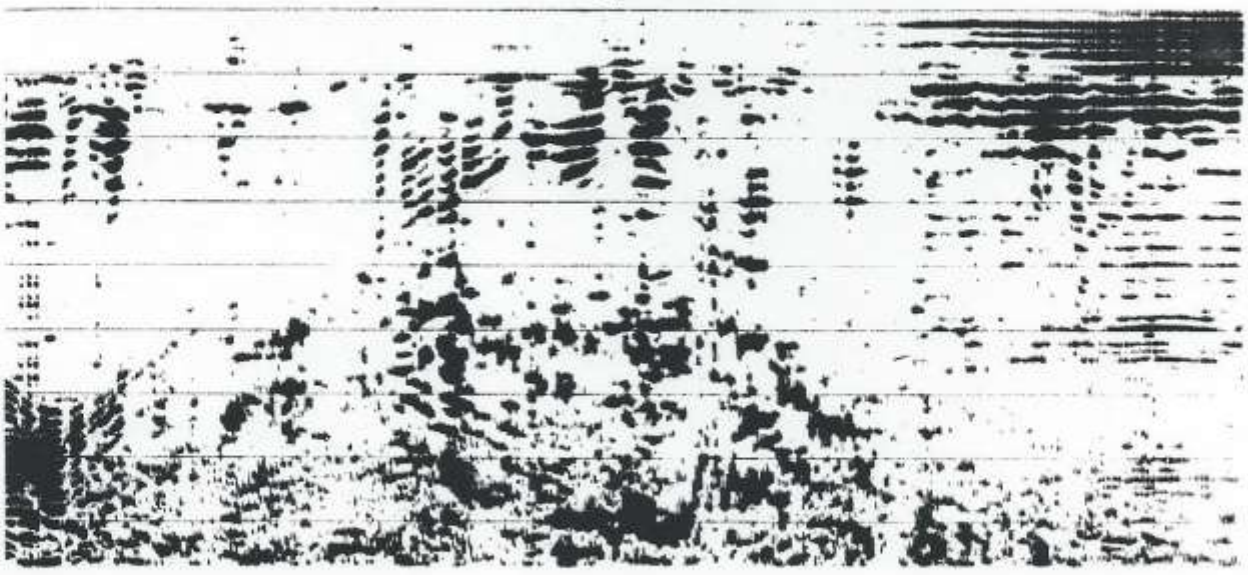

y = 0 m

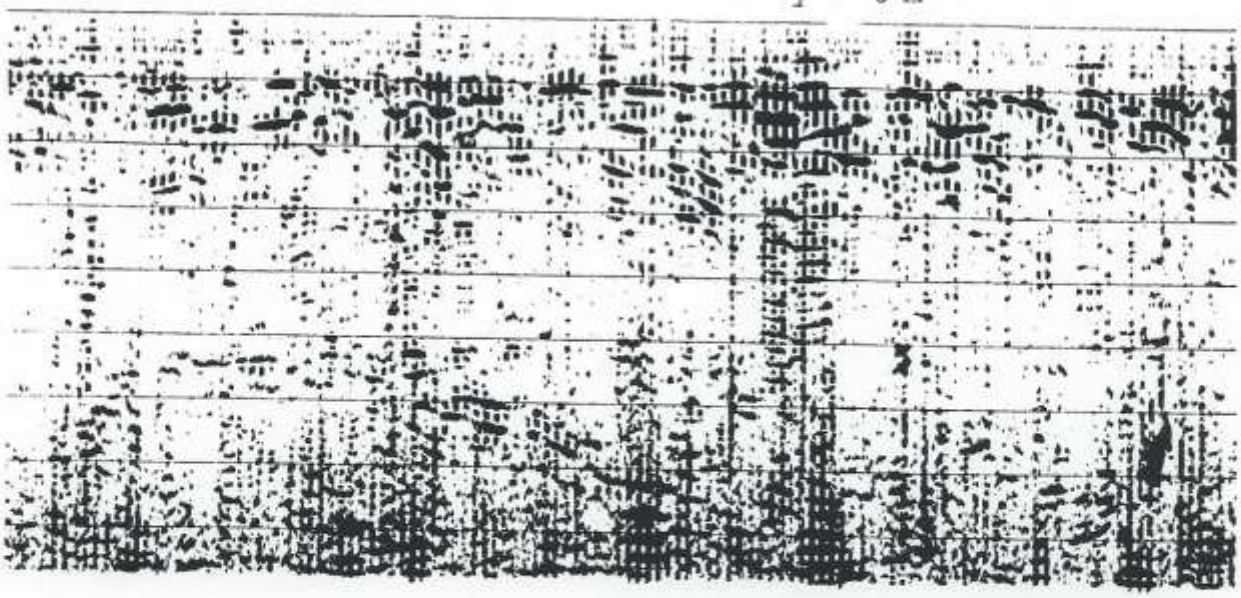

y = -2 m

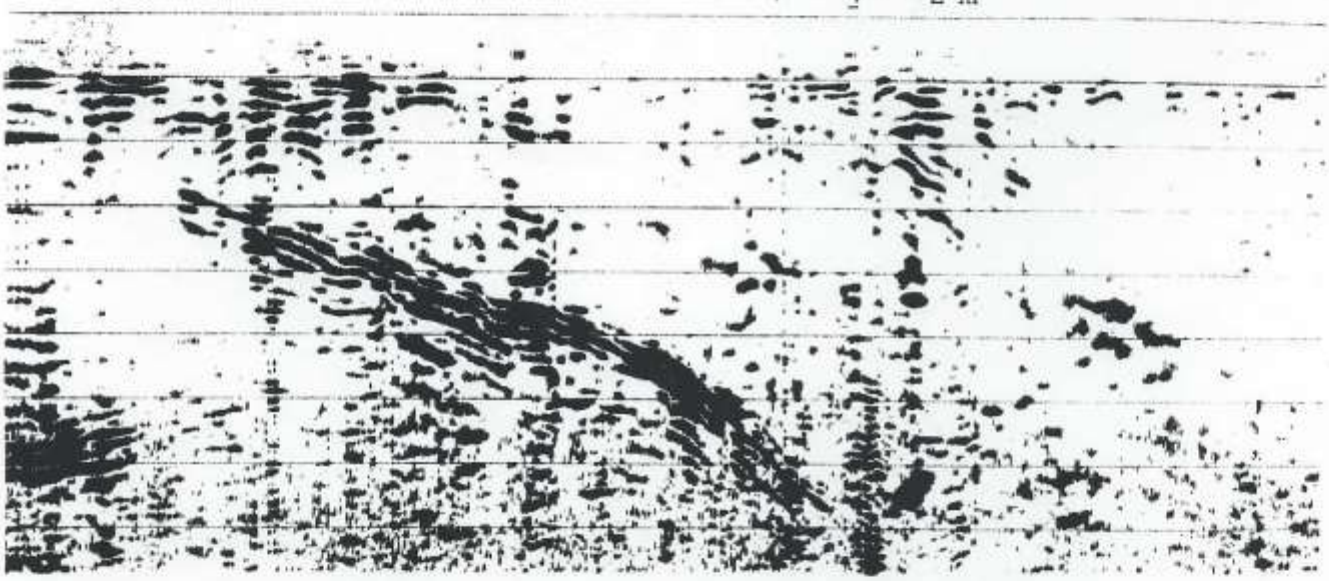

y = -4 m

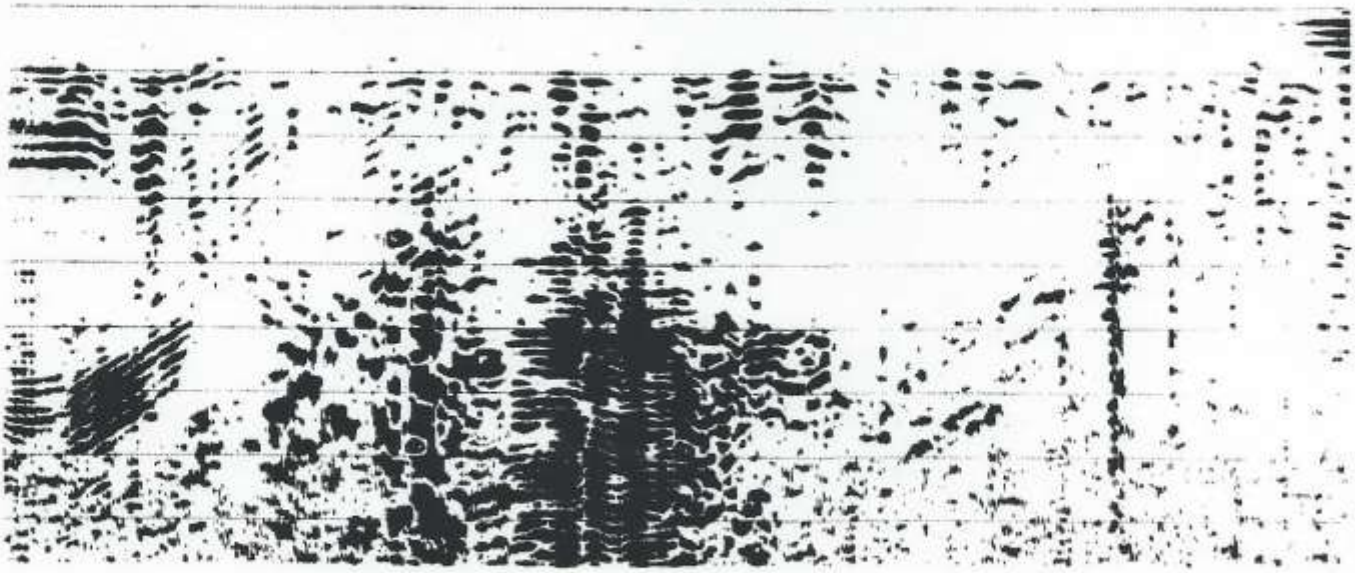

y = -6 m

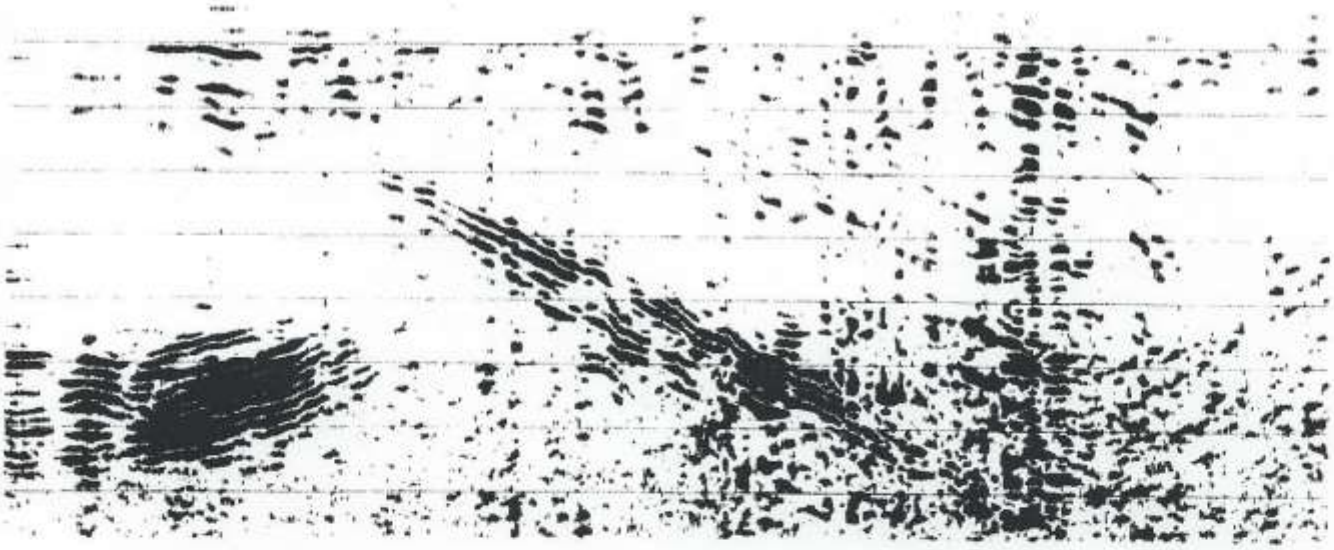

y = -8 m

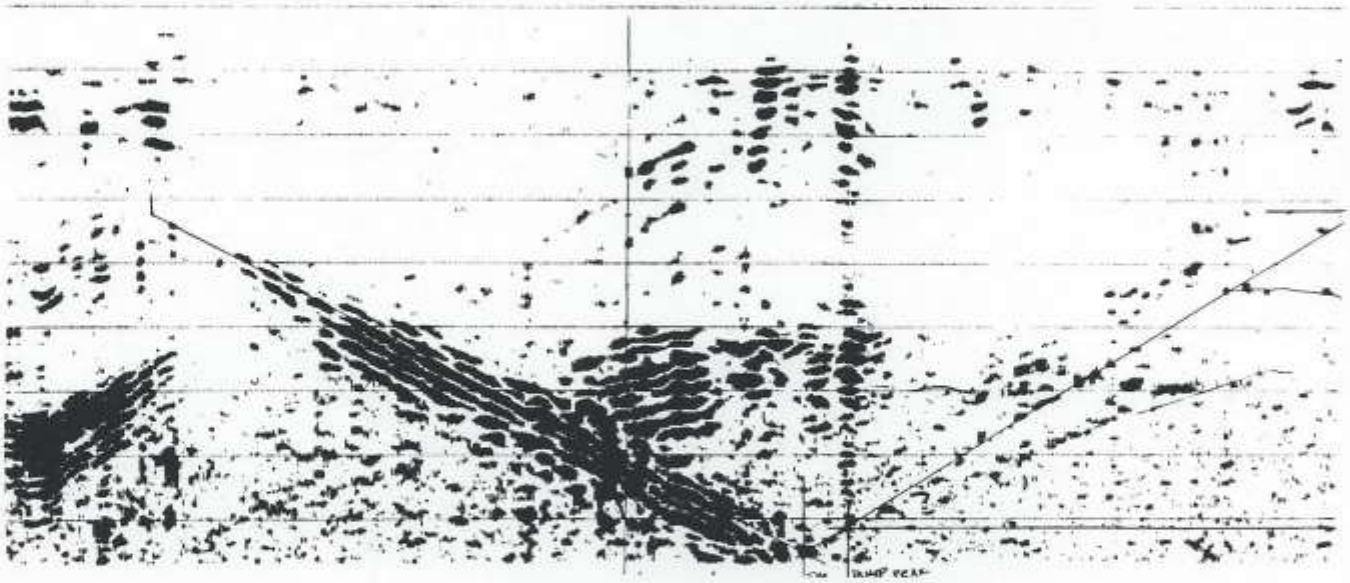

y = -10 m

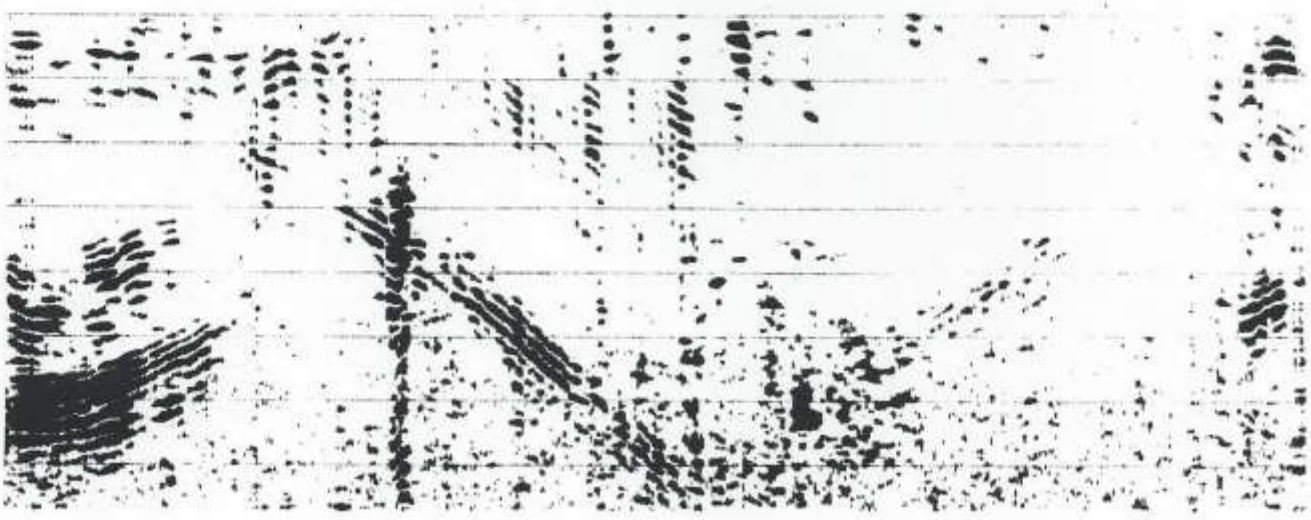

y = -12 m

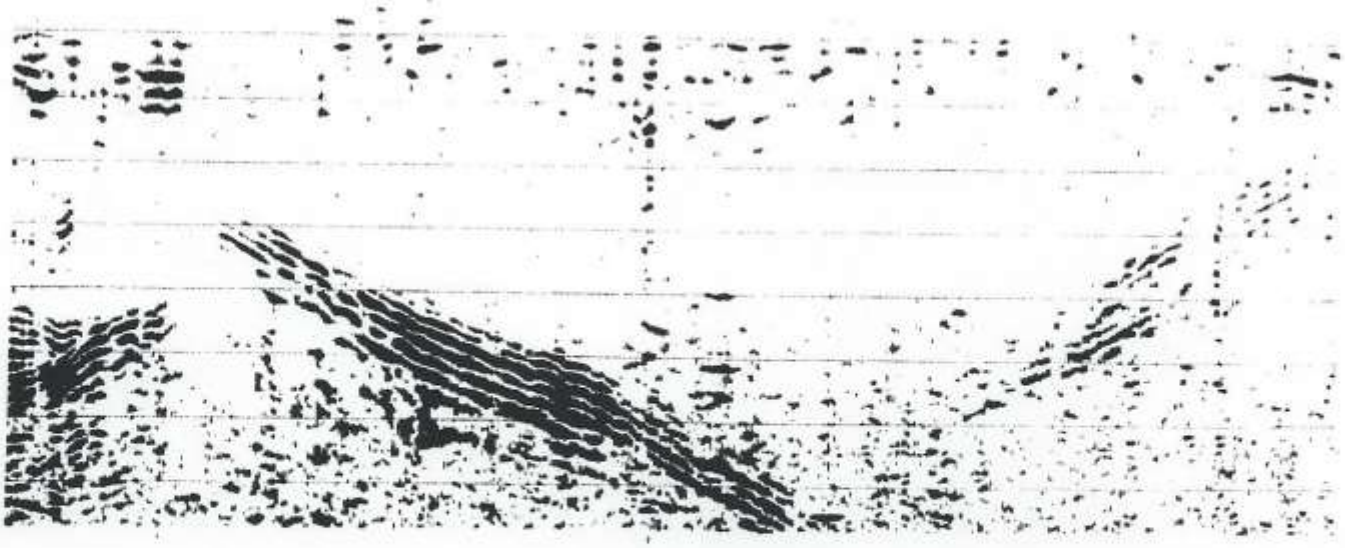

y = -14 m

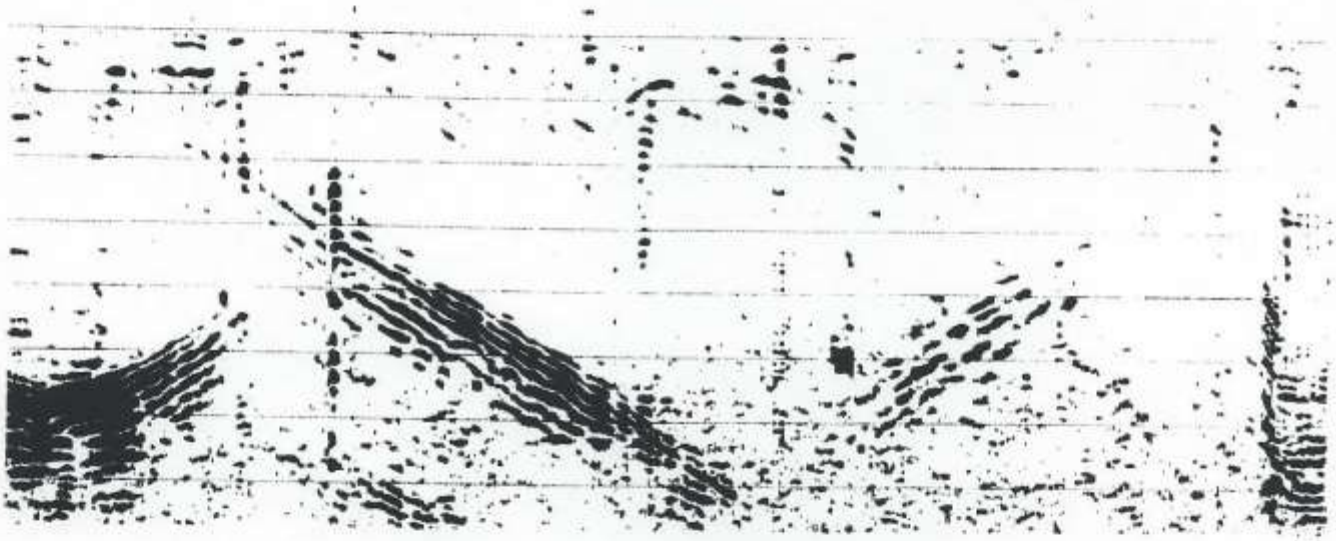

y = -16 m

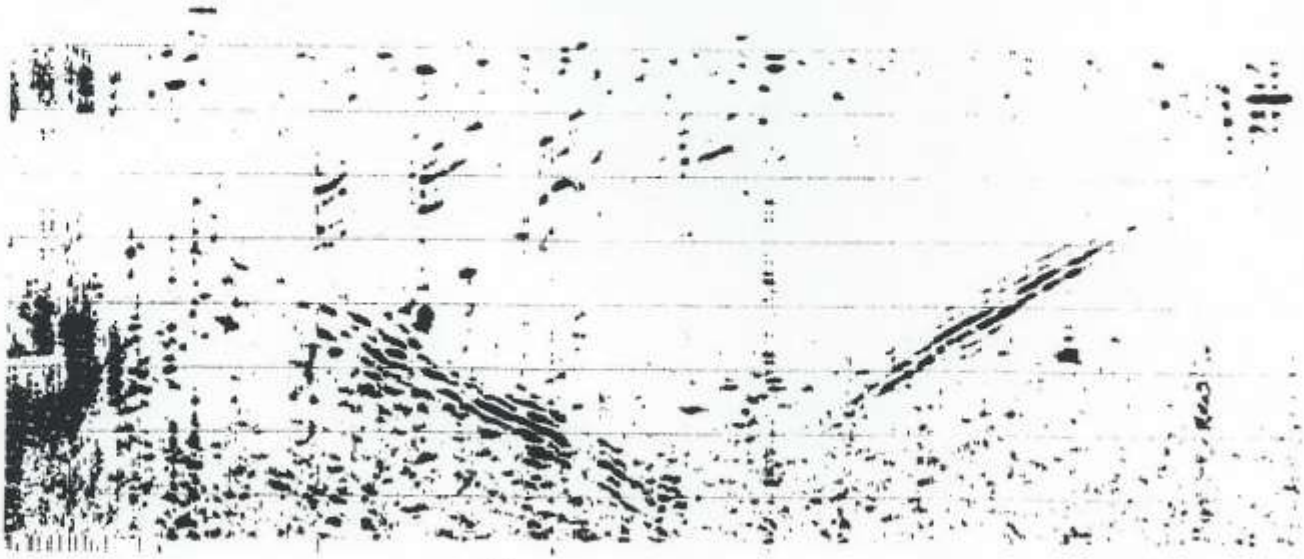

y = -18 m

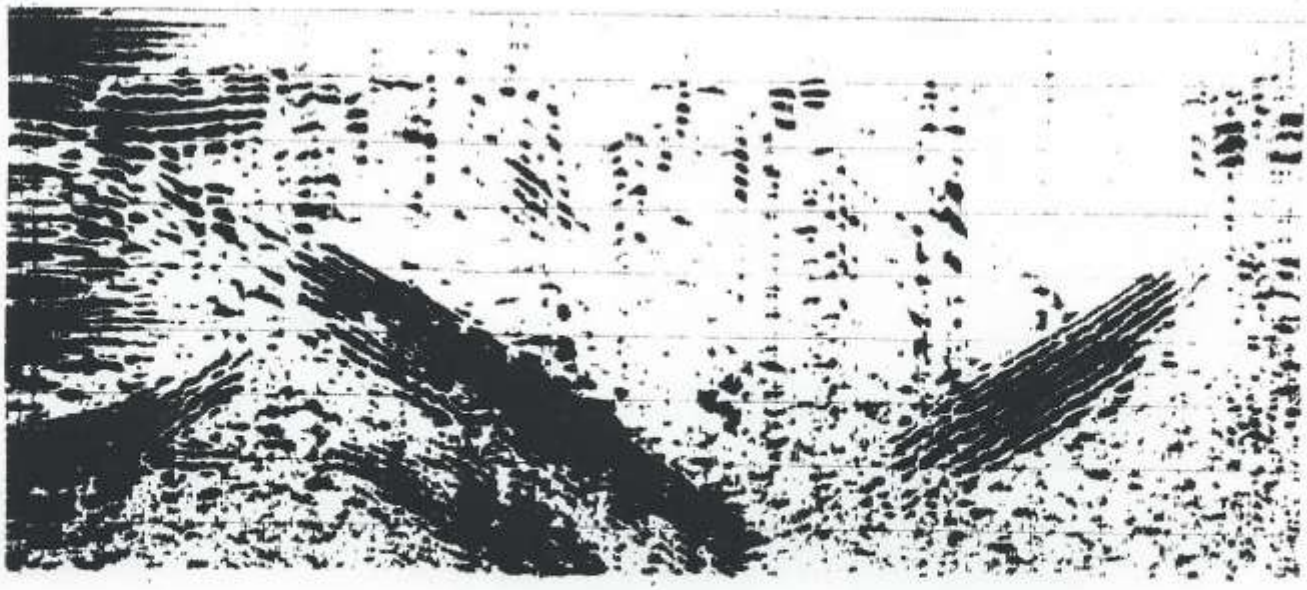

y = -20 m

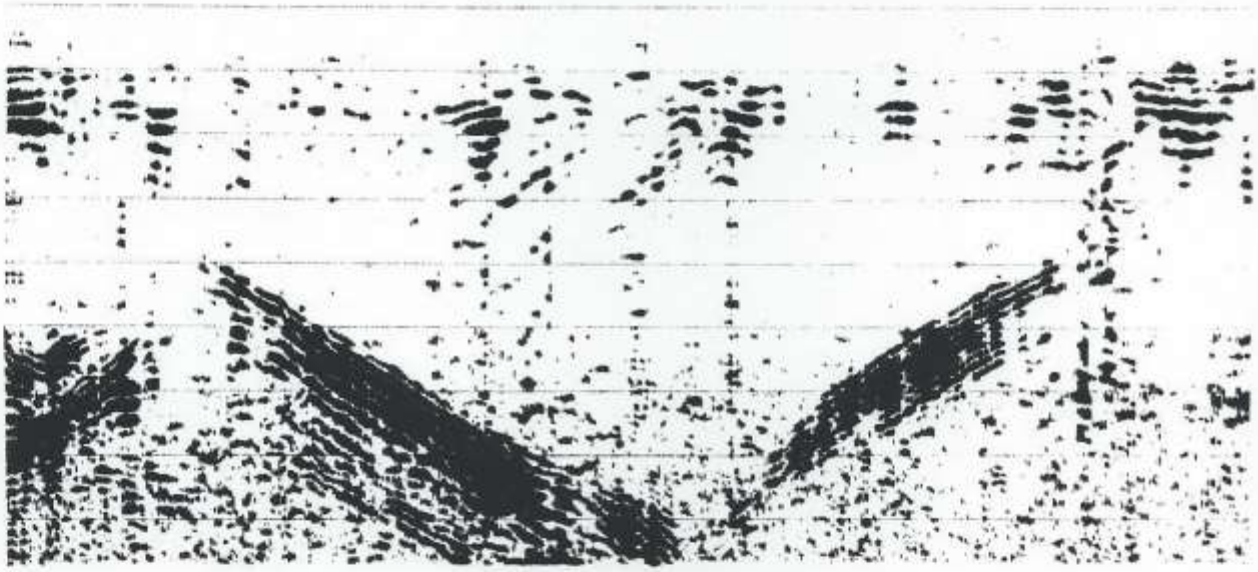

y = -22 m

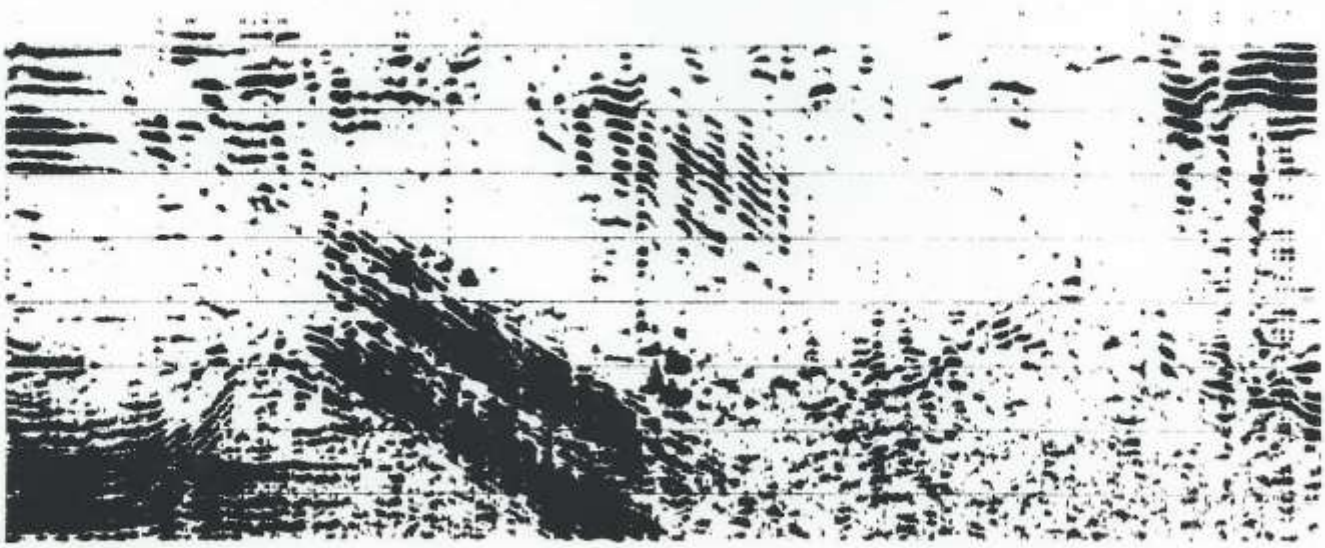

y = -24 m

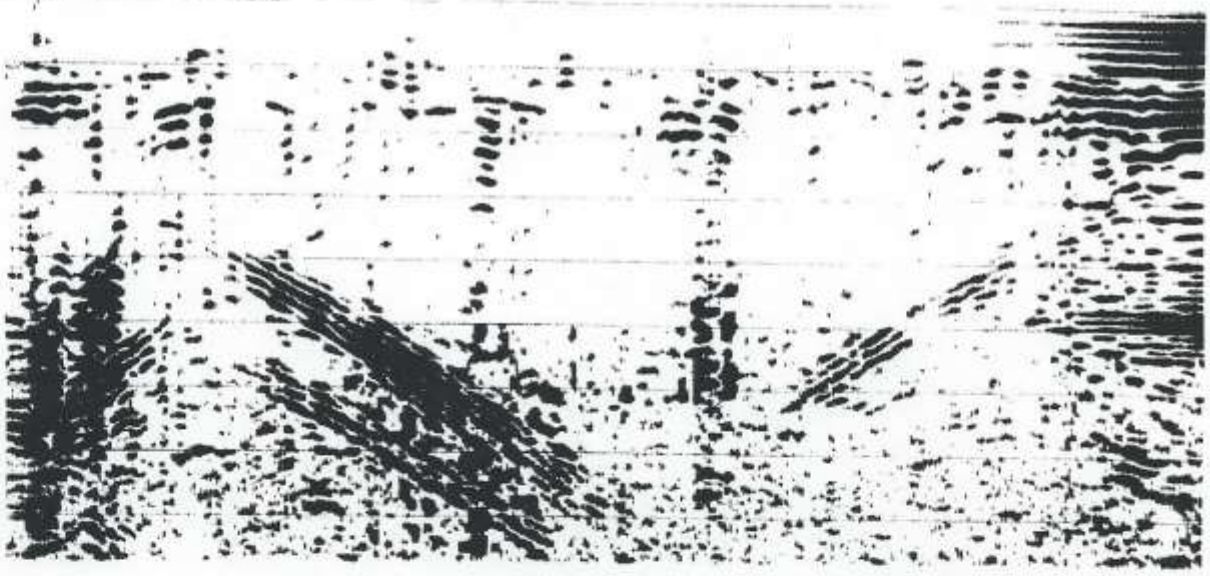

y = -26 m

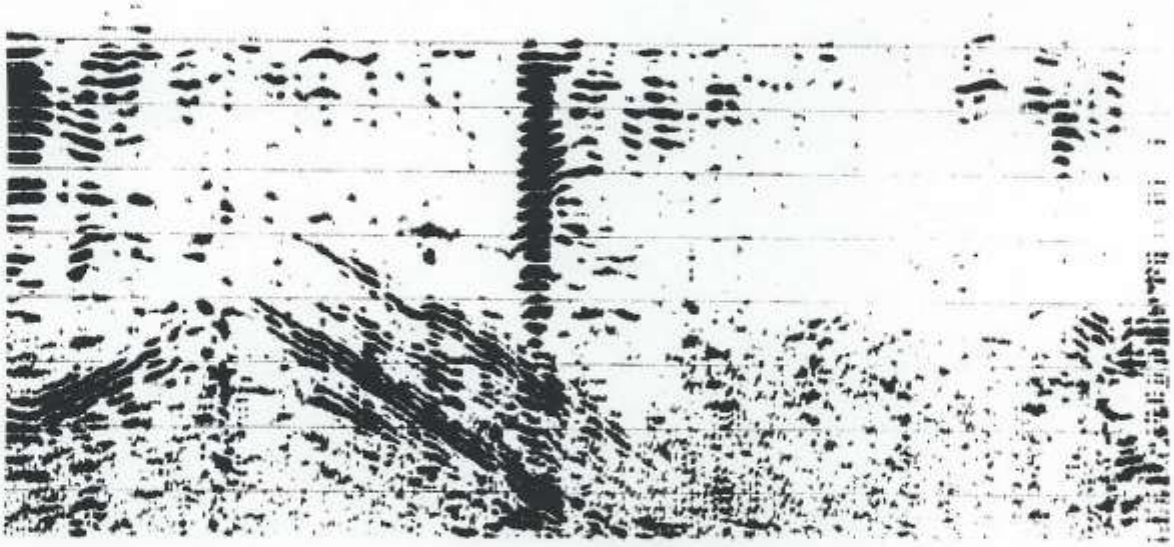

y = -28 m

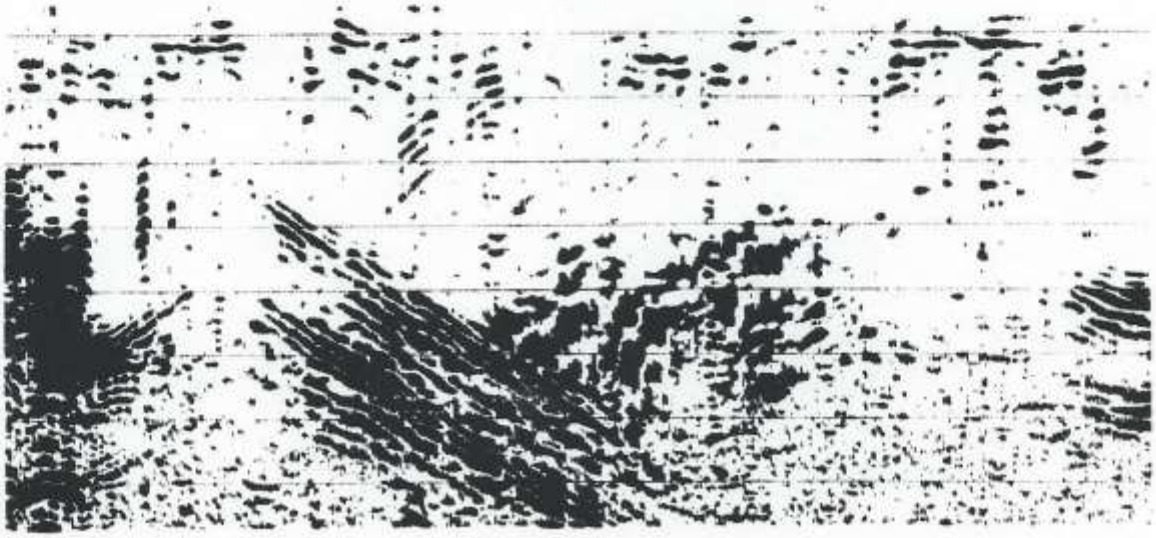

y = -30 m

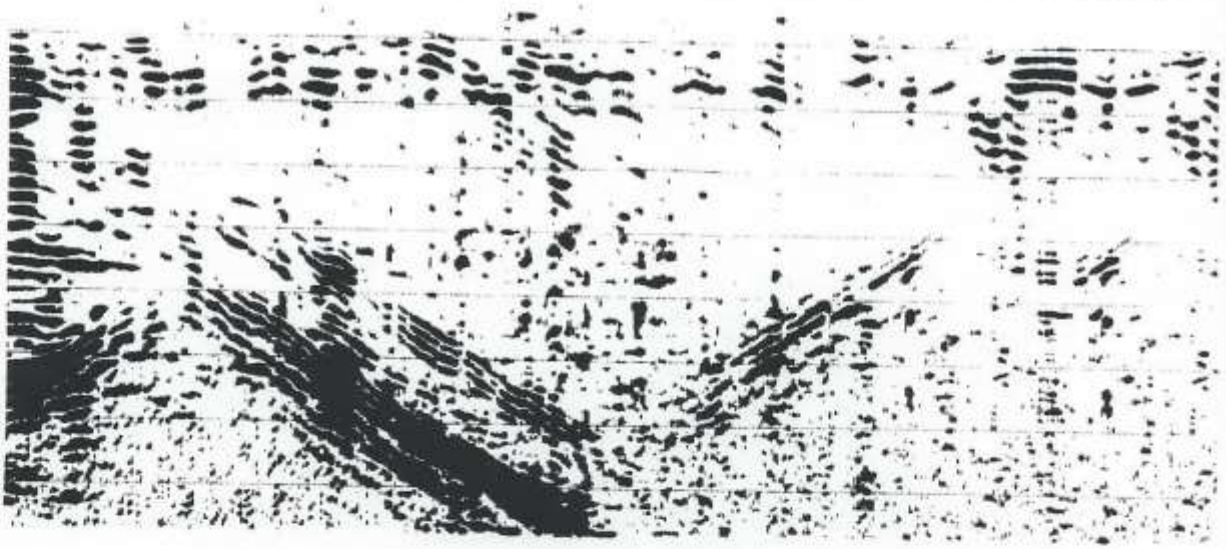

y = -32 m

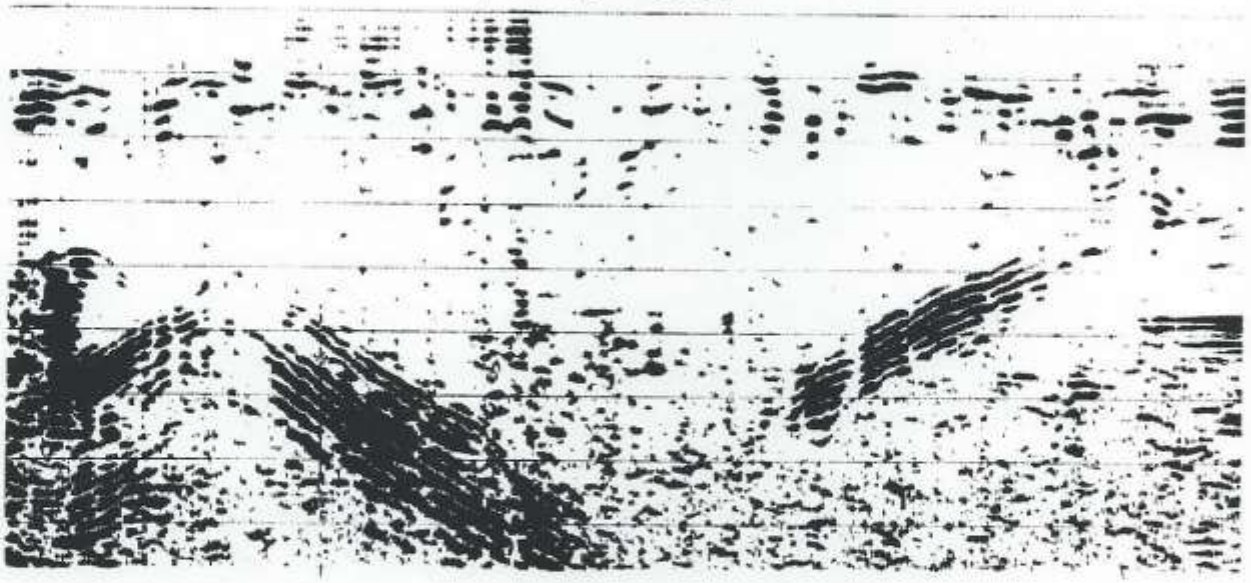

y = -34 m

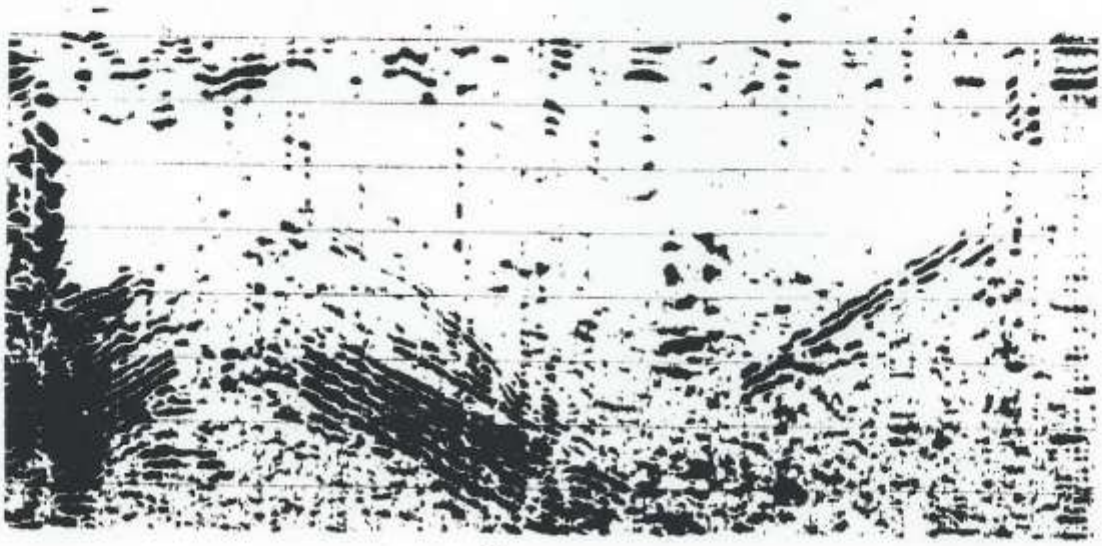

y = -36 m

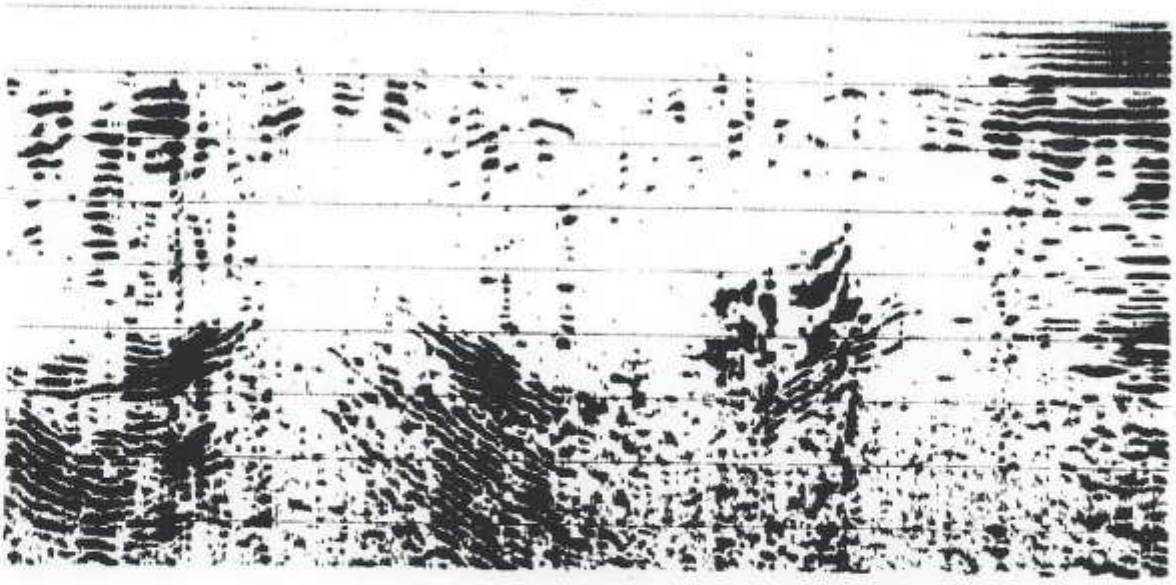

y = -38 m

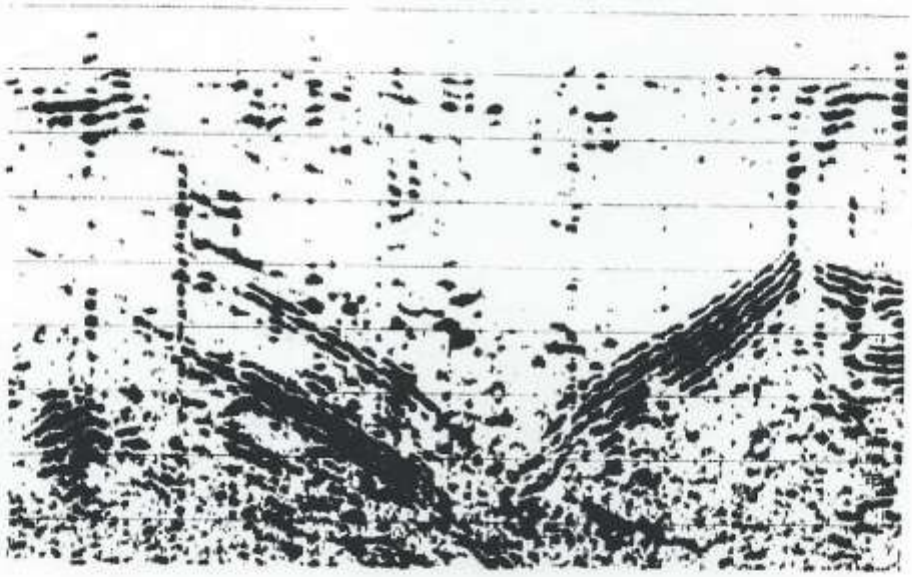

y = -40 m

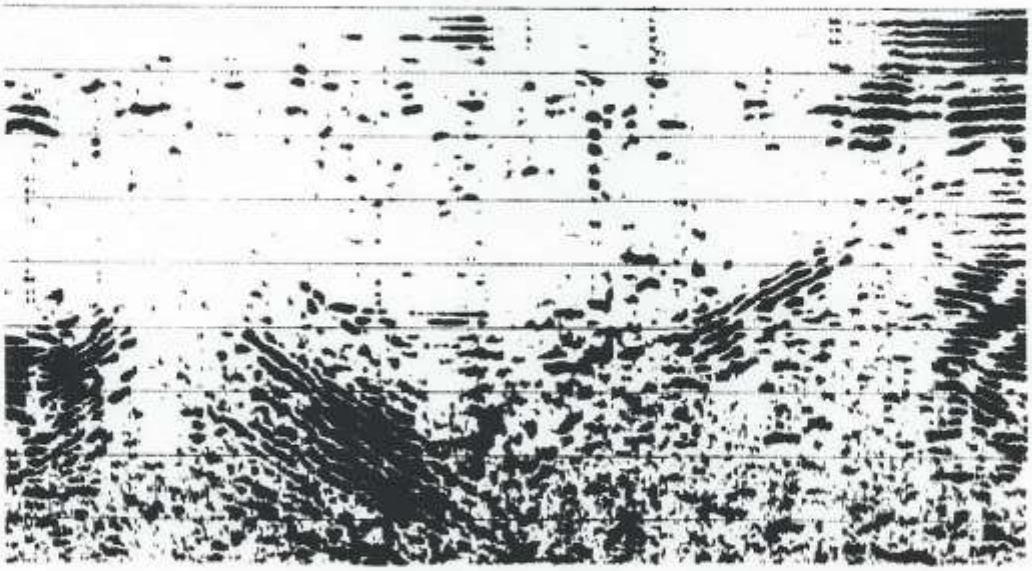

y = -42 m

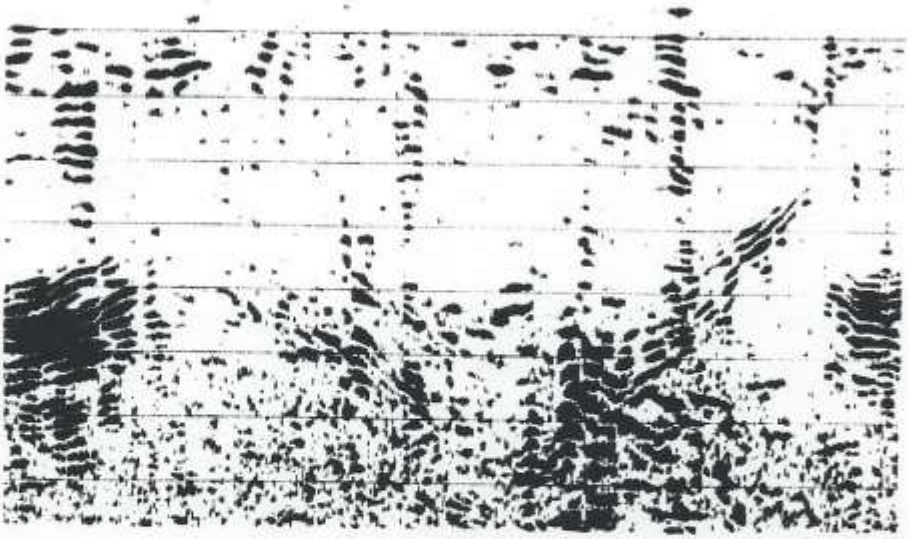

y = -44 m

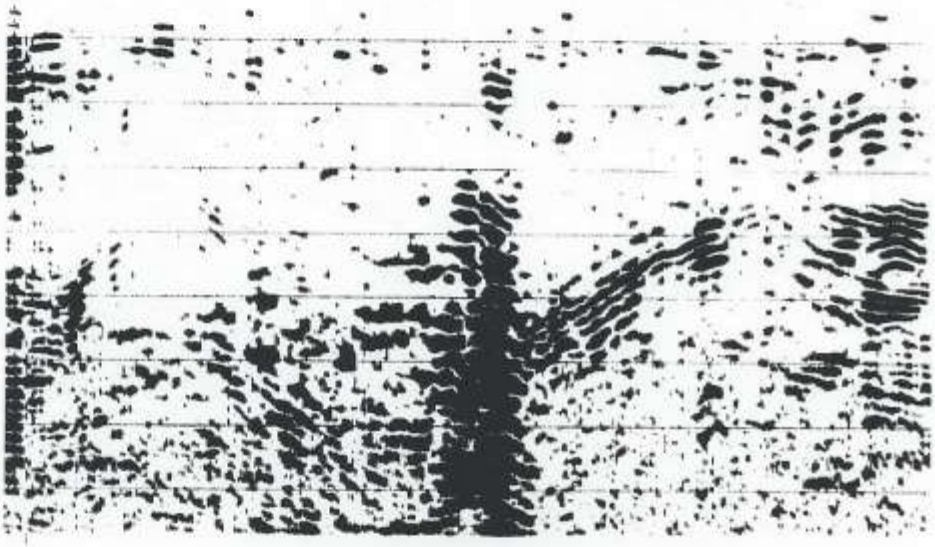

y = -46 m

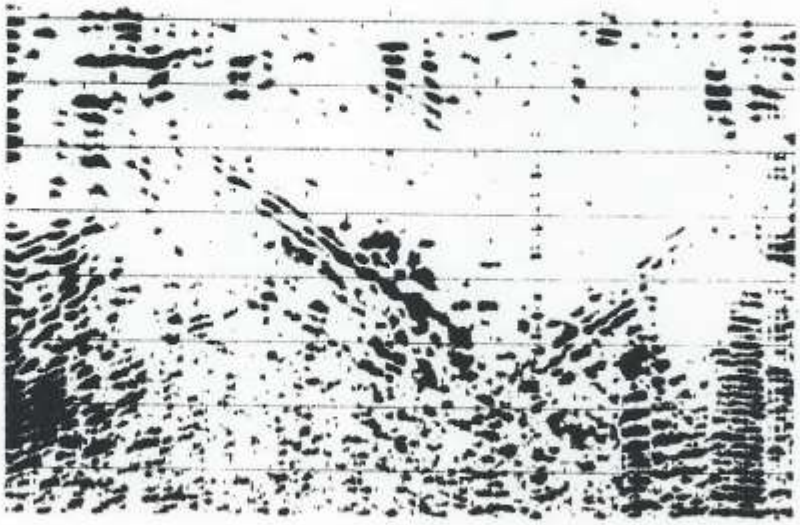

y = -48 m

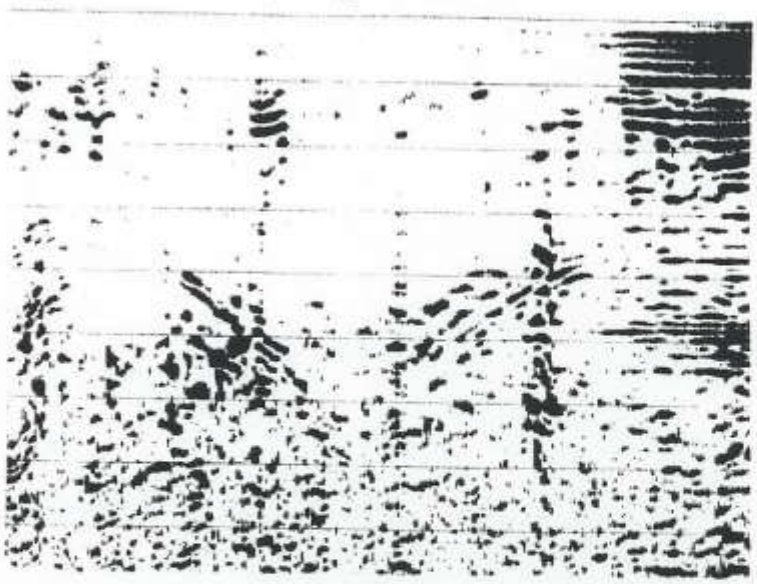

y = -50 m

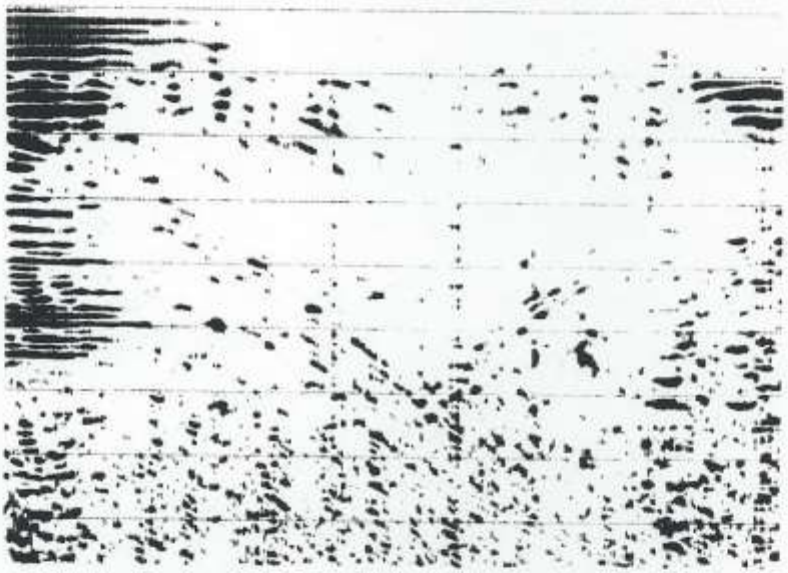

y = -52 m

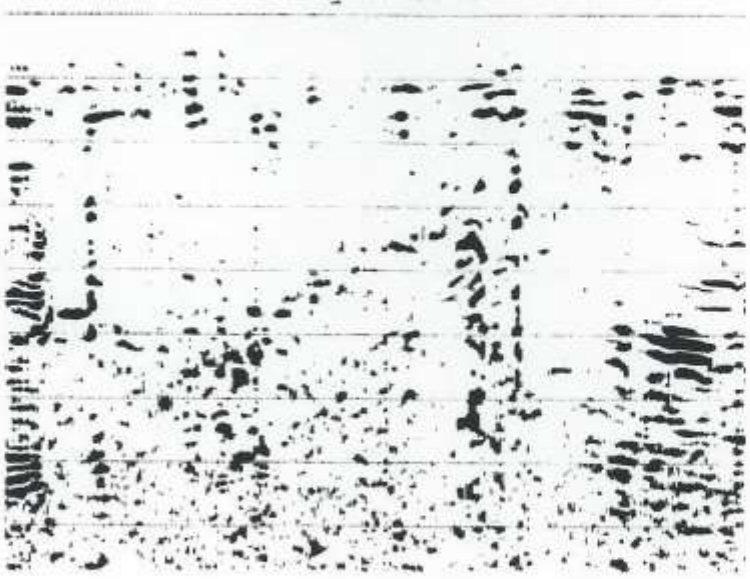

y = -54 m

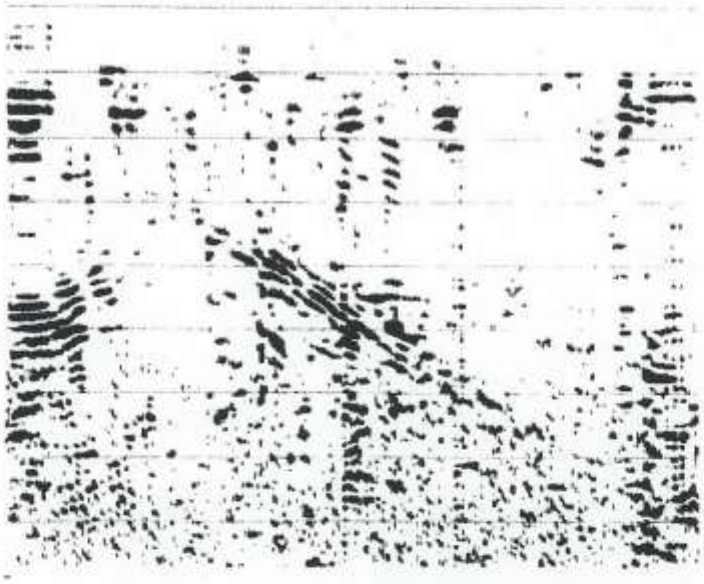

y = -56 m

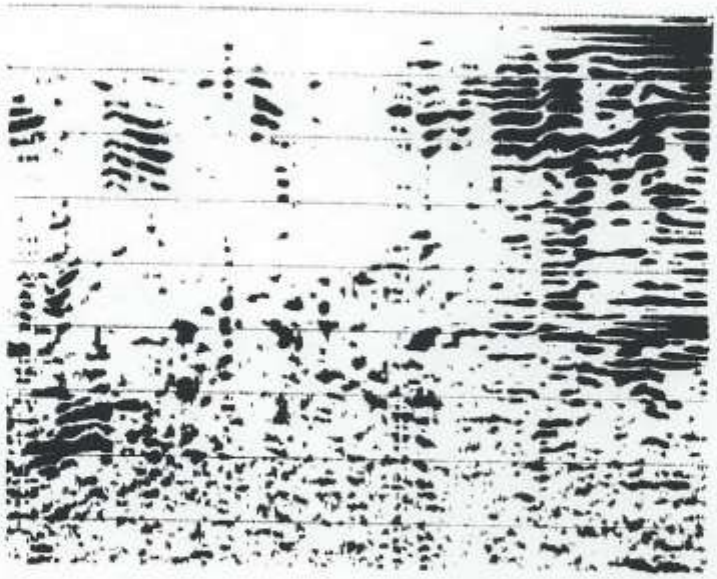

y = -58 m

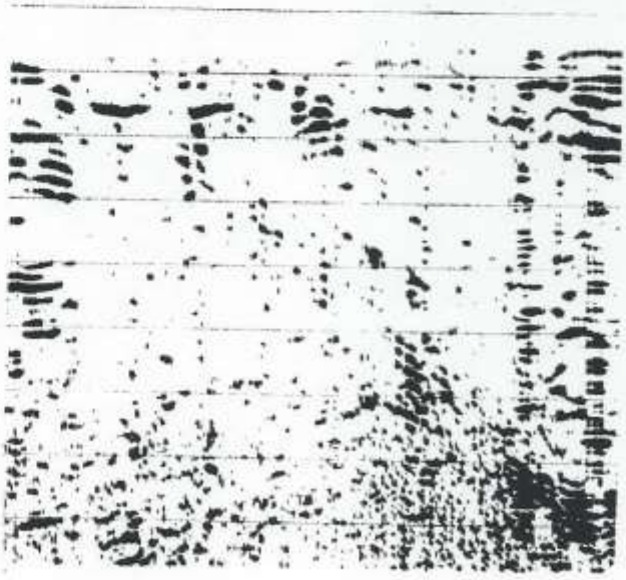

y = -60 m

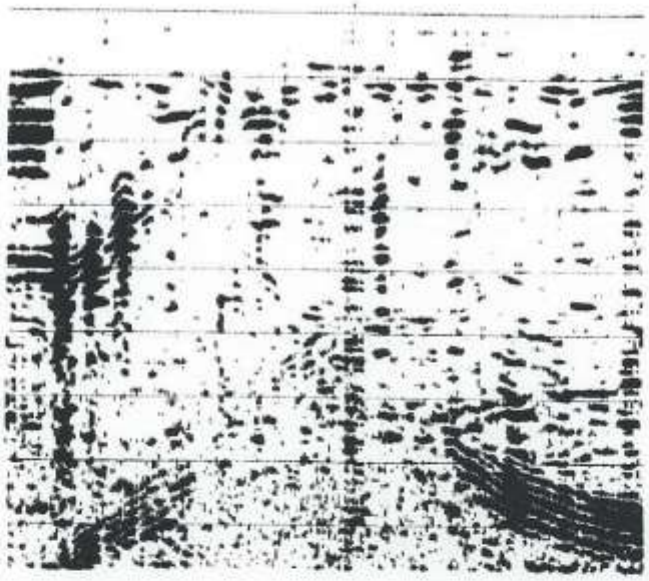

y = -62 m

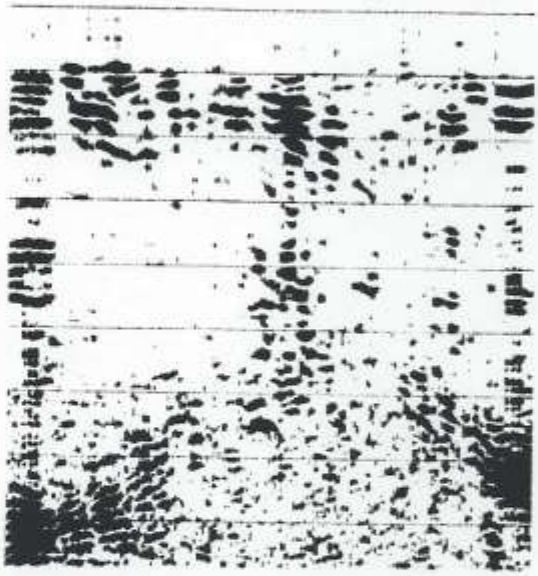

y = -64 m

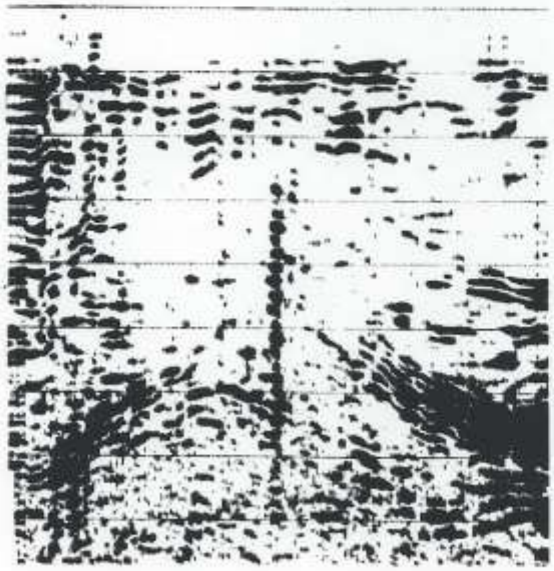


y = −66 m

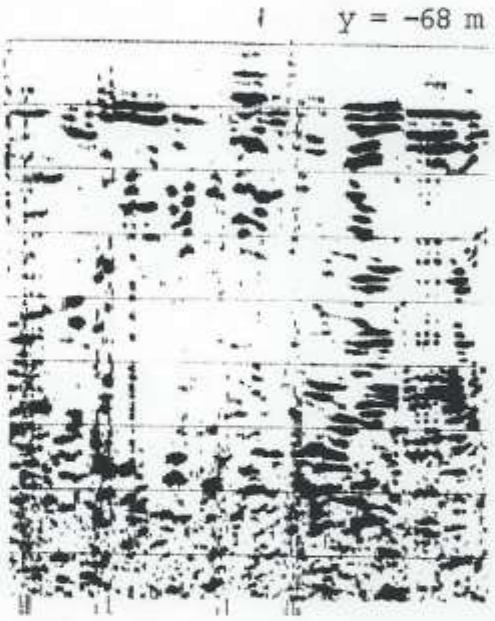
y = −68 m

MAGNETOMETER DATA

Table 1 lists the x-y locations and field values for 1177 measurements of the total magnetic field. These measurements were made on a square grid of points spaced two meters apart. Correction for the temporal variations in the magnetic field was provided for by returning to a base station approximately every 30 minutes to take a reference reading. The linearly interpolated time corrections are also shown in Table 1 together with the corrected field values. The units are nanotesla.

Figure 8 is a contour plot of the variation of the total magnetic field obtained from the corrected field values of Table 1 minus a reference value of 47500 nanotestas. The most noticeable feature in Figure 8 is a strong anomaly centered at approximately x=14 m, y=7 m. The good correlation between the location of this anomaly and the rock outcrop suggest a close relationship. The simplest interpretation is that the calc-schist rock has a lower magnetic mineral content than the surrounding soil resulting in a reduced value for the observed field in the vicinity of the outcropping rock. This interpretation implies that the rock unit is limited in its lateral extent, since the anomaly covers a relatively small area, but suggests that the rock unit has considerable vertical extent because of the large amplitude (~400 nanotestas). Core drilling can provide definitive answers to the questions as to the extent of this rock unit and its relationship to the rest of the structure.

A second anomaly of similar character but of smaller amplitude is centered at x=-6 m, y=-10 m. There is also an outcrop of the calc-schist rock near this position on the site. This second instance of correlation between the outcrop of low magnetic mineral content rock and a local minimum in the observed magnetic field provides strong support for the conclusion that both features in the magnetic field pattern denote the presence of bodies of the calc-schist rock.

A final observation from Figure 8 is the almost steplike change in the magnetic field amplitude by approximately 100 nanotestas at a y-position of -20 m. We offer no explanation for this feature except for the possibility of a change in the rock type of the basement rocks beneath the site.

In conclusion we emphasize again the benefits of core drilling to provide the ability to make definitive interpretations from these data.

Table 1 Coordinates, magnetic field readings, temporal corrections, and corrected field values for the Noah's Ark site. Units are meters and nanotestas.

x	y	meas. field	corr.	corr. field
0.0	80.0	47479.0	24.0	47455.0
0.0	78.0	47463.6	24.0	47439.6
0.0	76.0	47450.1	24.0	47426.1
0.0	74.0	47449.7	24.1	47425.6
0.0	72.0	47451.2	24.1	47427.1
0.0	70.0	47468.6	24.1	47444.5
0.0	68.0	47485.5	24.1	47461.4
0.0	66.0	47486.5	24.2	47462.3
0.0	64.0	47489.5	24.2	47465.3
0.0	62.0	47499.9	24.2	47475.7
0.0	60.0	47520.5	24.2	47496.3
0.0	58.0	47554.5	24.3	47530.2
0.0	56.0	47577.3	24.3	47553.0
0.0	54.0	47590.6	24.3	47566.3
0.0	52.0	47583.2	24.3	47558.9
0.0	50.0	47570.7	24.4	47546.3
0.0	48.0	47569.2	24.4	47544.8
0.0	46.0	47574.4	24.4	47550.0
0.0	44.0	47588.8	24.4	47564.4
0.0	42.0	47606.2	24.5	47581.7
0.0	40.0	47604.4	24.5	47579.9
0.0	38.0	47594.3	24.5	47569.8
0.0	36.0	47589.5	24.5	47565.0
0.0	34.0	47587.7	24.6	47563.1
0.0	32.0	47587.6	24.6	47563.0
0.0	30.0	47572.2	24.6	47547.6
0.0	28.0	47564.0	24.6	47539.4
0.0	26.0	47567.0	24.7	47542.3
0.0	24.0	47574.4	24.7	47549.7
0.0	22.0	47588.8	24.7	47564.1
0.0	20.0	47601.3	24.7	47576.6
0.0	18.0	47609.3	24.8	47584.5
0.0	16.0	47617.0	24.8	47592.2
0.0	14.0	47618.8	24.8	47594.0
0.0	12.0	47610.0	24.8	47585.2
0.0	10.0	47608.7	24.8	47583.9
0.0	8.0	47597.9	24.9	47573.0
0.0	6.0	47606.7	24.9	47581.8
0.0	4.0	47614.5	24.9	47589.6
0.0	2.0	47618.2	24.9	47593.3
0.0	0.0	47613.1	24.9	47588.2
0.0	-2.0	47591.1	24.9	47566.2
0.0	-4.0	47606.4	25.0	47581.4
0.0	-6.0	47648.7	25.0	47623.7
0.0	-8.0	47603.0	25.0	47578.0
0.0	-10.0	47559.6	25.0	47534.6
0.0	-12.0	47558.9	25.0	47533.9
0.0	-14.0	47596.1	25.1	47571.0
0.0	-16.0	47645.1	25.1	47620.0
0.0	-18.0	47705.1	25.1	47680.0
0.0	-20.0	47742.1	25.1	47717.0
0.0	-22.0	47739.9	25.1	47714.8
0.0	-24.0	47735.2	25.2	47710.0
0.0	-26.0	47734.0	25.2	47708.8
0.0	-28.0	47732.6	25.2	47707.4
0.0	-30.0	47728.3	25.2	47703.1
0.0	-32.0	47724.3	25.2	47699.1
0.0	-34.0	47722.7	25.3	47697.4
0.0	-36.0	47725.6	25.3	47700.3
0.0	-38.0	47727.4	25.3	47702.1
0.0	-40.0	47725.7	25.3	47700.4
0.0	-42.0	47728.5	25.3	47703.2
0.0	-44.0	47732.0	25.3	47706.7
0.0	-46.0	47735.1	25.4	47709.7
0.0	-48.0	47733.9	25.4	47708.5
0.0	-50.0	47728.6	25.4	47703.2
0.0	-52.0	47723.7	25.4	47698.3
0.0	-54.0	47715.9	25.4	47690.5
0.0	-56.0	47705.1	25.5	47679.6
0.0	-58.0	47688.2	25.5	47662.7
0.0	-60.0	47664.0	25.5	47638.5
0.0	-62.0	47651.5	25.5	47626.0
0.0	-64.0	47648.4	25.5	47622.9
0.0	-66.0	47642.7	25.6	47617.1
0.0	-68.0	47626.5	25.6	47600.9
-2.0	-68.0	47630.4	25.6	47604.8
-2.0	-66.0	47637.3	25.6	47611.7
-2.0	-64.0	47640.8	25.6	47615.2
-2.0	-62.0	47643.4	25.6	47617.7
-2.0	-60.0	47660.5	25.7	47634.8

x	y	meas. field	corr.	corr. field
-2.0	-58.0	47687.3	25.7	47661.6
-2.0	-56.0	47704.9	25.7	47679.2
-2.0	-54.0	47718.2	25.7	47692.5
-2.0	-52.0	47727.2	25.7	47701.5
-2.0	-50.0	47733.7	25.8	47707.9
-2.0	-48.0	47734.2	25.8	47708.4
-2.0	-46.0	47731.5	25.8	47705.7
-2.0	-44.0	47727.8	25.8	47702.0
-2.0	-42.0	47729.1	25.8	47703.3
-2.0	-40.0	47732.3	25.9	47706.4
-2.0	-38.0	47732.4	25.9	47706.5
-2.0	-36.0	47729.5	25.9	47703.6
-2.0	-34.0	47724.7	25.9	47698.8
-2.0	-32.0	47723.3	25.9	47697.4
-2.0	-30.0	47732.4	26.0	47706.4
-2.0	-28.0	47735.2	26.0	47709.2
-2.0	-26.0	47733.4	26.0	47707.4
-2.0	-24.0	47734.2	26.0	47708.2
-2.0	-22.0	47745.2	26.0	47719.2
-2.0	-20.0	47740.3	26.0	47714.3
-2.0	-18.0	47690.5	26.1	47664.4
-2.0	-16.0	47637.2	26.1	47611.1
-2.0	-14.0	47576.5	26.1	47550.4
-2.0	-12.0	47540.5	26.1	47514.4
-2.0	-10.0	47539.5	26.1	47513.4
-2.0	-8.0	47584.8	26.2	47558.6
-2.0	-6.0	47669.8	26.2	47643.6
-2.0	-4.0	47662.7	26.2	47636.5
-2.0	-2.0	47615.2	26.2	47589.0
-2.0	0.0	47599.8	26.2	47573.6
-2.0	2.0	47594.1	26.3	47567.8
-2.0	4.0	47583.9	26.3	47557.6
-2.0	6.0	47586.9	26.3	47560.6
-2.0	8.0	47585.9	26.3	47559.6
-2.0	10.0	47590.1	26.3	47563.8
-2.0	12.0	47598.1	26.4	47571.7
-2.0	14.0	47612.2	26.4	47585.8
-2.0	16.0	47612.1	26.4	47585.7
-2.0	18.0	47606.8	26.4	47580.4
-2.0	20.0	47600.9	26.4	47574.5
-2.0	22.0	47593.2	26.4	47566.8
-2.0	24.0	47587.1	26.5	47560.6
-2.0	26.0	47579.8	26.5	47553.3
-2.0	28.0	47578.6	26.5	47552.1
-2.0	30.0	47582.3	26.4	47555.9
-2.0	32.0	47586.8	26.4	47560.4
-2.0	34.0	47586.6	26.4	47560.2
-2.0	36.0	47584.5	26.4	47558.1
-2.0	38.0	47586.5	26.4	47560.1
-2.0	40.0	47633.3	26.4	47606.9
-2.0	42.0	47609.8	26.3	47583.5
-2.0	44.0	47587.5	26.3	47561.2
-2.0	46.0	47580.4	26.3	47554.1
-2.0	48.0	47582.7	26.3	47556.4
-2.0	50.0	47585.4	26.3	47559.1
-2.0	52.0	47593.7	26.2	47567.5
-2.0	54.0	47602.0	26.2	47575.8
-2.0	56.0	47594.8	26.2	47568.6
-2.0	58.0	47566.6	26.2	47540.4
-2.0	60.0	47540.4	26.2	47514.2
-2.0	62.0	47522.1	26.2	47495.9
-2.0	64.0	47504.8	26.1	47478.7
-2.0	66.0	47499.5	26.1	47473.4
-2.0	68.0	47499.7	26.1	47473.6
-2.0	70.0	47491.7	26.1	47465.6
-2.0	72.0	47480.8	26.1	47454.7
-2.0	74.0	47472.2	26.1	47446.2
-2.0	76.0	47473.9	26.0	47447.9
-2.0	78.0	47486.8	26.0	47460.8
-2.0	80.0	47501.1	26.0	47475.1
-4.0	80.0	47514.1	26.0	47488.1
-4.0	78.0	47516.1	26.0	47490.1
-4.0	76.0	47508.7	25.9	47482.8
-4.0	74.0	47509.2	25.9	47483.3
-4.0	72.0	47519.7	25.9	47493.8
-4.0	70.0	47516.8	25.9	47490.9
-4.0	68.0	47515.3	25.9	47489.4
-4.0	66.0	47513.1	25.9	47487.2
-4.0	64.0	47526.0	25.8	47500.2
-4.0	62.0	47545.1	25.8	47519.3

x	y	meas. field	corr.	corr. field
-4.0	60.0	47566.4	25.8	47540.6
-4.0	58.0	47596.4	25.8	47570.6
-4.0	56.0	47613.9	25.8	47588.1
-4.0	54.0	47612.8	25.7	47587.1
-4.0	52.0	47604.0	25.7	47578.3
-4.0	50.0	47598.9	25.7	47573.2
-4.0	48.0	47592.9	25.7	47567.2
-4.0	46.0	47593.8	25.7	47568.1
-4.0	44.0	47593.3	25.7	47567.6
-4.0	42.0	47599.0	25.6	47573.4
-4.0	40.0	47602.3	25.6	47576.7
-4.0	38.0	47573.3	25.6	47547.7
-4.0	36.0	47578.7	25.6	47553.1
-4.0	34.0	47591.6	25.6	47566.0
-4.0	32.0	47599.3	25.5	47573.8
-4.0	30.0	47595.5	25.5	47570.0
-4.0	28.0	47592.8	25.5	47567.3
-4.0	26.0	47592.1	25.5	47566.6
-4.0	24.0	47597.8	25.5	47572.3
-4.0	22.0	47600.7	25.5	47575.2
-4.0	20.0	47603.2	25.4	47577.8
-4.0	18.0	47606.5	25.4	47581.1
-4.0	16.0	47611.6	25.4	47586.2
-4.0	14.0	47595.7	25.4	47570.3
-4.0	12.0	47578.0	25.3	47552.7
-4.0	10.0	47577.6	25.3	47552.3
-4.0	8.0	47581.1	25.3	47555.8
-4.0	6.0	47571.5	25.3	47546.2
-4.0	4.0	47566.2	25.2	47541.0
-4.0	2.0	47593.0	25.2	47567.8
-4.0	0.0	47622.7	25.2	47597.5
-4.0	-2.0	47661.8	25.2	47636.6
-4.0	-4.0	47687.0	25.1	47661.9
-4.0	-6.0	47649.2	25.1	47624.1
-4.0	-8.0	47573.1	25.1	47548.0
-4.0	-10.0	47526.9	25.1	47501.8
-4.0	-12.0	47545.3	25.0	47520.3
-4.0	-14.0	47594.5	25.0	47569.5
-4.0	-16.0	47639.7	25.0	47614.7
-4.0	-18.0	47694.7	25.0	47669.7
-4.0	-20.0	47733.9	24.9	47709.0
-4.0	-22.0	47746.5	24.9	47721.6
-4.0	-24.0	47736.2	24.9	47711.3
-4.0	-26.0	47736.1	24.9	47711.3
-4.0	-28.0	47741.6	24.8	47716.8
-4.0	-30.0	47732.6	24.8	47707.8
-4.0	-32.0	47728.0	24.8	47703.2
-4.0	-34.0	47732.0	24.7	47707.3
-4.0	-36.0	47737.8	24.7	47713.1
-4.0	-38.0	47742.5	24.7	47717.8
-4.0	-40.0	47742.6	24.7	47717.9
-4.0	-42.0	47736.8	24.6	47712.2
-4.0	-44.0	47733.0	24.6	47708.4
-4.0	-46.0	47738.3	24.6	47713.7
-4.0	-48.0	47743.5	24.6	47718.9
-4.0	-50.0	47743.1	24.5	47718.6
-4.0	-52.0	47741.0	24.5	47716.5
-4.0	-54.0	47716.6	24.5	47692.1
-4.0	-56.0	47703.4	24.5	47678.9
-4.0	-58.0	47678.5	24.4	47654.1
-4.0	-60.0	47658.5	24.4	47634.1
-4.0	-62.0	47650.7	24.4	47626.3
-4.0	-64.0	47638.4	24.4	47614.0
-4.0	-66.0	47628.4	24.3	47604.1
-4.0	-68.0	47619.4	24.3	47595.1
-6.0	-64.0	47631.5	24.3	47607.2
-6.0	-62.0	47652.3	24.3	47628.0
-6.0	-60.0	47658.3	24.2	47634.1
-6.0	-58.0	47673.1	24.2	47648.9
-6.0	-56.0	47701.3	24.2	47677.1
-6.0	-54.0	47722.9	24.1	47698.8
-6.0	-52.0	47734.0	24.1	47709.9
-6.0	-50.0	47744.7	24.1	47720.6
-6.0	-48.0	47745.8	24.1	47721.7
-6.0	-46.0	47741.2	24.0	47717.2
-6.0	-44.0	47735.8	24.0	47711.8
-6.0	-42.0	47738.6	24.0	47714.6
-6.0	-40.0	47740.8	24.0	47716.8
-6.0	-38.0	47739.4	23.9	47715.5
-6.0	-36.0	47734.8	23.9	47710.9

x	y	meas. field	corr.	corr. field
-6.0	-34.0	47723.6	23.9	47699.7
-6.0	-32.0	47719.8	23.9	47695.9
-6.0	-30.0	47727.6	23.8	47703.8
-6.0	-28.0	47728.4	23.8	47704.6
-6.0	-26.0	47725.0	23.8	47701.2
-6.0	-24.0	47721.4	23.8	47697.6
-6.0	-22.0	47720.6	23.7	47696.9
-6.0	-20.0	47710.9	23.7	47687.2
-6.0	-18.0	47659.0	23.7	47635.3
-6.0	-16.0	47626.1	23.7	47602.4
-6.0	-14.0	47586.8	23.6	47563.2
-6.0	-12.0	47544.5	23.6	47520.9
-6.0	-10.0	47520.7	23.6	47497.1
-6.0	-8.0	47568.3	23.6	47544.8
-6.0	-6.0	47663.7	23.5	47640.2
-6.0	-4.0	47698.0	23.5	47674.5
-6.0	-2.0	47675.4	23.5	47651.9
-6.0	0.0	47646.0	23.4	47622.6
-6.0	2.0	47601.6	23.4	47578.2
-6.0	4.0	47570.7	23.4	47547.3
-6.0	6.0	47566.7	23.4	47543.3
-6.0	8.0	47566.0	23.3	47542.7
-6.0	10.0	47563.3	23.3	47540.0
-6.0	12.0	47557.8	23.3	47534.5
-6.0	14.0	47558.9	23.3	47535.6
-6.0	16.0	47571.8	23.2	47548.6
-6.0	18.0	47583.8	23.2	47560.6
-6.0	20.0	47594.0	23.2	47570.8
-6.0	22.0	47601.3	23.2	47578.1
-6.0	24.0	47602.0	23.1	47578.9
-6.0	26.0	47595.0	23.1	47571.9
-6.0	28.0	47590.8	23.1	47567.7
-6.0	30.0	47589.4	23.1	47566.3
-6.0	32.0	47587.2	23.1	47564.1
-6.0	34.0	47580.7	23.0	47557.7
-6.0	36.0	47572.6	23.0	47549.6
-6.0	38.0	47573.2	23.0	47550.2
-6.0	40.0	47575.9	23.0	47552.9
-6.0	42.0	47581.3	23.0	47558.3
-6.0	44.0	47588.5	23.0	47565.5
-6.0	46.0	47591.8	23.0	47568.8
-6.0	48.0	47593.5	23.0	47570.5
-6.0	50.0	47599.1	22.9	47576.2
-6.0	52.0	47603.4	22.9	47580.5
-6.0	54.0	47612.1	22.9	47589.2
-6.0	56.0	47616.5	22.9	47593.6
-6.0	58.0	47597.7	22.9	47574.8
-6.0	60.0	47574.4	22.9	47551.5
-6.0	62.0	47553.5	22.9	47530.6
-6.0	64.0	47531.2	22.9	47508.3
-6.0	66.0	47520.4	22.8	47497.6
-6.0	68.0	47524.0	22.8	47501.2
-6.0	70.0	47537.3	22.8	47514.5
-6.0	72.0	47546.8	22.8	47524.0
-8.0	72.0	47574.6	22.8	47551.8
-8.0	70.0	47577.0	22.8	47554.2
-8.0	68.0	47569.5	22.8	47546.7
-8.0	66.0	47561.6	22.8	47538.8
-8.0	64.0	47566.9	22.8	47544.1
-8.0	62.0	47578.8	22.7	47556.1
-8.0	60.0	47590.2	22.7	47567.5
-8.0	58.0	47609.8	22.7	47587.1
-8.0	56.0	47626.0	22.7	47603.3
-8.0	54.0	47624.4	22.7	47601.7
-8.0	52.0	47617.8	22.7	47595.1
-8.0	50.0	47612.3	22.7	47589.6
-8.0	48.0	47606.7	22.7	47584.0
-8.0	46.0	47604.8	22.6	47582.2
-8.0	44.0	47602.4	22.6	47579.8
-8.0	42.0	47593.6	22.6	47571.0
-8.0	40.0	47589.8	22.6	47567.2
-8.0	38.0	47587.4	22.6	47564.8
-8.0	36.0	47584.2	22.6	47561.6
-8.0	34.0	47579.7	22.6	47557.1
-8.0	32.0	47580.1	22.6	47557.5
-8.0	30.0	47588.0	22.5	47565.5
-8.0	28.0	47594.8	22.5	47572.3
-8.0	26.0	47607.4	22.5	47584.9
-8.0	24.0	47615.9	22.5	47593.4
-8.0	22.0	47609.4	22.5	47586.9

x	y	meas. field	corr.	corr. field
-8.0	20.0	47591.2	22.5	47568.7
-8.0	18.0	47571.7	22.6	47549.1
-8.0	16.0	47561.2	22.6	47538.6
-8.0	14.0	47560.3	22.6	47537.7
-8.0	12.0	47565.9	22.6	47543.3
-8.0	10.0	47577.8	22.6	47555.2
-8.0	8.0	47589.8	22.7	47567.1
-8.0	6.0	47599.2	22.7	47576.5
-8.0	4.0	47617.5	22.7	47594.8
-8.0	2.0	47642.2	22.7	47619.5
-8.0	0.0	47670.0	22.7	47647.3
-8.0	-2.0	47706.3	22.8	47683.5
-8.0	-4.0	47734.5	22.8	47711.7
-8.0	-6.0	47673.6	22.8	47650.8
-8.0	-8.0	47602.3	22.8	47579.5
-8.0	-10.0	47539.0	22.8	47516.2
-8.0	-12.0	47549.2	22.9	47526.3
-8.0	-14.0	47599.5	22.9	47576.6
-8.0	-16.0	47629.7	22.9	47606.8
-8.0	-18.0	47668.2	22.9	47645.3
-8.0	-20.0	47692.4	22.9	47669.5
-8.0	-22.0	47703.8	23.0	47680.8
-8.0	-24.0	47707.7	23.0	47684.7
-8.0	-26.0	47714.5	23.0	47691.5
-8.0	-28.0	47722.1	23.0	47699.1
-8.0	-30.0	47719.0	23.0	47696.0
-8.0	-32.0	47713.5	23.1	47690.4
-8.0	-34.0	47723.6	23.1	47700.5
-8.0	-36.0	47733.4	23.1	47710.3
-8.0	-38.0	47737.2	23.1	47714.1
-8.0	-40.0	47739.0	23.1	47715.9
-8.0	-42.0	47741.5	23.2	47718.3
-8.0	-44.0	47743.4	23.2	47720.2
-8.0	-46.0	47745.7	23.2	47722.5
-8.0	-48.0	47748.6	23.2	47725.4
-8.0	-50.0	47748.1	23.2	47724.9
-8.0	-52.0	47746.0	23.3	47722.7
-8.0	-54.0	47732.0	23.3	47708.7
-8.0	-56.0	47715.6	23.3	47692.3
-8.0	-58.0	47690.6	23.3	47667.3
-8.0	-60.0	47669.0	23.3	47645.7
-10.0	-60.0	47668.3	23.4	47644.9
-10.0	-58.0	47698.8	23.4	47675.4
-10.0	-56.0	47722.1	23.4	47698.7
-10.0	-54.0	47738.6	23.4	47715.2
-10.0	-52.0	47746.7	23.4	47723.3
-10.0	-50.0	47747.8	23.5	47724.3
-10.0	-48.0	47747.6	23.5	47724.1
-10.0	-46.0	47744.2	23.5	47720.7
-10.0	-44.0	47743.8	23.5	47720.3
-10.0	-42.0	47741.2	23.5	47717.7
-10.0	-40.0	47737.4	23.6	47713.8
-10.0	-38.0	47733.5	23.6	47709.9
-10.0	-36.0	47729.6	23.6	47706.0
-10.0	-34.0	47711.9	23.6	47688.3
-10.0	-32.0	47709.3	23.6	47685.7
-10.0	-30.0	47707.1	23.7	47683.4
-10.0	-28.0	47702.9	23.7	47679.2
-10.0	-26.0	47696.0	23.7	47672.3
-10.0	-24.0	47689.2	23.7	47665.5
-10.0	-22.0	47682.4	23.7	47658.7
-10.0	-20.0	47672.4	23.8	47648.6
-10.0	-18.0	47650.3	23.8	47626.5
-10.0	-16.0	47625.7	23.8	47601.9
-10.0	-14.0	47585.0	23.8	47561.2
-10.0	-12.0	47570.2	23.8	47546.4
-10.0	-10.0	47587.8	23.9	47563.9
-10.0	-8.0	47637.8	23.9	47613.9
-10.0	-6.0	47720.8	23.9	47696.9
-10.0	-4.0	47739.9	23.9	47716.0
-10.0	-2.0	47711.9	23.9	47688.0
-10.0	0.0	47683.9	24.0	47659.9
-10.0	2.0	47658.6	24.0	47634.6
-10.0	4.0	47644.5	24.0	47620.5
-10.0	6.0	47629.0	24.0	47605.0
-10.0	8.0	47613.1	24.0	47589.1
-10.0	10.0	47593.6	24.1	47569.5
-10.0	12.0	47587.3	24.1	47563.2
-10.0	14.0	47586.0	24.1	47561.9
-10.0	16.0	47580.8	24.1	47556.7

x	y	meas. field	corr.	corr. field
-10.0	18.0	47585.3	24.1	47561.2
-10.0	20.0	47599.7	24.2	47575.5
-10.0	22.0	47620.4	24.2	47596.2
-10.0	24.0	47625.5	24.2	47601.3
-10.0	26.0	47610.5	24.2	47586.3
-10.0	28.0	47597.6	24.2	47573.4
-10.0	30.0	47586.6	24.2	47562.4
-10.0	32.0	47582.8	24.2	47558.6
-10.0	34.0	47599.1	24.2	47574.9
-10.0	36.0	47607.5	24.2	47583.3
-10.0	38.0	47611.6	24.3	47587.3
-10.0	40.0	47610.8	24.3	47586.5
-10.0	42.0	47612.3	24.3	47588.0
-10.0	44.0	47613.3	24.3	47589.0
-10.0	46.0	47614.9	24.3	47590.6
-10.0	48.0	47615.6	24.3	47591.3
-10.0	50.0	47622.5	24.3	47598.2
-10.0	52.0	47626.2	24.3	47601.9
-10.0	54.0	47632.6	24.3	47608.3
-10.0	56.0	47632.9	24.3	47608.6
-10.0	58.0	47621.1	24.3	47596.8
-10.0	60.0	47613.2	24.3	47588.9
-10.0	62.0	47613.3	24.4	47588.9
-10.0	64.0	47613.9	24.4	47589.5
-10.0	66.0	47608.3	24.4	47583.9
-10.0	68.0	47596.5	24.4	47572.1
-12.0	60.0	47641.3	24.4	47616.9
-12.0	58.0	47646.2	24.4	47621.8
-12.0	56.0	47658.3	24.4	47633.9
-12.0	54.0	47662.3	24.4	47637.9
-12.0	52.0	47650.5	24.4	47626.1
-12.0	50.0	47646.2	24.4	47621.8
-12.0	48.0	47639.6	24.4	47615.2
-12.0	46.0	47632.1	24.4	47607.7
-12.0	44.0	47635.9	24.4	47611.5
-12.0	42.0	47636.6	24.5	47612.1
-12.0	40.0	47636.6	24.5	47612.1
-12.0	38.0	47641.6	24.5	47617.1
-12.0	36.0	47646.9	24.5	47622.4
-12.0	34.0	47639.6	24.5	47615.1
-12.0	32.0	47626.8	24.5	47602.3
-12.0	30.0	47612.8	24.5	47588.3
-12.0	28.0	47600.9	24.5	47576.4
-12.0	26.0	47613.8	24.5	47589.3
-12.0	24.0	47629.7	24.5	47605.2
-12.0	22.0	47634.3	24.5	47609.8
-12.0	20.0	47623.1	24.5	47598.6
-12.0	18.0	47613.1	24.5	47588.6
-12.0	16.0	47614.9	24.5	47590.4
-12.0	14.0	47619.6	24.4	47595.2
-12.0	12.0	47618.7	24.4	47594.3
-12.0	10.0	47623.2	24.4	47598.8
-12.0	8.0	47637.6	24.4	47613.2
-12.0	6.0	47657.0	24.4	47632.6
-12.0	4.0	47673.9	24.4	47649.5
-12.0	2.0	47685.9	24.4	47661.5
-12.0	0.0	47700.0	24.4	47675.6
-12.0	-2.0	47728.1	24.4	47703.7
-12.0	-4.0	47750.4	24.4	47726.0
-12.0	-6.0	47739.3	24.4	47714.9
-12.0	-8.0	47672.0	24.4	47647.6
-12.0	-10.0	47616.2	24.3	47591.9
-12.0	-12.0	47600.4	24.3	47576.1
-12.0	-14.0	47613.4	24.3	47589.1
-12.0	-16.0	47634.0	24.3	47609.7
-12.0	-18.0	47662.1	24.3	47637.8
-12.0	-20.0	47673.5	24.3	47649.2
-12.0	-22.0	47683.5	24.3	47659.2
-12.0	-24.0	47691.5	24.3	47667.2
-12.0	-26.0	47703.6	24.3	47679.3
-12.0	-28.0	47708.0	24.3	47683.7
-12.0	-30.0	47717.8	24.3	47693.5
-12.0	-32.0	47721.1	24.3	47696.8
-12.0	-34.0	47724.2	24.3	47699.9
-12.0	-36.0	47732.6	24.2	47708.4
-12.0	-38.0	47746.4	24.2	47722.2
-12.0	-40.0	47751.5	24.2	47727.3
-12.0	-42.0	47758.2	24.2	47734.0
-12.0	-44.0	47759.0	24.2	47734.8
-12.0	-46.0	47754.5	24.2	47730.3

x	y	meas. field	corr.	corr. field
-12.0	-48.0	47751.2	24.2	47727.0
-14.0	-40.0	47748.7	24.2	47724.5
-14.0	-38.0	47741.4	24.2	47717.2
-14.0	-36.0	47737.8	24.2	47713.6
-14.0	-34.0	47739.3	24.2	47715.1
-14.0	-32.0	47736.1	24.2	47711.9
-14.0	-30.0	47729.4	24.1	47705.3
-14.0	-28.0	47722.8	24.1	47698.7
-14.0	-26.0	47715.2	24.1	47691.1
-14.0	-24.0	47704.8	24.1	47680.7
-14.0	-22.0	47691.1	24.1	47667.0
-14.0	-20.0	47684.5	24.1	47660.4
-14.0	-18.0	47672.6	24.1	47648.5
-14.0	-16.0	47656.3	24.1	47632.2
-14.0	-14.0	47641.2	24.1	47617.1
-14.0	-12.0	47641.2	24.1	47617.1
-14.0	-10.0	47672.7	24.1	47648.6
-14.0	-8.0	47707.8	24.1	47683.7
-14.0	-6.0	47744.8	24.1	47720.7
-14.0	-4.0	47749.5	24.0	47725.5
-14.0	-2.0	47731.3	24.0	47707.3
-14.0	0.0	47717.4	24.0	47693.4
-14.0	2.0	47703.0	24.0	47679.0
-14.0	4.0	47691.9	24.0	47667.9
-14.0	6.0	47671.2	24.0	47647.2
-14.0	8.0	47656.5	24.0	47632.5
-14.0	10.0	47638.2	24.0	47614.2
-14.0	12.0	47639.4	24.0	47615.4
-14.0	14.0	47642.5	24.0	47618.5
-14.0	16.0	47637.0	24.0	47613.0
-14.0	18.0	47638.1	24.0	47614.1
-14.0	20.0	47641.6	23.9	47617.7
-14.0	22.0	47640.2	23.9	47616.3
-14.0	24.0	47628.4	23.9	47604.5
-14.0	26.0	47617.9	23.8	47594.1
-14.0	28.0	47633.5	23.7	47609.8
-14.0	30.0	47685.6	23.6	47662.0
-14.0	32.0	47700.1	23.5	47676.6
-14.0	34.0	47684.2	23.4	47660.8
-14.0	36.0	47669.9	23.4	47646.5
-14.0	38.0	47661.8	23.3	47638.5
-14.0	40.0	47655.5	23.2	47632.3
-14.0	42.0	47653.3	23.1	47630.2
-14.0	44.0	47654.0	23.0	47631.0
-14.0	46.0	47658.7	22.9	47635.8
-14.0	48.0	47661.4	22.8	47638.6
-14.0	50.0	47674.4	22.7	47651.7
-14.0	52.0	47680.0	22.6	47657.4
-14.0	54.0	47675.5	22.5	47653.0
-14.0	56.0	47669.4	22.4	47647.0
-16.0	52.0	47694.8	22.4	47672.4
-16.0	50.0	47694.8	22.3	47672.5
-16.0	48.0	47690.2	22.2	47668.0
-16.0	46.0	47691.2	22.1	47669.1
-16.0	44.0	47690.0	22.0	47668.0
-16.0	42.0	47696.8	21.9	47674.9
-16.0	40.0	47688.6	21.8	47666.8
-16.0	38.0	47687.3	21.7	47665.6
-16.0	36.0	47695.5	21.6	47673.9
-16.0	34.0	47698.9	21.5	47677.4
-16.0	32.0	47710.6	21.4	47689.2
-16.0	30.0	47711.7	21.4	47690.3
-16.0	28.0	47679.6	21.3	47658.3
-16.0	26.0	47651.2	21.2	47630.0
-16.0	24.0	47642.1	21.1	47621.0
-16.0	22.0	47645.7	21.0	47624.7
-16.0	20.0	47649.6	20.9	47628.7
-16.0	18.0	47649.6	20.8	47628.8
-16.0	16.0	47650.2	20.7	47629.5
-16.0	14.0	47656.9	20.6	47636.3
-16.0	12.0	47666.1	20.5	47645.6
-16.0	10.0	47674.1	20.4	47653.7
-16.0	8.0	47687.7	20.4	47667.3
-16.0	6.0	47699.1	20.3	47678.8
-16.0	4.0	47709.6	20.2	47689.4
-16.0	2.0	47718.8	20.1	47698.7
-16.0	0.0	47726.8	20.0	47706.8
-16.0	-2.0	47737.7	19.9	47717.8
-16.0	-4.0	47751.8	19.8	47732.0
-16.0	-6.0	47752.9	19.7	47733.2

x	y	meas. field	corr.	corr. field
-16.0	-8.0	47732.0	19.6	47712.4
-16.0	-10.0	47709.4	19.5	47689.9
-16.0	-12.0	47696.7	19.4	47677.3
-16.0	-14.0	47697.8	19.4	47678.5
-16.0	-16.0	47694.1	19.3	47674.8
-16.0	-18.0	47698.8	19.2	47679.6
-16.0	-20.0	47710.2	19.1	47691.1
-16.0	-22.0	47717.8	19.0	47698.8
-16.0	-24.0	47726.4	18.9	47707.5
2.0	80.0	47463.9	-0.4	47464.3
2.0	78.0	47457.3	-0.4	47457.7
2.0	76.0	47436.0	-0.5	47436.5
2.0	74.0	47420.9	-0.5	47421.4
2.0	72.0	47423.1	-0.6	47423.7
2.0	70.0	47437.9	-0.6	47438.5
2.0	68.0	47450.6	-0.7	47451.3
2.0	66.0	47451.8	-0.7	47452.5
2.0	64.0	47447.3	-0.8	47448.1
2.0	62.0	47453.5	-0.8	47454.3
2.0	60.0	47475.1	-0.9	47476.0
2.0	58.0	47519.9	-0.9	47520.8
2.0	56.0	47543.8	-1.0	47544.8
2.0	54.0	47563.2	-1.0	47564.2
2.0	52.0	47552.5	-1.1	47553.6
2.0	50.0	47533.2	-1.1	47534.3
2.0	48.0	47542.5	-1.2	47543.7
2.0	46.0	47559.7	-1.2	47560.9
2.0	44.0	47566.2	-1.3	47567.5
2.0	42.0	47571.5	-1.3	47572.8
2.0	40.0	47571.5	-1.4	47572.9
2.0	38.0	47571.4	-1.4	47572.8
2.0	36.0	47568.3	-1.5	47569.8
2.0	34.0	47566.3	-1.5	47567.8
2.0	32.0	47571.2	-1.6	47572.8
2.0	30.0	47556.8	-1.6	47558.4
2.0	28.0	47532.4	-1.7	47534.1
2.0	26.0	47541.4	-1.7	47543.1
2.0	24.0	47542.1	-1.8	47543.9
2.0	22.0	47566.0	-1.8	47567.8
2.0	20.0	47579.2	-1.9	47581.1
2.0	18.0	47585.5	-1.9	47587.4
2.0	16.0	47593.5	-1.9	47595.4
2.0	14.0	47594.3	-1.9	47596.2
2.0	12.0	47574.0	-2.0	47576.0
2.0	10.0	47556.0	-2.0	47558.0
2.0	8.0	47571.7	-2.0	47573.7
2.0	6.0	47584.4	-2.0	47586.4
2.0	4.0	47581.5	-2.1	47583.6
2.0	2.0	47564.4	-2.1	47566.5
2.0	0.0	47562.6	-2.1	47564.7
2.0	-2.0	47561.0	-2.2	47563.2
2.0	-4.0	47561.9	-2.2	47564.1
2.0	-6.0	47588.7	-2.2	47590.9
2.0	-8.0	47589.5	-2.2	47591.7
2.0	-10.0	47565.0	-2.3	47567.3
2.0	-12.0	47560.0	-2.3	47562.3
2.0	-14.0	47582.0	-2.3	47584.3
2.0	-16.0	47628.8	-2.3	47631.1
2.0	-18.0	47673.9	-2.4	47676.3
2.0	-20.0	47690.2	-2.4	47692.6
2.0	-22.0	47705.0	-2.4	47707.4
2.0	-24.0	47705.1	-2.4	47707.5
2.0	-26.0	47705.5	-2.5	47708.0
2.0	-28.0	47704.7	-2.5	47707.2
2.0	-30.0	47701.0	-2.5	47703.5
2.0	-32.0	47696.0	-2.6	47698.6
2.0	-34.0	47693.8	-2.6	47696.4
2.0	-36.0	47694.5	-2.6	47697.1
2.0	-38.0	47697.1	-2.6	47699.7
2.0	-40.0	47698.7	-2.7	47701.4
2.0	-42.0	47702.2	-2.7	47704.9
2.0	-44.0	47707.5	-2.7	47710.2
2.0	-46.0	47710.5	-2.7	47713.2
2.0	-48.0	47706.0	-2.8	47708.8
2.0	-50.0	47699.9	-2.8	47702.7
2.0	-52.0	47694.1	-2.8	47696.9
2.0	-54.0	47685.2	-2.9	47688.1
2.0	-56.0	47673.5	-2.9	47676.4
2.0	-58.0	47649.5	-2.9	47652.4
2.0	-60.0	47633.1	-2.9	47636.0

x	y	meas. field	corr.	corr. field
2.0	-62.0	47624.5	-3.0	47627.5
2.0	-64.0	47619.6	-3.0	47622.6
2.0	-66.0	47607.8	-3.0	47610.8
2.0	-68.0	47586.8	-3.0	47589.8
4.0	-68.0	47575.4	-3.1	47578.5
4.0	-66.0	47596.4	-3.1	47599.5
4.0	-64.0	47616.8	-3.1	47619.9
4.0	-62.0	47629.2	-3.1	47632.3
4.0	-60.0	47640.5	-3.2	47643.7
4.0	-58.0	47659.3	-3.2	47662.5
4.0	-56.0	47676.3	-3.2	47679.5
4.0	-54.0	47683.6	-3.3	47686.9
4.0	-52.0	47693.1	-3.3	47696.4
4.0	-50.0	47699.4	-3.3	47702.7
4.0	-48.0	47705.0	-3.3	47708.3
4.0	-46.0	47708.5	-3.4	47711.9
4.0	-44.0	47704.2	-3.4	47707.6
4.0	-42.0	47699.5	-3.4	47702.9
4.0	-40.0	47697.3	-3.4	47700.7
4.0	-38.0	47693.5	-3.5	47697.0
4.0	-36.0	47689.1	-3.5	47692.6
4.0	-34.0	47688.3	-3.5	47691.8
4.0	-32.0	47689.9	-3.6	47693.5
4.0	-30.0	47694.3	-3.6	47697.9
4.0	-28.0	47697.8	-3.6	47701.4
4.0	-26.0	47698.7	-3.6	47702.3
4.0	-24.0	47698.2	-3.7	47701.9
4.0	-22.0	47686.3	-3.7	47690.0
4.0	-20.0	47660.3	-3.7	47664.0
4.0	-18.0	47652.7	-3.7	47656.4
4.0	-16.0	47637.6	-3.8	47641.4
4.0	-14.0	47597.9	-3.8	47601.7
4.0	-12.0	47585.3	-3.8	47589.1
4.0	-10.0	47586.0	-3.9	47589.9
4.0	-8.0	47579.4	-3.9	47583.3
4.0	-6.0	47561.3	-3.9	47565.2
4.0	-4.0	47542.4	-3.9	47546.3
4.0	-2.0	47535.8	-4.0	47539.8
4.0	0.0	47530.3	-4.0	47534.3
4.0	2.0	47540.4	-4.0	47544.4
4.0	4.0	47560.7	-4.0	47564.7
4.0	6.0	47574.5	-4.1	47578.6
4.0	8.0	47566.0	-4.1	47570.1
4.0	10.0	47547.0	-4.1	47551.1
4.0	12.0	47569.6	-4.1	47573.7
4.0	14.0	47588.8	-4.2	47593.0
4.0	16.0	47591.1	-4.2	47595.3
4.0	18.0	47584.4	-4.2	47588.6
4.0	20.0	47576.1	-4.3	47580.4
4.0	22.0	47564.1	-4.3	47568.4
4.0	24.0	47538.0	-4.3	47542.3
4.0	26.0	47527.9	-4.3	47532.2
4.0	28.0	47512.3	-4.3	47516.6
4.0	30.0	47553.2	-4.2	47557.4
4.0	32.0	47576.9	-4.2	47581.1
4.0	34.0	47562.3	-4.2	47566.5
4.0	36.0	47558.3	-4.2	47562.5
4.0	38.0	47558.8	-4.2	47563.0
4.0	40.0	47559.3	-4.1	47563.4
4.0	42.0	47564.7	-4.1	47568.8
4.0	44.0	47560.8	-4.1	47564.9
4.0	46.0	47559.6	-4.1	47563.7
4.0	48.0	47550.1	-4.1	47554.2
4.0	50.0	47531.3	-4.0	47535.3
4.0	52.0	47530.3	-4.0	47534.3
4.0	54.0	47537.0	-4.0	47541.0
4.0	56.0	47532.4	-4.0	47536.4
4.0	58.0	47508.2	-4.0	47512.2
4.0	60.0	47473.2	-3.9	47477.1
4.0	62.0	47446.3	-3.9	47450.2
4.0	64.0	47444.7	-3.9	47448.6
4.0	66.0	47455.9	-3.9	47459.8
4.0	68.0	47453.6	-3.9	47457.5
4.0	70.0	47439.8	-3.8	47443.6
4.0	72.0	47426.6	-3.8	47430.4
4.0	74.0	47420.4	-3.8	47424.2
4.0	76.0	47436.2	-3.8	47440.0
6.0	68.0	47502.1	8.1	47494.0
6.0	66.0	47512.8	8.2	47504.6
6.0	64.0	47508.4	8.2	47500.2

x	y	meas. field	corr.	corr. field
6.0	62.0	47511.4	8.3	47503.1
6.0	60.0	47522.6	8.3	47514.3
6.0	58.0	47542.1	8.4	47533.7
6.0	56.0	47539.7	8.4	47531.3
6.0	54.0	47524.0	8.5	47515.5
6.0	52.0	47528.3	8.5	47519.8
6.0	50.0	47558.3	8.6	47549.7
6.0	48.0	47574.9	8.6	47566.2
6.0	46.0	47580.3	8.7	47571.6
6.0	44.0	47577.5	8.8	47568.7
6.0	42.0	47575.8	8.8	47567.0
6.0	40.0	47573.3	8.9	47564.4
6.0	38.0	47573.1	8.9	47564.2
6.0	36.0	47579.4	9.0	47570.4
6.0	34.0	47584.7	9.0	47575.7
6.0	32.0	47589.2	9.1	47580.1
6.0	30.0	47568.2	9.1	47559.1
6.0	28.0	47541.4	9.2	47532.2
6.0	26.0	47550.0	9.3	47540.7
6.0	24.0	47566.3	9.3	47557.0
6.0	22.0	47588.2	9.3	47578.9
6.0	20.0	47597.2	9.3	47587.9
6.0	18.0	47606.8	9.3	47597.5
6.0	16.0	47613.3	9.3	47604.0
6.0	14.0	47610.7	9.2	47601.5
6.0	12.0	47598.6	9.2	47589.4
6.0	10.0	47583.7	9.2	47574.5
6.0	8.0	47584.8	9.2	47575.6
6.0	6.0	47584.6	9.2	47575.4
6.0	4.0	47556.6	9.2	47547.4
6.0	2.0	47527.3	9.2	47518.1
6.0	0.0	47513.9	9.2	47504.7
6.0	-2.0	47519.5	9.2	47510.3
6.0	-4.0	47540.8	9.1	47531.7
6.0	-6.0	47565.3	9.1	47556.2
6.0	-8.0	47583.6	9.1	47574.5
6.0	-10.0	47602.7	9.1	47593.6
6.0	-12.0	47615.7	9.1	47606.6
6.0	-14.0	47632.9	9.1	47623.8
6.0	-16.0	47649.9	9.1	47640.8
6.0	-18.0	47659.3	9.1	47650.2
6.0	-20.0	47671.5	9.1	47662.4
6.0	-22.0	47695.7	9.0	47686.7
6.0	-24.0	47706.6	9.0	47697.6
6.0	-26.0	47707.8	9.0	47698.8
6.0	-28.0	47708.2	9.0	47699.2
6.0	-30.0	47706.2	9.0	47697.2
6.0	-32.0	47703.7	9.0	47694.7
6.0	-34.0	47706.7	9.0	47697.7
6.0	-36.0	47711.4	9.0	47702.4
6.0	-38.0	47717.2	9.0	47708.2
6.0	-40.0	47715.4	8.9	47706.5
6.0	-42.0	47717.0	8.9	47708.1
6.0	-44.0	47723.1	8.9	47714.2
6.0	-46.0	47724.6	8.9	47715.7
6.0	-48.0	47719.6	8.9	47710.7
6.0	-50.0	47712.0	8.9	47703.1
6.0	-52.0	47706.9	8.9	47698.0
6.0	-54.0	47702.2	8.9	47693.3
6.0	-56.0	47696.1	8.9	47687.2
6.0	-58.0	47674.9	8.8	47666.1
6.0	-60.0	47660.3	8.8	47651.5
6.0	-62.0	47647.1	8.8	47638.3
6.0	-64.0	47626.7	8.8	47617.9
6.0	-66.0	47606.0	8.8	47597.2
6.0	-68.0	47581.9	8.8	47573.1
8.0	-68.0	47588.4	8.8	47579.6
8.0	-66.0	47604.4	8.8	47595.6
8.0	-64.0	47627.2	8.8	47618.4
8.0	-62.0	47662.4	8.8	47653.6
8.0	-60.0	47677.6	8.7	47668.9
8.0	-58.0	47697.8	8.7	47689.1
8.0	-56.0	47710.7	8.7	47702.0
8.0	-54.0	47711.1	8.7	47702.4
8.0	-52.0	47706.9	8.7	47698.2
8.0	-50.0	47712.2	8.7	47703.5
8.0	-48.0	47719.5	8.7	47710.8
8.0	-46.0	47729.4	8.7	47720.7
8.0	-44.0	47729.6	8.7	47720.9
8.0	-42.0	47723.4	8.6	47714.8

x	y	meas. field	corr.	corr. field
8.0	-40.0	47723.8	8.6	47715.2
8.0	-38.0	47729.4	8.6	47720.8
8.0	-36.0	47722.3	8.6	47713.7
8.0	-34.0	47709.4	8.6	47700.8
8.0	-32.0	47705.8	8.6	47697.2
8.0	-30.0	47705.5	8.6	47696.9
8.0	-28.0	47706.9	8.6	47698.3
8.0	-26.0	47701.8	8.6	47693.2
8.0	-24.0	47695.2	8.5	47686.7
8.0	-22.0	47687.5	8.5	47679.0
8.0	-20.0	47674.7	8.5	47666.2
8.0	-18.0	47658.7	8.5	47650.2
8.0	-16.0	47652.5	8.5	47644.0
8.0	-14.0	47642.0	8.5	47633.5
8.0	-12.0	47625.6	8.5	47617.1
8.0	-10.0	47599.0	8.5	47590.5
8.0	-8.0	47574.0	8.5	47565.5
8.0	-6.0	47546.4	8.4	47538.0
8.0	-4.0	47528.6	8.4	47520.2
8.0	-2.0	47503.6	8.4	47495.2
8.0	0.0	47494.5	8.4	47486.1
8.0	2.0	47520.6	8.4	47512.2
8.0	4.0	47550.7	8.4	47542.3
8.0	6.0	47580.8	8.4	47572.4
8.0	8.0	47596.0	8.4	47587.6
8.0	10.0	47605.1	8.4	47596.7
8.0	12.0	47613.0	8.3	47604.7
8.0	14.0	47615.7	8.3	47607.4
8.0	16.0	47618.2	8.3	47609.9
8.0	18.0	47610.3	8.3	47602.0
8.0	20.0	47601.3	8.3	47593.0
8.0	22.0	47590.7	8.3	47582.4
8.0	24.0	47579.9	8.3	47571.6
8.0	26.0	47563.0	8.3	47554.7
8.0	28.0	47564.6	8.4	47556.2
8.0	30.0	47568.9	8.4	47560.5
8.0	32.0	47577.1	8.4	47568.7
8.0	34.0	47584.7	8.5	47576.2
8.0	36.0	47583.3	8.5	47574.8
8.0	38.0	47571.3	8.6	47562.7
8.0	40.0	47572.4	8.6	47563.8
8.0	42.0	47566.0	8.6	47557.4
8.0	44.0	47568.8	8.7	47560.1
8.0	46.0	47570.2	8.7	47561.5
8.0	48.0	47569.4	8.7	47560.7
8.0	50.0	47548.3	8.8	47539.5
8.0	52.0	47519.2	8.8	47510.4
8.0	54.0	47516.8	8.8	47508.0
8.0	56.0	47534.3	8.9	47525.4
8.0	58.0	47546.6	8.9	47537.7
8.0	60.0	47544.5	8.9	47535.6
8.0	62.0	47539.3	9.0	47530.3
8.0	64.0	47528.6	9.0	47519.6
10.0	60.0	47550.4	9.1	47541.3
10.0	58.0	47553.6	9.1	47544.5
10.0	56.0	47553.3	9.1	47544.2
10.0	54.0	47549.2	9.2	47540.0
10.0	52.0	47553.4	9.2	47544.2
10.0	50.0	47575.1	9.2	47565.9
10.0	48.0	47581.6	9.3	47572.3
10.0	46.0	47578.6	9.3	47569.3
10.0	44.0	47577.4	9.3	47568.1
10.0	42.0	47577.8	9.4	47568.4
10.0	40.0	47582.5	9.4	47573.1
10.0	38.0	47588.4	9.5	47578.9
10.0	36.0	47593.0	9.5	47583.5
10.0	34.0	47592.9	9.5	47583.4
10.0	32.0	47588.6	9.6	47579.0
10.0	30.0	47583.0	9.6	47573.4
10.0	28.0	47584.0	9.6	47574.4
10.0	26.0	47586.5	9.7	47576.8
10.0	24.0	47592.7	9.7	47583.0
10.0	22.0	47600.7	9.8	47590.9
10.0	20.0	47609.3	9.9	47599.4
10.0	18.0	47624.6	9.9	47614.7
10.0	16.0	47632.7	10.0	47622.7
10.0	14.0	47637.3	10.1	47627.2
10.0	12.0	47632.4	10.2	47622.2
10.0	10.0	47632.3	10.2	47622.1
10.0	8.0	47601.0	10.3	47590.7

x	y	meas. field	corr.	corr. field
10.0	6.0	47511.5	10.4	47501.1
10.0	4.0	47465.6	10.5	47455.1
10.0	2.0	47451.0	10.6	47450.4
10.0	0.0	47472.8	10.6	47462.2
10.0	-2.0	47508.1	10.7	47497.4
10.0	-4.0	47535.0	10.8	47524.2
10.0	-6.0	47564.2	10.9	47553.3
10.0	-8.0	47580.6	10.9	47569.7
10.0	-10.0	47609.7	11.0	47598.7
10.0	-12.0	47629.9	11.1	47618.8
10.0	-14.0	47645.9	11.2	47634.7
10.0	-16.0	47655.8	11.3	47644.5
10.0	-18.0	47665.7	11.3	47654.4
10.0	-20.0	47671.8	11.4	47660.4
10.0	-22.0	47685.2	11.5	47673.7
10.0	-24.0	47690.3	11.6	47678.7
10.0	-26.0	47698.5	11.6	47686.9
10.0	-28.0	47702.0	11.7	47690.3
10.0	-30.0	47703.2	11.8	47691.4
10.0	-32.0	47705.6	11.9	47693.7
10.0	-34.0	47715.8	12.0	47703.8
10.0	-36.0	47727.7	12.0	47715.7
10.0	-38.0	47738.8	12.1	47726.7
10.0	-40.0	47729.3	12.2	47717.1
10.0	-42.0	47721.9	12.3	47709.6
10.0	-44.0	47728.0	12.4	47715.6
10.0	-46.0	47725.0	12.4	47712.6
10.0	-48.0	47717.5	12.5	47705.0
10.0	-50.0	47707.3	12.6	47694.7
10.0	-52.0	47713.8	12.7	47701.1
10.0	-54.0	47735.7	12.7	47723.0
10.0	-56.0	47752.8	12.8	47740.0
10.0	-58.0	47725.1	12.9	47712.2
10.0	-60.0	47701.2	13.0	47688.2
10.0	-62.0	47675.3	13.1	47662.2
10.0	-64.0	47632.6	13.1	47619.5
12.0	-60.0	47699.9	13.2	47686.7
12.0	-58.0	47736.6	13.3	47723.3
12.0	-56.0	47754.8	13.4	47741.4
12.0	-54.0	47759.2	13.4	47745.8
12.0	-52.0	47734.4	13.5	47720.9
12.0	-50.0	47712.4	13.6	47698.8
12.0	-48.0	47714.3	13.7	47700.6
12.0	-46.0	47718.7	13.8	47704.9
12.0	-44.0	47719.4	13.8	47705.6
12.0	-42.0	47717.0	13.9	47703.1
12.0	-40.0	47720.3	14.0	47706.3
12.0	-38.0	47728.6	14.1	47714.5
12.0	-36.0	47723.4	14.1	47709.3
12.0	-34.0	47711.1	14.2	47696.9
12.0	-32.0	47707.9	14.3	47693.6
12.0	-30.0	47707.8	14.4	47693.4
12.0	-28.0	47704.8	14.5	47690.3
12.0	-26.0	47699.8	14.5	47685.3
12.0	-24.0	47692.8	14.6	47678.2
12.0	-22.0	47685.1	14.7	47670.4
12.0	-20.0	47675.9	14.8	47661.1
12.0	-18.0	47666.3	14.8	47651.5
12.0	-16.0	47659.2	14.9	47644.3
12.0	-14.0	47644.3	15.0	47629.3
12.0	-12.0	47632.7	15.1	47617.6
12.0	-10.0	47606.0	15.2	47590.8
12.0	-8.0	47588.3	15.2	47573.1
12.0	-6.0	47572.1	15.3	47556.8
12.0	-4.0	47555.9	15.4	47540.5
12.0	-2.0	47508.8	15.5	47493.3
12.0	0.0	47467.4	15.5	47451.9
12.0	2.0	47384.8	15.6	47369.2
12.0	4.0	47372.5	15.7	47356.8
12.0	6.0	47482.1	15.8	47466.3
12.0	8.0	47603.3	15.9	47587.4
12.0	10.0	47666.3	15.9	47650.4
12.0	12.0	47667.7	16.0	47651.7
12.0	14.0	47676.0	16.1	47659.9
12.0	16.0	47658.5	16.2	47642.3
12.0	18.0	47638.5	16.3	47622.2
12.0	20.0	47622.6	16.3	47606.3
12.0	22.0	47607.0	16.4	47590.6
12.0	24.0	47602.8	16.5	47586.3
12.0	26.0	47610.3	16.6	47593.7

x	y	meas. field	corr.	corr. field
12.0	28.0	47615.5	16.6	47598.9
12.0	30.0	47610.4	16.7	47593.7
12.0	32.0	47613.5	16.8	47596.7
12.0	34.0	47608.8	16.9	47591.9
12.0	36.0	47601.9	17.0	47584.9
12.0	38.0	47600.7	17.0	47583.7
12.0	40.0	47598.8	17.1	47581.7
12.0	42.0	47597.4	17.2	47580.2
12.0	44.0	47596.9	17.3	47579.6
12.0	46.0	47596.1	17.3	47578.8
12.0	48.0	47593.8	17.4	47576.4
12.0	50.0	47585.8	17.5	47568.3
12.0	52.0	47575.0	17.6	47557.4
14.0	44.0	47607.1	17.7	47589.4
14.0	42.0	47608.3	17.7	47590.6
14.0	40.0	47612.4	17.8	47594.6
14.0	38.0	47616.0	17.9	47598.1
14.0	36.0	47621.6	18.0	47603.6
14.0	34.0	47640.6	18.0	47622.6
14.0	32.0	47642.4	18.1	47624.3
14.0	30.0	47650.2	18.2	47632.0
14.0	28.0	47653.5	18.3	47635.2
14.0	26.0	47633.2	18.4	47614.8
14.0	24.0	47623.3	18.4	47604.9
14.0	22.0	47630.6	18.4	47612.2
14.0	20.0	47644.9	18.4	47626.6
14.0	18.0	47658.8	18.3	47640.5
14.0	16.0	47695.0	18.3	47676.7
14.0	14.0	47717.4	18.3	47699.1
14.0	12.0	47739.2	18.3	47720.9
14.0	10.0	47727.7	18.2	47709.5
14.0	8.0	47639.2	18.2	47621.0
14.0	6.0	47374.6	18.2	47356.4
14.0	4.0	47297.1	18.2	47279.0
14.0	2.0	47378.4	18.1	47360.3
14.0	0.0	47464.5	18.1	47446.4
14.0	-2.0	47551.3	18.1	47533.2
14.0	-4.0	47575.2	18.1	47557.2
14.0	-6.0	47588.5	18.0	47570.5
14.0	-8.0	47591.2	18.0	47573.2
14.0	-10.0	47610.3	18.0	47592.3
14.0	-12.0	47627.6	18.0	47609.7
14.0	-14.0	47648.2	17.9	47630.3
14.0	-16.0	47659.3	17.9	47641.4
14.0	-18.0	47672.4	17.9	47654.5
14.0	-20.0	47688.5	17.9	47670.7
14.0	-22.0	47697.9	17.8	47680.1
14.0	-24.0	47707.5	17.8	47689.7
14.0	-26.0	47709.2	17.8	47691.4
14.0	-28.0	47710.7	17.8	47692.9
14.0	-30.0	47711.8	17.7	47694.1
14.0	-32.0	47707.9	17.7	47690.2
14.0	-34.0	47705.1	17.7	47687.4
14.0	-36.0	47707.6	17.7	47690.0
14.0	-38.0	47714.0	17.6	47696.4
14.0	-40.0	47716.7	17.6	47699.1
14.0	-42.0	47719.0	17.6	47701.4
14.0	-44.0	47716.7	17.6	47699.2
14.0	-46.0	47717.5	17.5	47700.0
14.0	-48.0	47721.8	17.5	47704.3
14.0	-50.0	47733.4	17.5	47715.9
14.0	-52.0	47748.4	17.5	47730.9
14.0	-54.0	47760.7	17.4	47743.3
14.0	-56.0	47749.1	17.4	47731.7
14.0	-58.0	47713.6	17.4	47696.2
14.0	-60.0	47693.7	17.4	47676.4
16.0	-56.0	47709.6	17.3	47692.3
16.0	-54.0	47722.6	17.3	47705.3
16.0	-52.0	47742.4	17.3	47725.1
16.0	-50.0	47743.0	17.3	47725.8
16.0	-48.0	47733.6	17.2	47716.4
16.0	-46.0	47724.3	17.2	47707.1
16.0	-44.0	47717.5	17.2	47700.3
16.0	-42.0	47714.6	17.2	47697.5
16.0	-40.0	47710.7	17.1	47693.6
16.0	-38.0	47699.4	17.1	47682.3
16.0	-36.0	47691.2	17.1	47674.1
16.0	-34.0	47691.9	17.1	47674.9
16.0	-32.0	47696.5	17.0	47679.5
16.0	-30.0	47701.1	17.0	47684.1

x	y	meas. field	corr.	corr. field
16.0	-28.0	47704.6	17.0	47687.6
16.0	-26.0	47708.7	17.0	47691.7
16.0	-24.0	47709.6	16.9	47692.7
16.0	-22.0	47706.2	16.9	47689.3
16.0	-20.0	47699.0	16.9	47682.1
16.0	-18.0	47687.3	16.9	47670.5
16.0	-16.0	47671.5	16.8	47654.7
16.0	-14.0	47648.8	16.8	47632.0
16.0	-12.0	47632.2	16.8	47615.4
16.0	-10.0	47605.0	16.8	47588.2
16.0	-8.0	47591.6	16.7	47574.9
16.0	-6.0	47579.5	16.7	47562.8
16.0	-4.0	47572.4	16.7	47555.7
16.0	-2.0	47536.6	16.7	47520.0
16.0	0.0	47480.1	16.6	47463.5
16.0	2.0	47398.4	16.6	47381.8
16.0	4.0	47375.6	16.6	47359.0
16.0	6.0	47495.1	16.6	47478.6
16.0	8.0	47640.4	16.5	47623.9
16.0	10.0	47718.9	16.5	47702.4
16.0	12.0	47733.7	16.5	47717.2
16.0	14.0	47716.4	16.5	47699.9
16.0	16.0	47699.2	16.4	47682.8
16.0	18.0	47678.8	16.4	47662.4
16.0	20.0	47658.1	16.4	47641.7
16.0	22.0	47641.4	16.4	47625.1
16.0	24.0	47630.7	16.3	47614.4
16.0	26.0	47635.9	16.2	47619.7
16.0	28.0	47640.1	16.0	47624.1
16.0	30.0	47636.5	15.9	47620.6
16.0	32.0	47631.2	15.8	47615.4
16.0	34.0	47626.0	15.7	47610.3
16.0	36.0	47613.7	15.5	47598.2
18.0	20.0	47669.9	15.4	47654.5
18.0	18.0	47682.2	15.3	47666.9
18.0	16.0	47705.3	15.2	47690.1
18.0	14.0	47718.0	15.0	47703.0
18.0	12.0	47719.3	14.9	47704.4
18.0	10.0	47701.4	14.8	47686.6
18.0	8.0	47660.0	14.7	47645.3
18.0	6.0	47600.3	14.5	47585.8
18.0	4.0	47535.1	14.4	47520.7
18.0	2.0	47488.6	14.3	47474.3
18.0	0.0	47509.9	14.2	47495.7
18.0	-2.0	47546.1	14.0	47532.1
18.0	-4.0	47570.5	13.9	47556.6
18.0	-6.0	47588.4	13.8	47574.6
18.0	-8.0	47599.9	13.7	47586.2
18.0	-10.0	47622.9	13.5	47609.4
18.0	-12.0	47647.3	13.4	47633.9
18.0	-14.0	47677.4	13.3	47664.1
18.0	-16.0	47688.3	13.2	47675.1
18.0	-18.0	47703.2	13.0	47690.2
18.0	-20.0	47710.3	12.9	47697.4
18.0	-22.0	47712.7	12.8	47699.9
18.0	-24.0	47709.6	12.7	47696.9
18.0	-26.0	47707.3	12.5	47694.8
18.0	-28.0	47704.5	12.4	47692.1
18.0	-30.0	47704.9	12.3	47692.6
18.0	-32.0	47705.6	12.2	47693.4
18.0	-34.0	47697.6	12.0	47685.6
18.0	-36.0	47699.6	11.9	47687.7
18.0	-38.0	47711.4	11.8	47699.6
18.0	-40.0	47724.4	11.7	47712.7
18.0	-42.0	47732.9	11.5	47721.4
18.0	-44.0	47743.9	11.4	47732.5
18.0	-46.0	47740.7	11.3	47729.4
18.0	-48.0	47733.2	11.2	47722.0
18.0	-50.0	47724.3	11.0	47713.3
18.0	-52.0	47717.7	10.9	47706.8
20.0	-48.0	47719.1	10.8	47708.3
20.0	-46.0	47718.1	10.7	47707.4
20.0	-44.0	47723.8	10.5	47713.3
20.0	-42.0	47732.2	10.4	47721.8
20.0	-40.0	47728.2	10.3	47717.9
20.0	-38.0	47710.5	10.2	47700.3
20.0	-36.0	47708.4	10.0	47698.4
20.0	-34.0	47708.3	9.9	47698.4
20.0	-32.0	47715.9	9.8	47706.1
20.0	-30.0	47716.8	9.7	47707.1

x	y	meas. field	corr.	corr. field
20.0	-28.0	47717.0	9.5	47707.5
20.0	-26.0	47717.2	9.4	47707.8
20.0	-24.0	47714.9	9.3	47705.6
20.0	-22.0	47714.5	9.2	47705.3
20.0	-20.0	47712.6	9.0	47703.6
20.0	-18.0	47707.5	8.9	47698.6
20.0	-16.0	47701.2	8.8	47692.4
20.0	-14.0	47689.6	8.7	47680.9
20.0	-12.0	47674.3	8.5	47665.8
20.0	-10.0	47647.1	8.4	47638.7
20.0	-8.0	47626.6	8.3	47618.3
20.0	-6.0	47607.1	8.2	47598.9
20.0	-4.0	47587.9	8.0	47579.9
20.0	-2.0	47564.8	7.9	47556.9
20.0	0.0	47550.0	7.8	47542.2
20.0	2.0	47558.6	7.7	47550.9
20.0	4.0	47580.8	7.5	47573.3
20.0	6.0	47620.3	7.4	47612.9
20.0	8.0	47656.9	7.3	47649.6
22.0	4.0	47601.6	7.3	47594.3
22.0	2.0	47589.3	7.3	47582.0
22.0	0.0	47579.6	7.3	47572.3
22.0	-2.0	47588.6	7.3	47581.3
22.0	-4.0	47601.6	7.3	47594.3
22.0	-6.0	47628.9	7.3	47621.6
22.0	-8.0	47647.1	7.3	47639.8
22.0	-10.0	47674.3	7.3	47667.0
22.0	-12.0	47688.7	7.3	47681.4
22.0	-14.0	47701.4	7.3	47694.1
22.0	-16.0	47707.8	7.3	47700.5
22.0	-18.0	47709.9	7.3	47702.6
22.0	-20.0	47709.0	7.3	47701.7
22.0	-22.0	47703.6	7.3	47696.3
22.0	-24.0	47708.1	7.3	47700.8
22.0	-26.0	47718.5	7.3	47711.2
22.0	-28.0	47708.3	7.3	47701.0
22.0	-30.0	47703.8	7.3	47696.5
22.0	-32.0	47697.4	7.3	47690.1
22.0	-34.0	47691.8	7.3	47684.5
22.0	-36.0	47685.7	7.3	47678.4
22.0	-38.0	47683.1	7.3	47675.8
22.0	-40.0	47686.4	7.3	47679.1
24.0	-28.0	47680.3	7.3	47673.0
24.0	-26.0	47687.2	7.3	47679.9
24.0	-24.0	47686.8	7.3	47679.5
24.0	-22.0	47685.8	7.3	47678.5
24.0	-20.0	47692.6	7.3	47685.3
24.0	-18.0	47705.8	7.3	47698.5
24.0	-16.0	47707.9	7.3	47700.6
24.0	-14.0	47700.0	7.3	47692.7
24.0	-12.0	47694.7	7.3	47687.4
24.0	-10.0	47673.0	7.3	47665.7
24.0	-8.0	47657.1	7.3	47649.8
24.0	-6.0	47632.6	7.3	47625.3
24.0	-4.0	47617.6	7.3	47610.3
24.0	-2.0	47604.9	7.3	47597.6
24.0	0.0	47600.9	7.3	47593.6

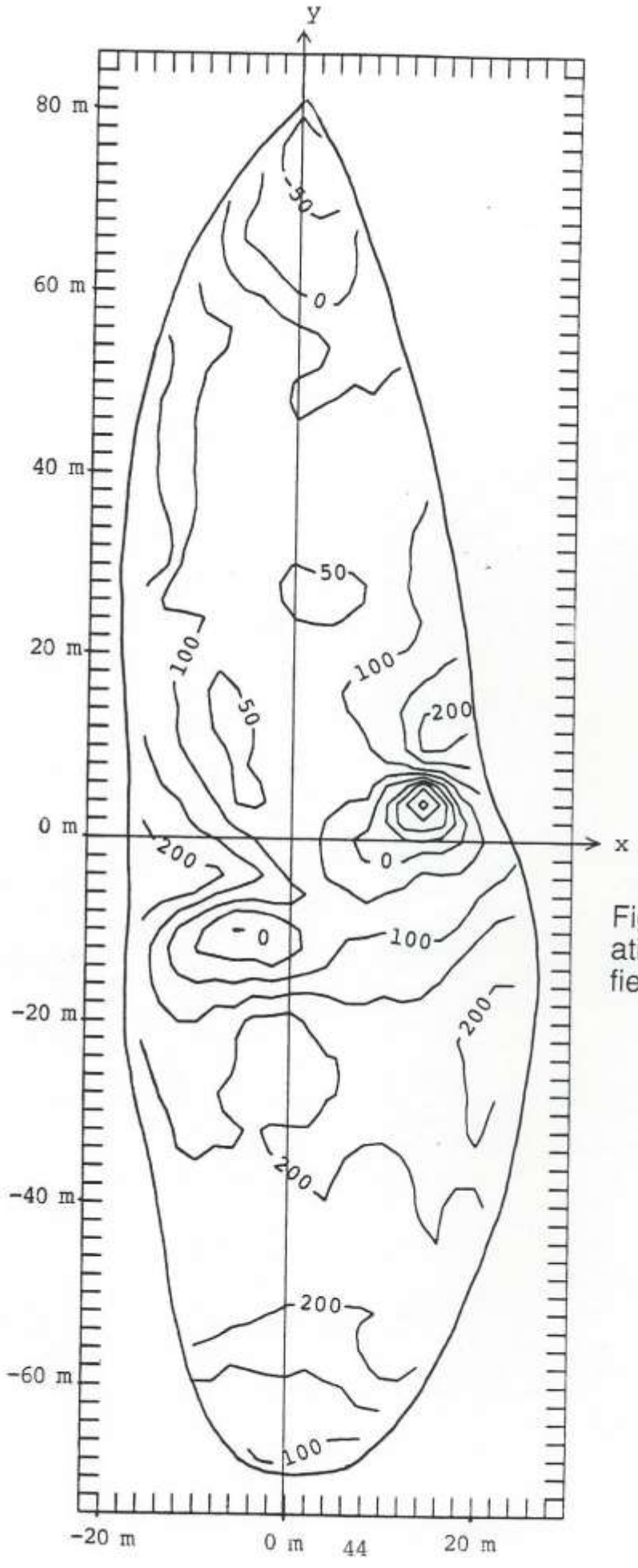

Fig. 8 Contours of the variation of the total magnetic field in units of nanoteslas.

SEISMOGRAPH DATA

Figures 9-11 are plots of seismic travel times versus distance for three lines on the site. Figure 9 is for a line between points x=0, y=68 m and x=0, y=-4 m, with the seismic source at x=0, y=74 m. Figure 10 refers to a line between points x=0, y=0 and x=0, y=-76 m, with the source at x=0, y=-6 m. Figure 11 pertains to a line between points x=0, y=68 m and x=-10 m, y=-4 m with the source located x=-10 m, y=0. Points plotted in these figures represent the actual measured data. Line segments represent a best-fit approximation to the data, with each line segment pertaining to a separate subsurface layer. The slope of each line segment corresponds to the apparent seismic velocity in the layer.

Under the assumption that the subsurface layers are of uniform thickness, the thickness D of the topmost layer can be expressed by the formula

$$D = 1/2\, q\sqrt{(v_2 - v_1)/(v_2 + v_1)}$$

where q is the distance at which line segments for layers one and two intersect, v_1 is the apparent velocity of layer one, and v_2 is the apparent velocity of layer two. This formula gives a thickness for the surface layer of 5.9 m for the line of Figure 9, 2.3 m for the line of Figure 10, and 7.9 m for the line of Figure 11. Since the lines of Figures 9 and 10 are essential the same except that the seismic source is at opposite ends, and yet the apparent thickness of the top layer is noticeably different, obviously indicates the top layer is not of uniform thickness. Since the line with the source near the rock outcrop gives the shallower value, it is probably that this rock body is influencing the results.

The most important conclusion that can be inferred from these data is that a material of moderately high seismic velocity (2400-3300 m/s) lies at relatively shalow depth (6-8 m). The layer observed in Figure 10 with a velocity of 1500 m/s is conjectured to be the calc-schist rock that outcrops near the middle of the site. If this interpretation is correct, the the material responsible for the higher velocities (2400-3300 m/s) is different from the calc-schist. These conclusions are consistent with those reached in considering the radar results. It therefore seems reasonable to assume that the high velocity material observed in the seismograph data is the same material responsible for the strong radar reflections at 4-8 m depth in the radar data. Again core drilling can resolve the large uncertainties in the interpretation of these measurements and provide a clear answer as to the nature of the material which gives the strong radar reflections.

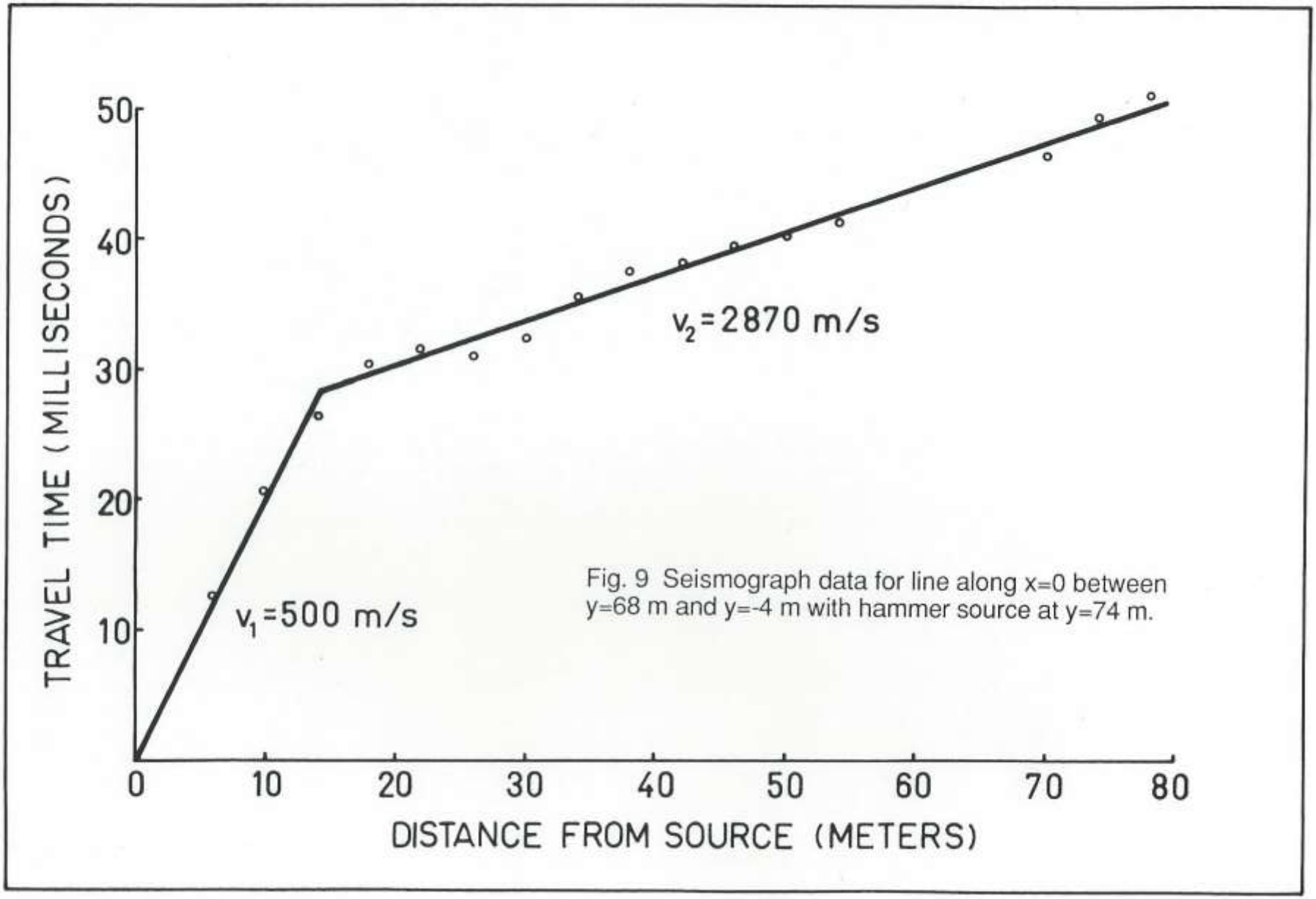

Fig. 9 Seismograph data for line along x=0 between y=68 m and y=-4 m with hammer source at y=74 m.

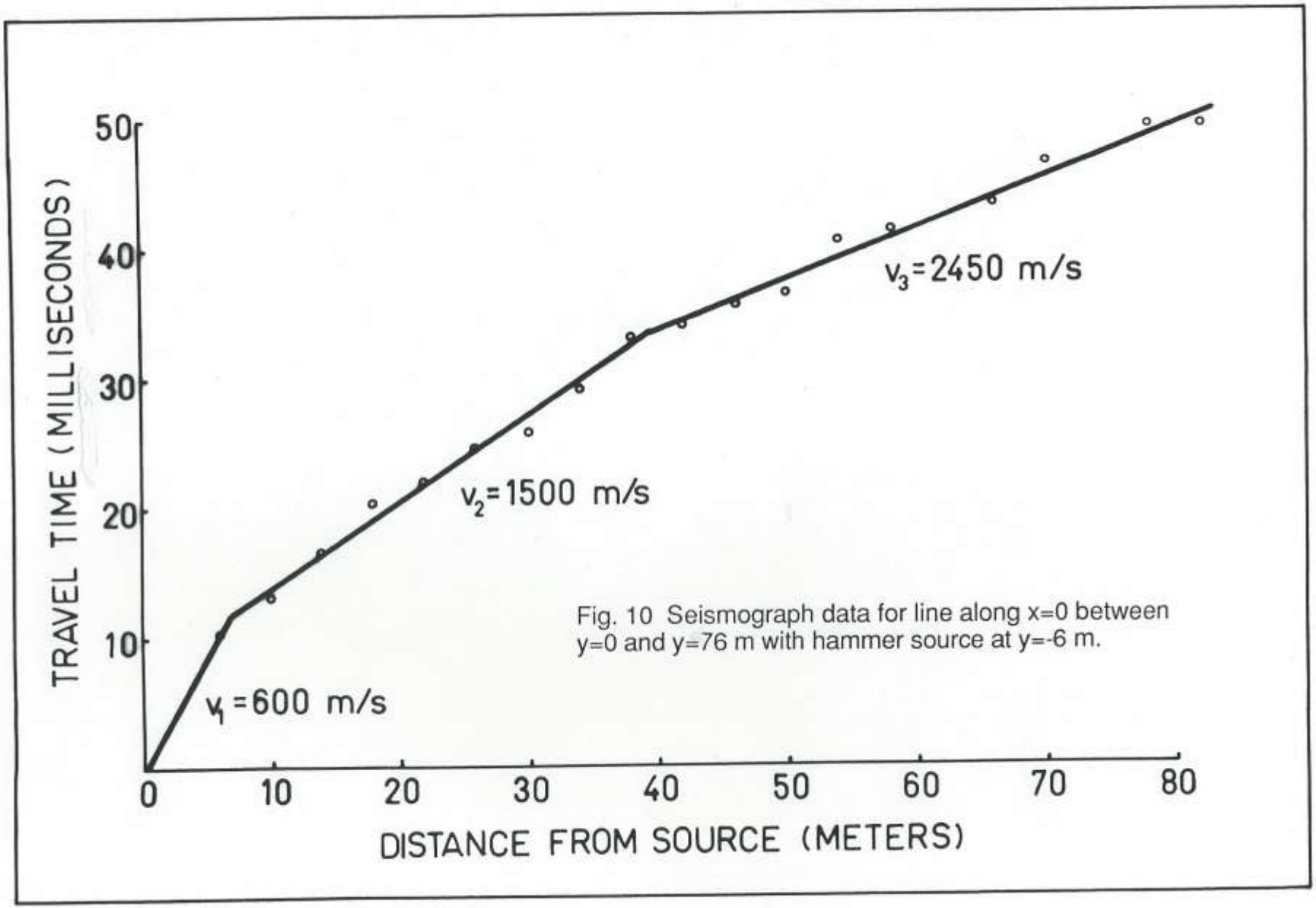

Fig. 10 Seismograph data for line along x=0 between y=0 and y=76 m with hammer source at y=-6 m.

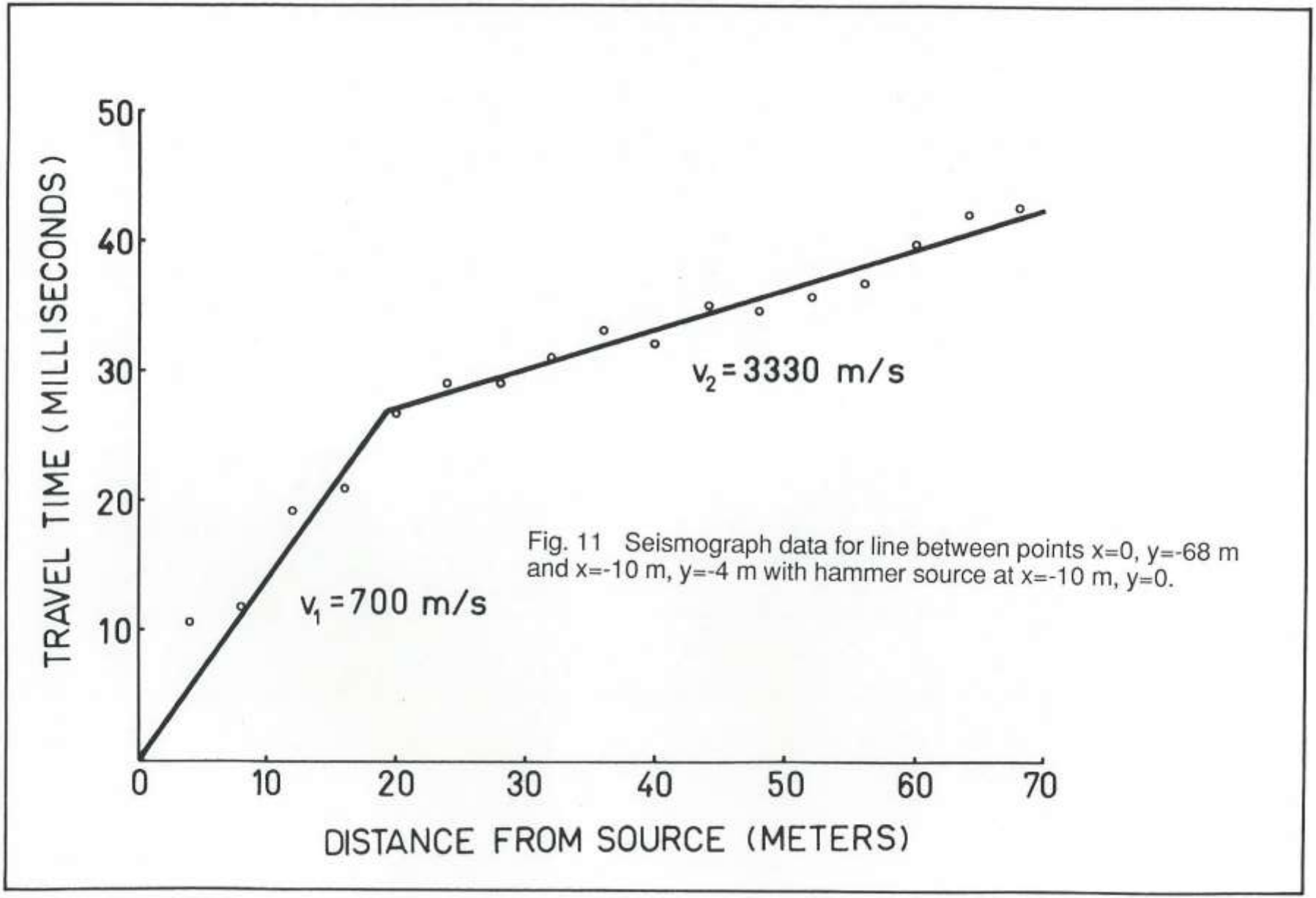

Fig. 11 Seismograph data for line between points x=0, y=-68 m and x=-10 m, y=-4 m with hammer source at x=-10 m, y=0.

CONCLUSIONS

We conclude that the data from our geophysical investigations in no way conflict with the proposition that the unusual boat-shaped site near Mahser village contains the remains of Noah's Ark. Indeed, the existence of remains of a large man-made structure in the site is an attractive way to account for the highly anomalous feature of the extensive, almost planar, reflector observed in the radar data. However, without actual samples of the subsurface materials we feel that definitive interpretations of our data are not possible. On the other hand, we believe samples obtainable through core drilling a small number of holes in the site can provide the information required which, together with the geophysical data we already have, can allow very solid conclusions to be reached. We therefore urge the Turkish authorities to support efforts to conduct core drilling as early in 1988 as weather conditions allow.

We want to express our thanks to Prof. Dr. Hurşit Ertuğrul, Rector of Atatürk University, for sponsoring this joint research project. We also thank Mr. Rüşdü Naiboğlu (Emeritus General), Director for Security Affairs, and Mrs. Reyyan Ödemiş, Director of the Department of Foreign Affairs, Turkish Prime Ministry, as well as the Governor of Ağri for their sincere efforts and assistance in making this project a success.

10 November 1987, Erzurum